DELFT UNIVERSITY OF TECHNOLOGY

Hydrodynamic Modeling of Estuarine Clay Mineral Distribution: The Ravenglass Estuary Analogue

by

Robbin Bauhuis

To obtain the degree of Master of Science at the Delft University of Technology

in the

Faculty of Civil Engineering and Geosciences

Thesis committee:	Dr. J. Storms,	TU Delft,
	Prof. Dr. A. W. Martinus,	TU Delft
	Dr. C. Chassagne,	TU Delft
	Prof. R. Worden	Universtity of Liverpool

To be defended on: 01-09-2021

Abstract

The presence of clay-coated sand grains in oil and gas sandstone reservoirs has been linked to unusually high reservoir properties. In order to predict and understand its distribution, numerous studies have been done using the present-day Ravenglass Estuary as an analogue. It was concluded that the distribution of clay minerals played an important role, which was in turn strongly influenced by hydrodynamic processes. However, current knowledge of estuarine hydrodynamics cannot fully explain the observed distribution of the clay minerals.

This study aims to improve on the current understanding of hydro- and morphodynamic controls on estuarine clay mineral distribution by using hydrodynamic modeling in Delft3D. A simplified model was made and different simulations were ran in order to distill and study the effects of different hydrodynamic effects, and the approximation of clay mineral behaviour as cohesive sediment Delft3D. In addition, this study has a focus on the overall use of hydrodynamic modeling for the prediction and explanation of sediment distribution, something which is rarely done.

The results of this study did not approach present-day clay mineral distribution, and the findings do not suggest or disprove that this can be done or that clay mineral distribution can be predicted. Key processes were identified to be the interaction between marine- and fluvial currents and the wave orientation. Both processes are strongly influenced by estuary geometry and hence, very local-specific. Results suggest that further modeling work on hydrodynamics in the Ravenglass Estuary could further improve current understanding on it's effects on sediment distribution and may play a role in the prediction of clay mineral distribution in the future. Lastly, this report makes recommendations on future studies.

Contents

List of Figures

List of Tables

Introduction

1.1 Background

While the porosity and permeability of sandstone reservoirs generally decreases with depth, a significant number of studies link unusually high reservoir properties with the presence of clay-coated sand grains, which spikes the interest of the petroleum industry (Ehrenberg, 1993),(Worden and Morad, 2000). These grain coats increase reservoir properties because their occurrence prevents pore-filling quartz cementation in the sandstone when exposed to higher pressures and temperature in the subsurface (Ehrenberg, 1993), (Griffiths et al., 2019a). Grain coats may consist of different types of clay minerals or compositions of clay minerals (Wooldridge et al., 2018a). Positive influences on reservoir quality have been reported for illite-clay-coated grains, and more prominently, chlorite-clay-coated grains (Ehrenberg, 1993) (Pittman et al., 1992).

In order to predict the locations of grain coats in reservoirs, a number of mineralogical and sedimentological studies have been done on the Ravenglass Estuary in NW England as analogue to better understand clay mineral distribution and the formation and distribution of clay-coated grains in marginal-shallow marine systems ((Daneshvar, 2015), (Griffiths et al., 2018), (Griffiths et al., 2019a), (Worden et al., 2020), (Wooldridge et al., 2017b), (Wooldridge et al., 2018a)). It was reported that the heterogeneous distribution of grain coats can be predicted with knowledge of the grain size, clay fraction and depositional facies and are governed by the surface-based hydrological segretation of the clay mineral assemblage and biological clay-coat formation (Wooldridge et al., 2017b), (Wooldridge et al., 2018b). Mineral distribution is controlled by the grain size of specific minerals and estuarine hydrodynamics (Griffiths et al., 2019a). More specifically, clay mineral distribution patterns are strongly influences by sediment supply and are subsequently modified by hydrodynamic processes (Griffiths et al., 2019b). In addition, the ability of clay coats to inhibit quartz cementation is a function of its mineralogical composition (Wooldridge et al., 2018a). So, in order to predict the occurrence of clay coats and it's implications for reservoir quality, one would need to understand the distribution of clay minerals.

1.2 Problem

Estuarine hydrodynamics are the main control on clay mineral and grain coat distribution. They can be very complex and vary greatly between different estuaries, where local-specific conditions can exert a strong control on clay mineral distribution (Griffiths et al., 2019a). However, current understanding of estuarine hydrodynamics and sedimentology don't fully explain the clay mineral distributions in the Ravenglass estuary. To illustrate, relatively high concentrations of chlorite are found in estuary dunes and tidal bars and relatively high concentrations of kaolinite are found in fluvial sediments (Griffiths et al., 2019b). In addition, against common convention, the occurrence of grain coats in the Ravenglass Estuary is most extensive in sediment composed of fine grained sand containing 3.5 to 13.0 % clay fraction, associated with tidal-flat facies (Wooldridge et al., 2017b).

1.3 Objective and Research Questions

To gain more insight on the effect of estuarine hydrodynamics on the distribution of clay minerals, and the implications thereof for predicting clay-coated grains, a hydrodynamic model of the Ravenglass Estuary was made in Delft3D. Delft3D is a 2- and 3-dimensional modeling suite that includes hydrodynamics, sediment transport and morphology for fluvial, estuarine and coastal environments. While a model is always a simplified version of real life, it can improve our understanding of the effects of certain hydro- and morphodynamic conditions and allows for studies on timescales from minutes to centuries. Currently little modeling work is done on the distribution of clay minerals and its reservoir implications. Because of that, this study also discusses and comments on the use of modeling in this context.

Main research question: **"Why do clay minerals accumulate at specific locations in the present-day Ravenglass Estuary and what implication does that have as an analogue for clay mineral distribution in paralic depositional environments?".**

Research sub-questions:

1. What are the most important hydro- and morphodynamic processes in the Ravenglass Estuary that can lead to the observed clay mineral distributions?
2. What are the key hydrodynamic and morphodynamic processes in the Ravenglass Estuary as identified by hydrodynamic modeling in Delft3D?
3. How can the behaviour of chlorite, illite and kaolinite clay minerals be approximated in Delft3D?
4. Can hydro- and morphodynamic modeling explain and predict clay mineral distribution in the Ravenglass Estuary and what does this imply for the use of modeling and prediction of clay mineral distributions in other paralic depositional environments?

5. What do the results and analyses of the Ravenglass Estuary potentially mean for the distribution of clay minerals and clay-coated sand grains in various paralic depositional environments and can this be used as a reservoir analogue?

1.4 Scope

Because of time constraints and the simplifications in a model, the overall scope and exclusion of certain factors important to grain coat formation or clay mineral distribution are listed here in bullet points.

- This study is based on the previous mineralogical and sedimentological studies in the Ravenglass Estuary (Daneshvar,2015 , Griffiths et al, 2019a, 2019b, Worden et al, 2020, Wooldridge et al, 2017, 2018, 2019).
- This study focuses on the initial distribution of the three dominant clay minerals (Chlorite, Illite, Kaolinite) in the Ravenglass estuary, excluding reworking and erosion.
- The study uses post-processing of the modeling results to obtain necessary results.
- The model is in 3D, with bathymetry taken from LIDAR measurements.
- The simulated period is 6 months.
- The bulk of the modeling work is done with the use of the FLOW- and WAVE modules in Delft3D.
- The model defines three cohesive sediment classes, approximating the behaviour of chlorite, illite and kaolinite.
- The study will not take compositional variation of the three clay minerals into account.
- The model will not include authigenic (formed in-situ) mineral sources.
- The model will not include organic material or biological processes.
- Hydrological inputs (e.g. tides, waves, river discharges) are simplified but approximate real-life conditions taken from literature.

Literature Review

2.1 Estuarine Systems

While it is hardly possible to define or classify estuarine systems, and this is a great point of discussion among geologists, traditionally an estuary been defined as a semi-enclosed coastal body of water which has a free connection with the open sea and and within which 'seawater is measurably diluted with fresh water derived from the land' (Pritchard, 1967). Patterns of water circulation are mainly dominated by the interaction of river discharges, waves and tidal influences. Therefore a estuary can be divided in three sectors: (a) a marine or lower estuary, in free connection with the open sea: (b) a middle estuary subject to strong salt and freshwater mixing and (c) an upper or fluvial estuary, characterized by freshwater but subject to daily tidal action (Fairbridge, 1980). Due to the dynamic nature of these forces, for example: fluctuations in river discharge and spring-neap tides, the interfaces of these zones moving spatially up and down the river. This also demonstrated the spatially dynamic behaviour of hydrodynamic elements like saltwater dilation and stratification, wave influence and the degree of flood domination (Flemming, 2011).

An estuary can be either wave- or water-dominated (Reading, 1996) (Figure 2.1). A wave-dominated estuary may result in a sheltered 'lagoonal' or 'barrier-island' type system, as well as more open system like the 'open ended' or 'drowned valley' type estuaries (Reading, 1996). Wave-dominated estuaries have a common facies pattern that roughly consists of the following: a coarse grained marine sandbody at the barrier, washover, tidal inlet and tidal delta deposits. A relatively fine-grained facies at the centre and an inner bay head delta sand and gravel facies that is deposited mainly by the river, but reworked by tides and waves (Reading, 1996). Note that substantial differences can occur here based on the interaction of wave, tidal and fluvial forces, as well as sediment supply.

A tide-dominated estuary has tidal-current energy that exceeds the wave energy at the mouth of the estuary (Reading, 1996). These types are less enclosed than wave-dominated estuaries and are commonly funnel-shaped. The facies pattern roughly follow a tidal channel with sandy deposits, with muddy flats and marshes alongside this channel along the whole length of the estuary. Sandy bars may form along or in this channel, elongated in the flow direction. The most sinuous part of the channel is often in the zone where marine-influences and river-influences have roughly the same energy levels (Reading, 1996).

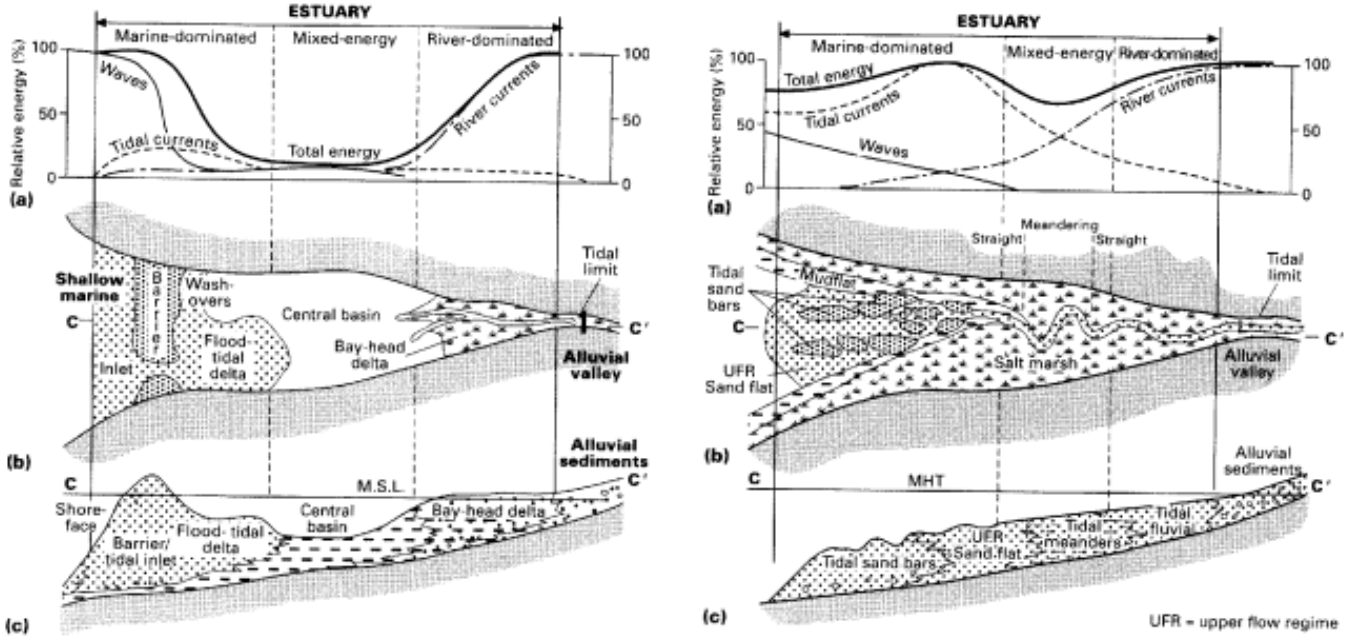

FIGURE 2.1: Distribution of energy levels (a), morphological components (b) and sedimentary facies (c) of wave-dominted (left) and tide-dominated (right) estuaries. (From (Dalrymple et al., 1992))

.

Other suggested ways of classifying estuaries have been done based on the degree of stratification of salt and fresh water. While this study won't strictly follow one of these classification systems, they do demonstrate an important part of the hydrodynamics within an estuary. The degree of stratification can say something about interaction between river and tidal currents, transportation and mixing of salt and sediments, density differences and effects of geometry of the estuary (Villars and Delvigne, 2001).

To illustrate, figures 2.2 and 2.3 show estuaries with a low- and high degree of stratification. Estuaries can also exist as intermediate types, with corresponding degrees of stratification. An estuary would tend to shift from well stratified to poorly stratified with i) increasing tidal velocities, ii) increasing width, and iii) decreasing depth (Villars and Delvigne, 2001).

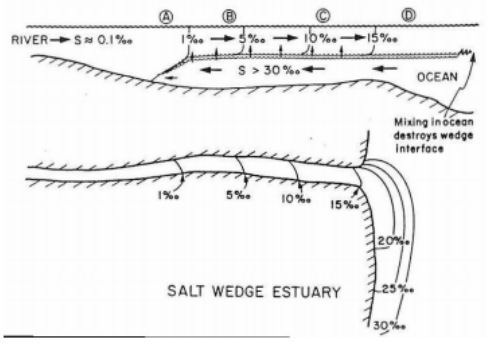

FIGURE 2.2: Example of estuary with a high degree of stratification or 'salt wedge estuary' (after (Villars and Delvigne, 2001)

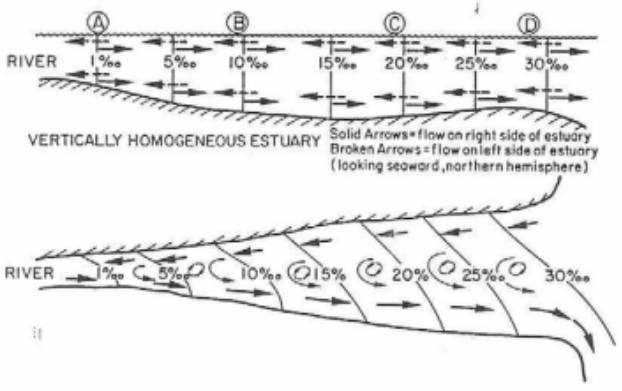

FIGURE 2.3: Example of estuary with a low degree of stratification or 'vertically homogeneous estuary' (after (Villars and Delvigne, 2001)

2.2 Sedimentary Processes in Estuarine Sedimentary Systems

Sediment can be deposited in estuaries by rivers, shore erosion, primary production, the sea and the atmosphere (Schubel, 1984). Sedimentary particles in suspension in estuaries are of relatively small size, 2 μm in diameter, and are mainly clay minerals and colloids which carry a negative surface charge (Daneshvar, 2015). Sediment distribution patterns in estuaries are complex and in addition to river- wave and tide-influences are also affected by atmospheric forcing, wind, climate, seasonal patterns and local flora and fauna (Perillo, 1995), (Wolanski and Elliott, 2014). Most estuaries are sites of tidal pulsing of sediments moving up the estuary under relatively low river flow and high tidal flow conditions, and the freshwater pulsing downstream of sediments under high river flow and weaker tidal conditions (Wolanski and Elliott, 2014). These factors contribute to sedimentary dynamics occuring at timescales of millenia (geomorphological) all the way down to hourly (ebb-flood).

The sediment in the lower estuary zone is derived from the sea and net bedload transport is seaward, whereas the middle estuary zone has a net convergence of fine grained sediments. Lastly, the upper estuary has seaward net transport of sediments, due to fluvial forces being dominant there (Dalrymple et al., 1992).

The main, process that results in the deposition of mud and clay minerals is flocculation due to the mixing of salt and fresh water. This is a result of a negative charge on the sheet-like surface of clay minerals. This attracts a double layer of cations, which increase the tendency to floc with other clay particles. The ionic nature of salt water increases suspended clay minerals potential to floc (Partheniades, 2009). These larger, heavier flocs are then more prone to settling. Note that these flocs can be described as thermodynamically reversable assemblies of solid clay particle, not as irreversable solid particle formations (Whitehouse et al., 1958).

Other factors that control settling rates of clay minerals are clay mineral lattice type, physical structure and initial solid particle size and shape (Whitehouse et al., 1958). Besides ionic composition of the water in which clay minerals settle, also water temperature effects settling (positively) (Whitehouse et al., 1958).

Flocculation results in most mud and clay being deposited in the middle zones of estuary (Flemming, 2011). This process is promoted by high levels of organic content and microbial activity (Flemming, 2011). Higher settling velocities of the larger flocs relative to local turbulance and residual current shear result in the deposition at times of low energy: slack tides. Data suggest that that the lower limit to overcome residual current shear is a settling velocity of 0.01 cm s^{-1}, which corresponds to a particle size in the range of several μm (Flemming, 2011). The upper limit of deposition is generally at the tidal limit as the lack of floc formation means the small particles can be easily re-suspended. The lower limit of deposition is determined by the point reached by the turbidity maximum during ebb tide (Flemming, 2011).

2.2.1 Controls on Clay Mineral Distribution

The distribution of clay mineral is controlled by a the grain size of specific minerals and estuarine hydrodynamics (Griffiths et al., 2019a), and related to mineral alteration processes in the hinterland and estuary settings (Dowey, 2012). Moreover, distribution is a heavily influenced by sediment supply and modification and reworking takes place after initial deposition by hydrodynamic processes (Dowey, 2012), (Griffiths et al., 2019b).

Estuarine hydrodynamics can vary significantly between different estuaries. Certain local-specific conditions can exert a strong control on clay mineral distribution. To illustrate, chlorite distribution on the outer parts of the Ravenglass Estuary has been strongly influenced by wave- and wind direction (Griffiths et al., 2019b). The tidal range, tidal limit and hence, the degree of landward intrusion of salt water are dependant on estuary elevation and geometry, location on the earth and river discharge (Villars and Delvigne, 2001). Increased flocculation and settling due to the presence of salt water is one of the main depositional processes of clay minerals (Partheniades, 2009).

Dowey, 2012 suggests a potential physical process that influences clay mineral distribution in the Leirárvogur Estuary, SW Iceland: A cyclic balance between flocculation due to increased salinity at high tide, and higher tidal flow velocities at the turbidity maximun that break up flocs or re-suspend material. The study also list likely-influencing hydrodynamic- and physical factors on the clay mineral distribution (all mentioned in this study in chapters 2.1 and 2.2), but can't exclude or quantify the degree of influence of any of them. It was also remarked that the physical characteristic of different clay minerals may be important in controlling their distribution (Dowey, 2012).

In the Anllóns Estuary, NW Spain, lower concentrations of clay minerals are found in areas of strong marine influence, together with a strong inverse relationship of carbonate content and clay mineral concentration (Dowey, 2012). Chlorite concentration is relatively high in close proximity to the main estuary channel, and relatively low in saltmarshes, intertidal- and shoreface environments (Dowey, 2012). Kaolinite concentration in the Leirárvogur Estuary is found to be higher in the marine-dominated part of the Anllóns estuary (Dowey, 2012). This may suggest that the ratio of fluvial- and marine currents and their interaction is one of the main hydrodynamic controls on clay material distribution. It also suggest that kaolinite settles out of water column with relatively high salinity. Definitive evidence for a specific estuarine hydrodynamic control lacks for the Anllóns estuary (Dowey, 2012).

One of the few studies that researched the hydrodynamic controls on mud (this study approximates the behaviour of clay minerals as a cohesive sediment, the same as mud) distribution with the use of modeling in Delft3D was done by van de Lageweg et al., 2018, the Scheldt estuary was used as an analogue. It was reported that tidal amplitudes only affect mud-flat size, but not mud-flat thickness. Higher tidal amplitudes result in higher tidal flow velocities, which prevent the deposition of mud. The main condition that determines mud distribution was reported to be the ratio of fluvial currents versus tidal currents. This ratio dictates the tidal flow velocities, which in turn dictates the location of deposition of mud. Tides tend to seperate sand and mud facies and low-energy fair-weather waves do prevent mud deposition at

the mouth, but do not influence hydrodynamics by forming barriers, bars or modifying the shape of the estuary mouth (van de Lageweg et al., 2018).

2.3 The Ravenglass Estuarine System

The Ravenglass Estuary is located in the North-West of England. It sits near the small town of Ravenglass, after which is named, in the county of Cumbria. It is made up from the tidal reaches of the rivers Irt, Mite and Esk that all join in this estuary to share a single relatively narrow (ca. 500m) inlet facing westward into the Irish sea (figures 2.4 and 2.5). The joint inlet, and hence the whole estuary complex, is a result of the extension of both the extensions of the Drigg Spit and the Eskmeals Dunes Spit (figure 2.6). The spits also protect most of the inner estuary of wave influences (Parsons et al., 2013). Figure 2.5 demonstrates the catchment area of the three rivers, extending roughly 20 km landwards.

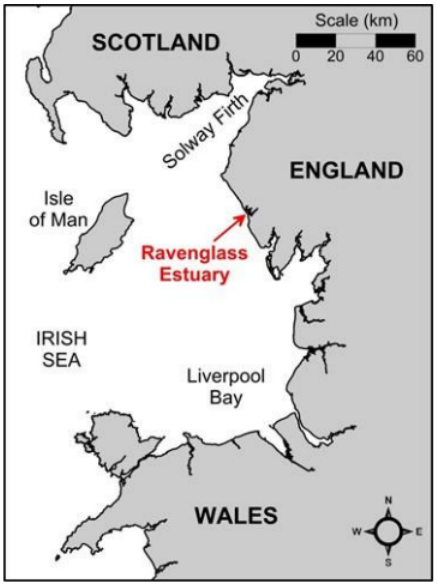

FIGURE 2.4: Location of the Ravenglass Estuary (Parsons et al., 2013)

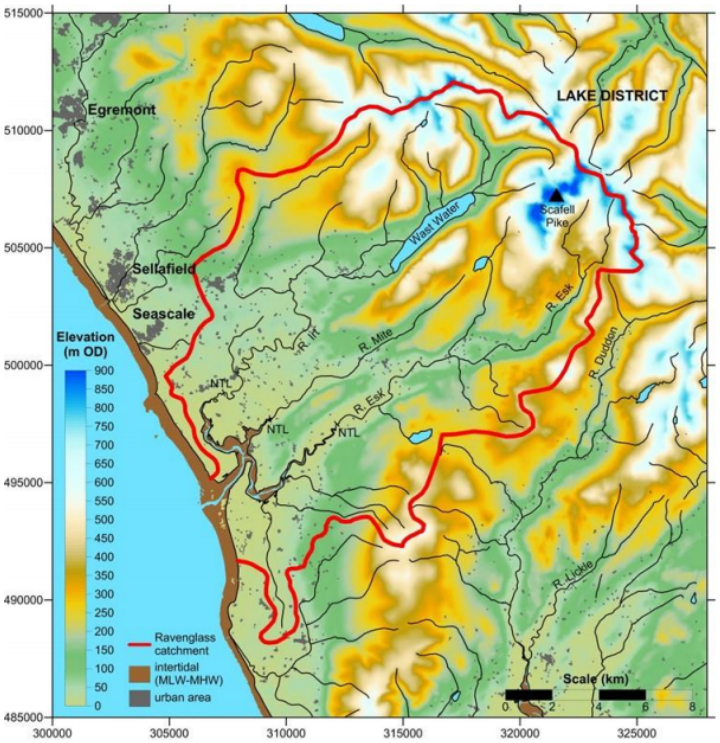

FIGURE 2.5: Catchment and Elevation of the Ravenglass Estuary (Parsons et al., 2013)

The estuary is macro-tidal with a mean spring tide tidal range of over 7 meters (Parsons et al., 2013). The spring tidal range can increase up to 8 meters with a neap tidal range up to 2.5 meters (National Oceanography Centre, 2021). The mean sea level is at 4.5 meters (National Oceanography Centre, 2021). The river discharges are relatively small, with mean flow rates of 3.4 m^3s^{-1} for the Irt, 4.2 m^3s^{-1} for the Esk and 0.4 m^3s^{-1} for the Mite (Boucher, 1999). Therefore the estuary largely empties of water during low tide (Daneshvar, 2015) and has relatively high tidal discharges and velocities (Boucher, 1999). This results in the penetration of seawater far up the Esk arm of estuary (Daneshvar, 2015). In addition, the shallow nature of the estuary and the corresponding frictional effects make these tidal cycles highly asymmetrical, resulting in slightly prolonged, outward ebb tidal flows in comparison to the inward flood tidal flows (Kelly and Emptage, 1991), (Griffiths et al., 2018).

The waves and wind influencing the Ravenglass Estuary are predominantly oriented in NNE to NE direction (Griffiths et al., 2018) (Parsons et al., 2013). The barrier spits shelter a large part of the inner estuary from wave influence, resulting in an outer estuary where predominantly wave-dominated processes occur. Following the same logic, the inner estuary houses more tide-dominant hydrodynamic processes (Wooldridge et al., 2017b).

The tidal range of the Ravenglass Estuary is demonstrated in figure 2.6. Daneshvar., 2015 and Assinder et al., 1985 report that stations A and D are measured as fresh water. Stations B and D and E are freshwater-dominated with minor dilutation by the salt water. For roughly 2 to 5 hours a day this creates brakish-water conditions at high tide. Lastly, station C and F are saltwater-dominated with minor freshwater incursions at low-tide (Daneshvar, 2015), (Assinder et al., 1985). Figure 2.6 also indicates the tidal limit as reported by Kelly and Emptage., 1991

Figure 2.7 shows the bedrock geology of the catchment area (Griffiths et al., 2019a). The catchment area consists of the Sherwood Sandstone Group, the Eskdale Granite, the Borrowdale volcanic group and the Skiddaw Group. Taking into account the provenances and discharges of the three rivers, the Ravenglass Estuary is predominantly fed by sediments from the Eskdale Granite through the Esk river and by sediments from both the Sherwood Sandstone Group and the Borowdale volcanic group through the river Irt (Griffiths et al., 2018).

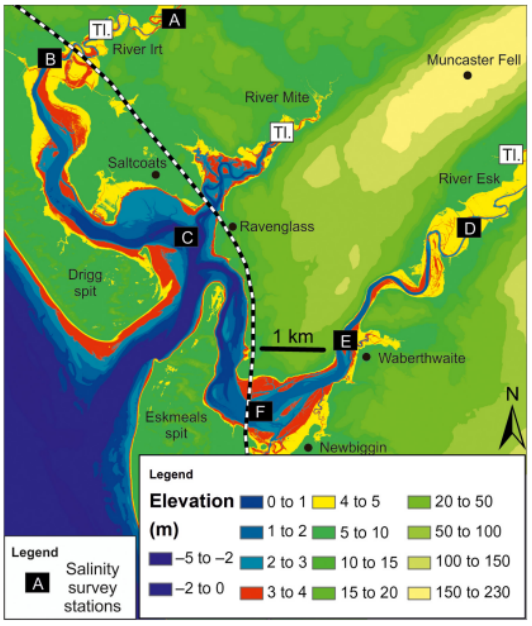

FIGURE 2.6: Bathymetry and salinity measurement stations in the Ravenglass Estuary (after (Daneshvar, 2015) and (Assinder et al., 1985) with tidal limits marked as 'Tl.' after (Kelly and Emptage, 1991)

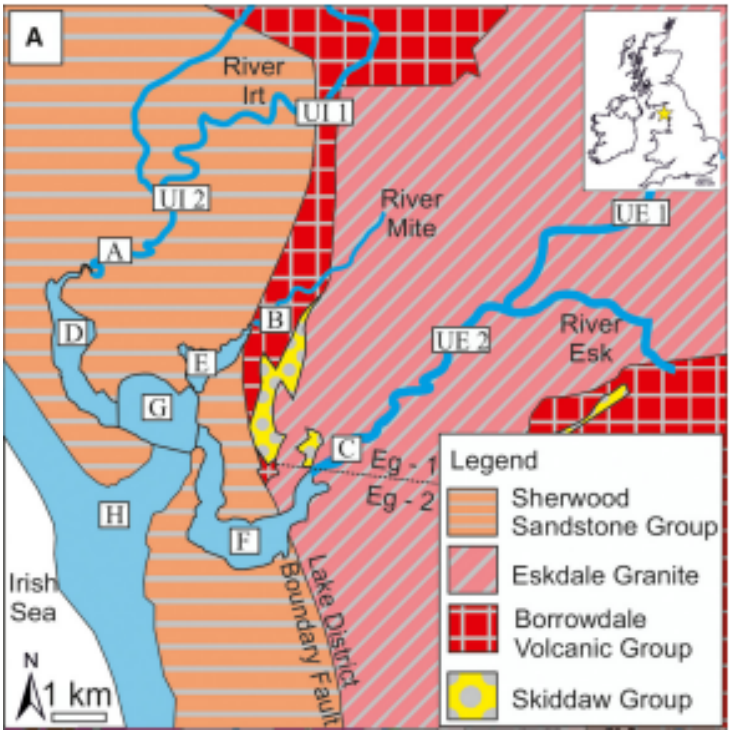

FIGURE 2.7: Provenance and and zonation of the Ravenglass Estuary (after (Griffiths et al., 2019a))

The Estuary only acts as a weak sink for sediment from the sea, mainly for fine-grained sediments (Parsons et al., 2013). It appears to be close to a state of equilibrium (Parsons et al., 2013).

2.3.1 Depositional Environments of the Ravenglass estuary

Field studies by (Griffiths et al., 2018) divided the Ravenglass estuary in nine depositional environments (De's).This is shown in figure 2.8.

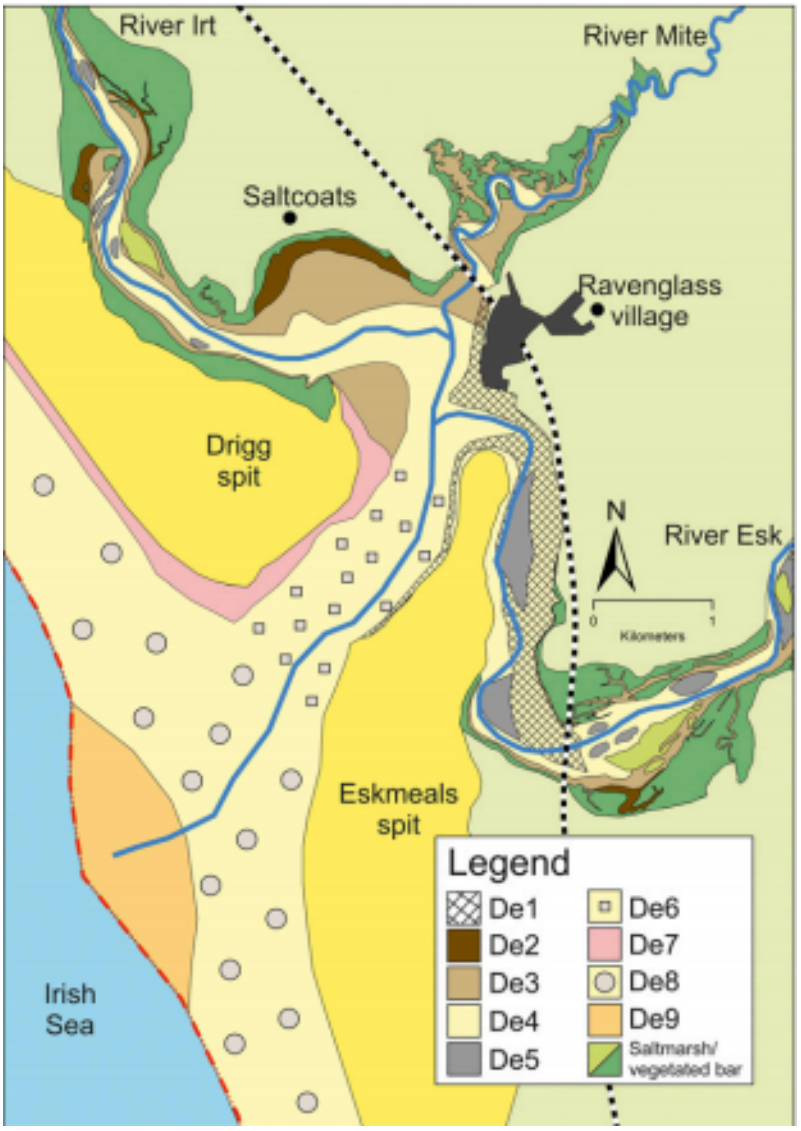

FIGURE 2.8: Distribution of estuarine depositonal environments in the Ravenglass estuary ((Griffiths et al., 2018)). De1, gravelbed; De2, mud-flat; De3, mixed-flat; De4, sand-flat; De5, tidal bars and dunes; De6, tidal-inlet; De7, backshore; De8, foreshore; and De9, pro-ebb delta.

The distribution of the depositional environments (figure 2.8) illustrate characteristic of both a tide- and wave-dominated estuary, the former in the inner estuary, the latter in the outer estuary. The outer estuary, inlet and central basin (estuary zones H and G as illustrated in figure 2.7) show a relatively small inlet, neighbouring two barrier-spits. In the inlet and foreshore/backshore there is minor clay fraction, moderately-well to well sorted, with medium grain sizes (250 to 500 μm) (Griffiths et al., 2018). In the central basin there is a gradation from sand flats to mixed-flats with decreasing mean grain size and sorting. At the start of the Esk estuary arm, there is gravel deposited mainly by the river, but reworked by the tides. These zones roughly follow the characteristic of wave-dominated estuaries as explained in chapter 2.1.

The arms of the estuary, mainly the Irt and Esk arms (or zones D and F) show some characteristics of tide-dominated estuaries. Elongated bars are formed alongside a clear relatively straight channel. This channel consist of sands (De4) with alongside marshes and some minor poorly sorted (Griffiths et al., 2018) mud-flats (De2) and mixed-flats (De3).

2.4 Clay minerals in the Ravenglass Estuary

This subchapter will go into the clay minerals present in the Ravenglass estuary in more detail. This will include basic mineralogy and their origins.

Figure 2.9 shows that the dominant minerals in the estuarine sands and silts is quartz , with smaller amounts of feldspars and clays/micas (Kelly and Emptage, 1991). Minor calcite and amphiboles are found in the rock fragments in the sediment, especially the sand grain size (Kelly and Emptage, 1991). The clay mineral content in the clay grain size fraction ($< 2\mu m$) is shown in figure 2.9. Note that the expandable clays consist of mainly mixed lattice clays including illite-smectite. The scope of this study consist of the clay minerals chlorite, illite and kaolinite.

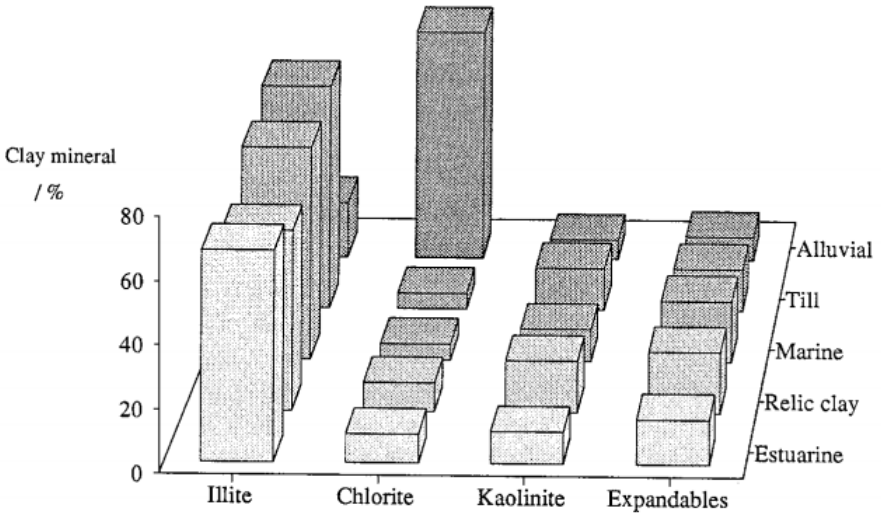

FIGURE 2.9: Mineral content in the clay grain size fraction in the Ravenglass Estuary devided by facies ((Boucher, 1999) after (Kelly and Emptage, 1991))

.

Daneshvar., 2015 reported that most clay minerals in the Ravenglass Estuary originated from the hinterland through the rivers. More specifically, it can be assumed that more clay minerals are being fed into the estuary by the river Irt than the river Esk. In addition, the data suggest that incoming seawater during flood tides has less clay minerals in suspension than the pre-existing water and that marine influx of clay minerals is minimal.

2.4.1 Chlorite

Chlorite is a sheet silicate mineral and has a generalized chemical composition of $(X,Y)_{(4–6)}(\text{Si,Al})_4O_{10}(OH,O)_8$. The X and Y in the formula represent divalent or trivalent ions in the octahedrally-coordinated layers, which commonly might include: Fe^{2+}, Fe^{3+}, Mg or Al (Worden et al., 2020). Due to the large amount of chemical compositions of chlorite, it is also referred to as the chlorite clay mineral group. The exact composition of a chlorite mineral is controlled by its origin (Worden et al., 2020). Chlorite is a relatively unreactive mineral, slow to undergo wheathering and alteration. Therefore chlorite is a common detrital mineral in sedimentary systems (Worden et al., 2020). It can occur in clastic lithics, in silt or clay grade matrix and as detrital clay coats in sedimentary systems (Griffiths et al., 2019a).

In the Ravenglass Estuary chlorite is present in the suspended sediment in the estuary itself, the local seawater and the Irt and Esk rivers (Daneshvar, 2015).

In the Ravenglass Estuary, there are two sources of suspended clay chlorite: i) transported from the hinterland into the system trough the rivers Irt and Esk and ii) generated in-site , presumably in the sediment column (Daneshvar, 2015). Chlorite dominates the clay mineral content coming into the estuary though the rivers (Daneshvar, 2015), (Griffiths et al., 2018).

2.4.2 Kaolinite

Kaolinite is a sheet silicate clay mineral and follows the chemical composition $Al_2Si_2O_5(OH)_4$. The mineral is formed by weathering or alteration of aluminiosilicates, most commonly in feldspar rich rocks such as granite (Nelson., 2014). Due to its crystalline and electric characteristics, it is less susceptible to flocculation due to ions present in salt water. Partheniades, 2009 reported that certain sediments, such as kaolinite, can even flocculate more readily in distilled rather than salt water due primarily to the attraction between their negatively charged surfaces and positively charged edges. In addition, it was found that the suspended behavior of kaolinite is dominated by mechanical processes when compared to physio-chemical processes or a combination of both processes for common clay minerals such as illite (Bennet and Hulbert, 1986).

In the Ravenglass Estuary Kaolinite is present in the suspended sediment in the estuary itself and the local seawater (Daneshvar, 2015). The clay mineral content in the estuary has two sources: i) created in-situ through diagenesis or alteration of other minerals (estuarine or lower-fluvial environment) and ii) washed into the estuary by the sea at high tide (Daneshvar, 2015).

2.4.3 Illite

Illite is a group of sheet silicates that follows the chemical composition $(K,H_3O)(Al,Mg,Fe)_2(Si,Al)_4O_{10}[(OH)_2(H_2O)]$. It is a product of altered or weathered Muscovite and feldspar or the re-crystallization of smectice in marine sediments (Deer et al., 1975).

In the Ravenglass Estuary illite is present in the suspended sediment in the estuary itself and the local seawater (Daneshvar, 2015). Suspended illite in the estuary has two sources: i) transported from the hinterland through the rivers (mainly Irt), it is a minor component relative to chlorite and ii) generated in-situ (estuarine or lower-fluvial environment) (Daneshvar, 2015).

2.5 Clay Mineral Distribution in the Ravenglass Estuary

This section will go into the clay mineral distribution in the Ravenglass estuary in terms of percentage of clay fraction (grain size $< 2\mu m$), devided per clay mineral.
To illustrate, figure 2.10 shows the distribution of the clay fraction as percentage of total sediment. The mineral distribution maps show the percentage of the clay fraction only, not of total sediment.

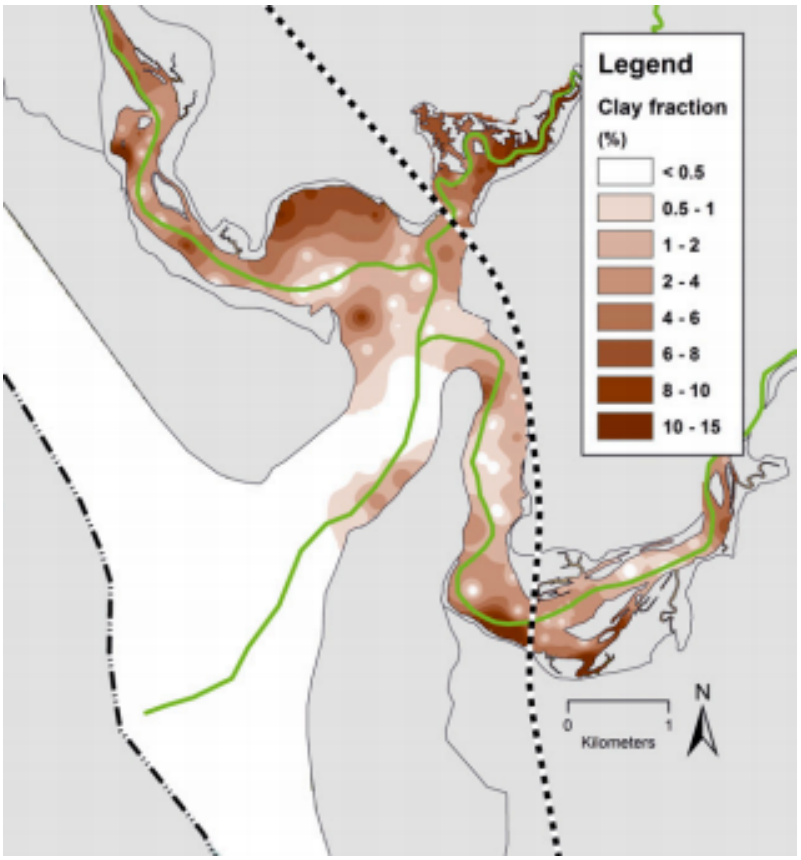

FIGURE 2.10: Interpolated clay fraction (percentage of grain size $< 2\mu m$ of total sediment) (Griffiths et al., 2019a)

2.5.1 Chlorite

Chlorite is typically most enriched in the coarsest grain fractions (Griffiths et al., 2019b). Figures 2.11 and 2.12 show that the higher energy areas like bars, dunes, northern foreshore, northern backshore and the channel axis are relatively rich in chlorite. Figure 2.12 shows the suggestion by (Griffiths et al., 2019b) that the rich foreshore and backshore is a result of the wave direction.

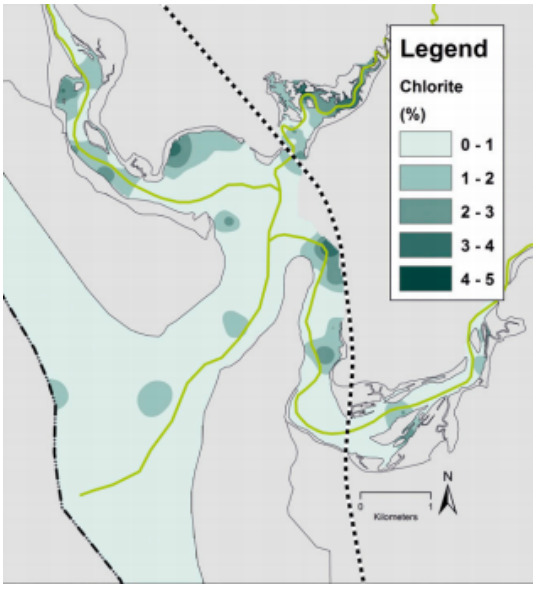

FIGURE 2.11: Interpolated map of chlorite as percentage of clay fraction (Griffiths et al., 2019a)

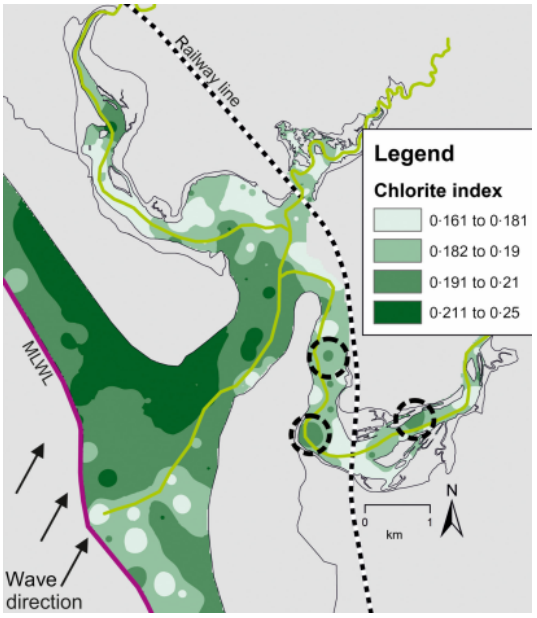

FIGURE 2.12: Interpolated map of chlorite index, i.e. percentage of the sum of chlorite, illite and kaolinite (Griffiths et al., 2019b)

2.5.2 Kaolinite

Figures 2.13 and 2.14 show that the outer estuary is relatively depleted of kaolinite. It is most abundant in fluvial sediment and relitively homogeneous in the area of tidal influence ((Griffiths et al., 2019b)).

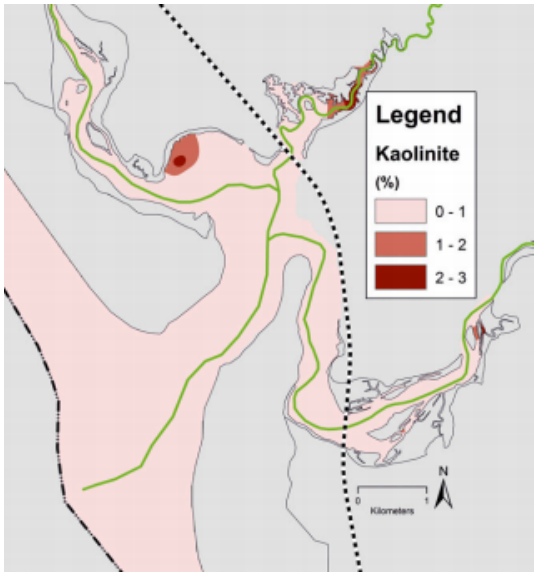

FIGURE 2.13: Interpolated map of kaolinite as percentage of clay fraction (Griffiths et al., 2019a)

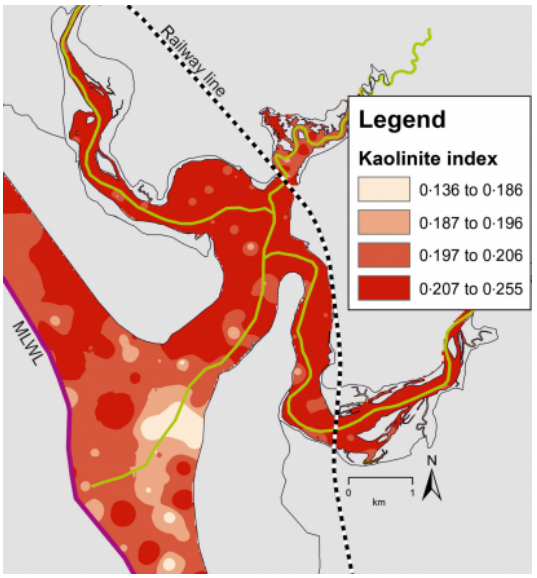

FIGURE 2.14: Interpolated map of kaolinite index, i.e. percentage of the sum of chlorite, illite and kaolinite (Griffiths et al., 2019b)

2.5.3 Illite

Illite is typically most enriched in the finest grain fractions (Griffiths et al., 2019b). Figures 2.15 and 2.16 show that illite is most abundant towards the margins. This coincides with the depositional environments mixed-flats and mud-flats. The higher energy area with high mean grain size and good sorting are relatively illite depleted. This includes bars, dunes and the channel axis. Figure 2.16 shows the depleted foreshore and backshore are a result of the wave direction.

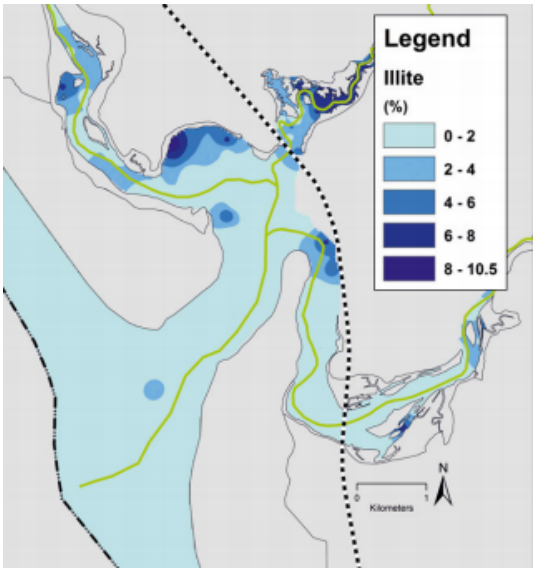

FIGURE 2.15: Interpolated map of illite as percentage of clay fraction (Griffiths et al., 2019a)

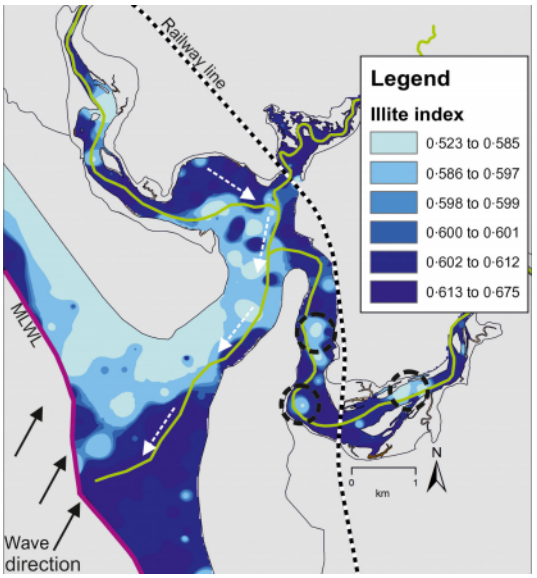

FIGURE 2.16: Interpolated map of illite index, i.e. percentage of the sum of chlorite, illite and kaolinite (Griffiths et al., 2019b)

2.6 Clay Coat Formation and Distribution

Two different types of clay coats exist: detrital clay coats, formed at or near the surface, and diagenetic clay coats. The formation of detrital clay coats generally consist of the attachment of detrital-clay minerals attaching to grain surfaces before compaction (Wooldridge et al., 2018a). This type of clay coat is of most interest in this study, and is also the focus of previous studies in the Ravenglass estuary. Detrital clay coats can occur in different morphologies, like ridged, clumped and bridged coats and on a wide range of degrees of coverage (Wooldridge et al., 2017b).

Typically detrital clay coats exist of a mix of phyllosilicates but they may also include some other clay fraction to silt fraction material (Griffiths et al., 2019b) or bioclastic debris (Dowey, 2012). It is reported that chlorite clay coats inhibit quartz cementation best, underlining the specific interest in chlorite in the petroleum industry (Worden and Morad, 2000), (Dowey, 2012). Other compositions are also reported to elevate porosity, such as illite- and mixed-mineralogy clay coats (Storvoll et al., 2002). The clay coat mineralogy is principally a function of the local, fluvially inputted clay mineral assemblage (Wooldridge et al., 2018a). The ability of clay coats to inhibit quartz cementation is a function of clay coat morphology and grain coverage, which is in turn a function of clay mineralogy (Wooldridge et al., 2018a).

The attachment of clay particles to sand grains in modern marginal systems was shown to primarily be a result of adhesive biofilms that acts as a glue (Wooldridge et al., 2017a). The biofilm is a product of microorganisms that live within the intertidal sediment and react to tidal- and daylight cycles (Wooldridge et al., 2017a). Both of these cycles are obviously dominantly present in a tide-dominated, shallow estuary like the Ravenglass estuary. After, the clay particles become attached to the sand grains. Proposed mechanisms for the introduction of clay to the biofilm include infiltration, bioturbation, inheritance or codeposition (Worden et al., 2020),(Wooldridge et al., 2017b). The distribution of clay coats are therefore

principally controlled by surface based processes local to the site of distribution and are formed in-situ (Wooldridge et al., 2018b)

The distribution of clay coats in the Ravenglass estuary is shown in figure 2.17. The five classes in the figure are described as follows (Wooldridge et al., 2017b):

1. Complete absence of attached clay coats.
2. Less than half of the grains have a small ($\sim$ 1–5%) surface area of attached clay coats.
3. Every grain exhibits at least $\sim$ 5–15% surface area of attached clay coats.
4. Clay coats observed on every grain with the majority exhibiting extensive ($\sim$ 15–30%) surface-area grain coverage.
5. Extensive $>$ 30% surface area covered by clay coats observed on every grain.

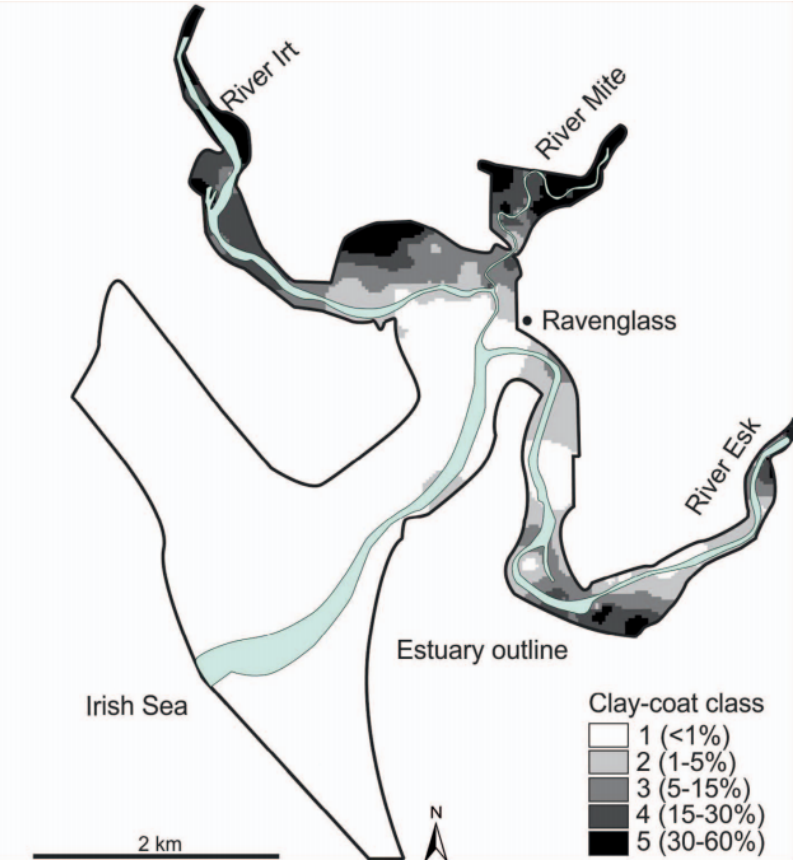

FIGURE 2.17: Distribution of surface clay-coated sand grains (Wooldridge et al., 2017b)

Another argument that emphasises the importance of understanding clay mineral distribution, is the so-called Goldilocks zone of optimum detrital clay-coat coverage. As is well known, high clay content between sand grains decreases porosity and permeability because it decreases pore throat connectivity and fill pores. At the same time, one would like high enough clay content so detrital clay coat coverage is sufficiently high for the inhibition of quartz cementation in the subsurface. In other words, the quantity of clay in sandstones should be not too high and not too low.
Wooldridge et al., 2017 proposed an optimum range of 3.5% to 13.0% of clay volume of total sediment

(based on the works of (Pittman et al., 1992) and (Heald and Baker, 1977)) where the clay quantity is not too high to fill pores but high enough to result in sufficient clay coat coverage for the inhibition of quartz cementation. This range is called 'Goldilocks zone of optimum detrital clay-coat coverage'. For the Ravenglass estuary, these zones are indicated in figure 2.18.

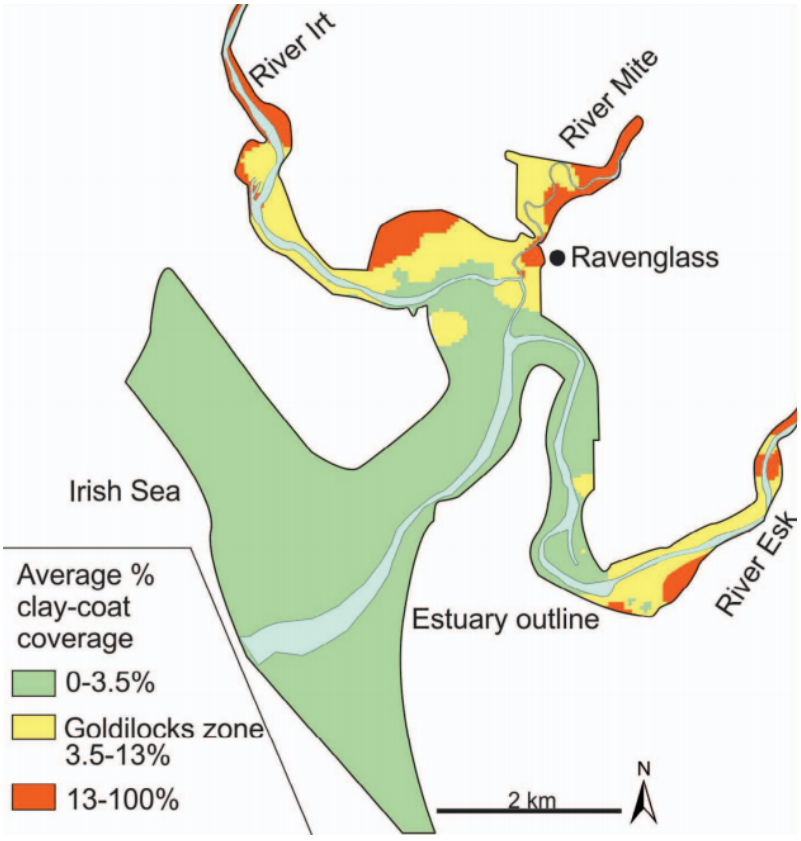

FIGURE 2.18: Indication of the Goldilocks zone of optimum detrital clay coat coverage (Wooldridge et al., 2017b)

Methodology

This chapter will first explain the reasoning behind the overall approach of this study in section 3.1. After, the different parts of the study are touched upon in more detail in sections 3.1.1 to 3.1.3. Lastly, the methodology relevant to computing the results (section 5) is explained, each in their own subsection. The exact input parameters are listed in chapter 4, along with the data the input is based on.

3.1 Modeling Strategy in Delft3D

The modeling work of this study is divided in four parts, that all contribute to two general goals. Schematically illustrated in fig 3.1.
The first goal is to distill the effect of hydrodynamic conditions and sediment properties on sediment distribution and improve the understanding of the hydrodynamics in the Ravenglass estuary and it's influence on sediment distribution.
The second goal: to test the sensitivity of the model. Knowing how sensitive the sediment distribution is to small changes in the conditions is vital when assessing the significance and implications of the results.

The basis of the modeling work is the base case, a very simplified approximation of the real-life estuary, only consisting of river discharges and tides as hydrodynamic input. This results in a sediment distribution of three types of sediment after a set simulated time.
Secondly, the base case model was ran three more times, each with a single change in the input parameters relative to the base case,these runs with a single change are also called scenario's. These resulted in a sediment distribution at the end of the simulated time as well, which then could be analysed and compared to the base case. This way, the effect of a single hydrodynamic condition is distilled.
Thirdly, waves were added to the model. Similar to the second step, three scenario's where ran again, this time allowing for distillation of the effect of waves on sediment distribution.
Fourth, the sediment in the model will consist of three cohesive sediment fractions, approximating the behaviour and properties of the dominant clay minerals in the real-life estuary: chlorite, illite and kaolinite. Two more runs are done subsequently with different sediment properties. this allows for the comparison of the clay mineral distribution with previous studies, and the distillation of the effects of sediment properties on clay mineral distribution.

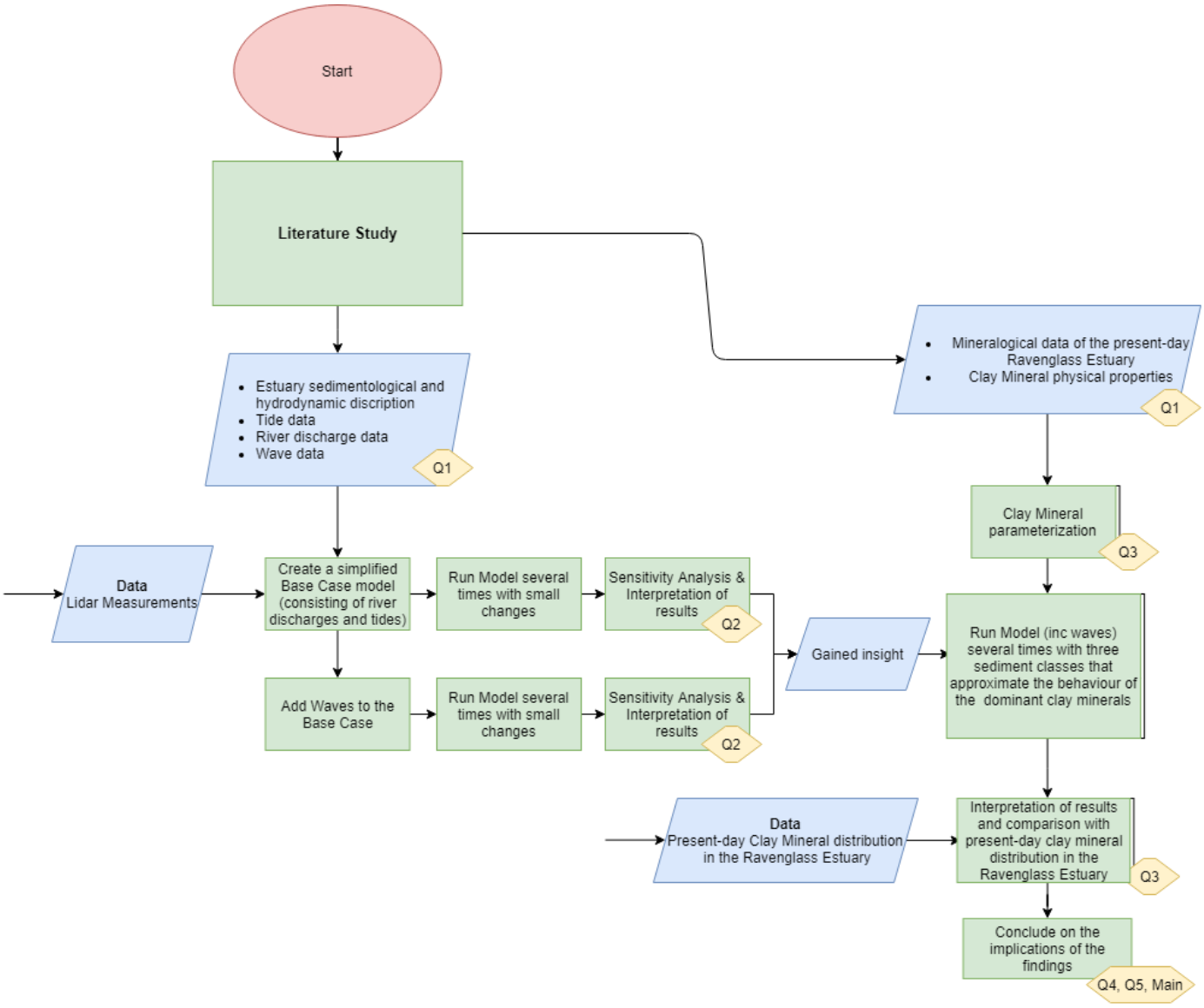

FIGURE 3.1: Schematic illustration of the workflow of this study, relevant research questions for each step depicted with the yellow diamonds

3.1.1 Base Case

The base case is a simplified version of the Ravenglass estuary. It consists of a domain made out of a grid and the bathymetry, bottom roughness, four boundary conditions that simulate the three rivers and the sea, and three different sediment fractions.
The sediment fractions consist of one cohesive sediment fraction (also called mud) and two non-cohesive sediment fractions (also referred to as sands). While the focus of this study is on clay minerals, which are simulated by cohesive sediment fractions, the sand fractions give information about the hydrodynamics in the Ravenglass estuary and realism of the model when analysed in the sensitivity analysis.

The base case was ran for a simulated time of 6 months, and results in a distribution of deposited sediment (i.e. is present in the sediment column according to Delft3D at the last time step of the simulation). All parameters used are listed in their corresponding chapter in section 4.

3.1.2 Sensitivity Analysis of the Base Case

3.1.2.1 Base Case Without Waves

Before adding waves to the model, it is important to know how sensitive the base case is. This is done by running the base case with a small change in conditions and comparing the results to the base case. In addition, it provides insight on the control of hydrodynamic condition on sediment distribution.

Three scenario's were ran. These are:

Scenario 1: Higher Mean Sea Level

Because the Ravenglass estuary is very shallow and the bed is exposed for the bulk of the time, most sediment is likely to occur through the main channels where flow occurs. A higher mean sea level will cover more of the estuary with water and might allow more sediment transport in other places. This can say something about the sensitivity of the base case with respect to the tidal-fluvial interaction where some assumptions were made.

Scenario 2: Initial Conditions for Suspended Sediment

Adding a relative large amount of suspended sediment at t=0 can say something about the dependence of sediment distribution on sediment supply, which is a strong influence on clay mineral distribution (Griffiths et al., 2019b). More specifically, large differences may indicate that the system is far from equilibrium and the simulated time may have to be increased to achieve this.

Scenario 3: Increased Horizontal Eddy Viscosity

Horizontal Eddy Viscosity has a direct positive relation to bed level turbulence in Delft3D.
The horizontal eddy viscosity in a model is dependant on the horizontal grid size and time step of a simulation and it can be used to increase stability of a numerical simulation. This scenario was chosen to analyse the effect of increased turbulence on sediment distribution, and also the possible sensitivity of the model due to the highly irregular grid shape and grid blocks sizes.

3.1.2.2 Base Case with Waves

To study the effect of waves on the sediment distribution in the Ravenglass estuary, three scenario's were ran. Because the shores of west England are sheltered by Ireland, the wave climate is relatively mild. Therefore it was chosen to study the effect of three different wave orientations and leave the peak period and wave height constant. In addition, wave direction is suggested as a possible local specific control on clay mineral distribution (Griffiths et al., 2019b). The first scenario has the most commonly observed orientation, which coincides with the orientation of the estuary inlet (Fugro GEOS, 2001).

The three scenario's are: **Scenario 1: Waves with an orientation of 200°**

A wave orientation of 200° is the dominant direction in the Ravenglass estuary and coincides with the orientation of the inlet, allowing for maximum energy transfer into the estuary. The wave orientation was mentioned as a possible strong control on clay mineral distribution, and local concentrations of chlorite have been identified as a result of wave energy dominant in south-west direction (Griffiths et al., 2019b). Also illustrated in figure 2.12.

Scenario 2: Waves with an orientation of 230°

This scenario has a wave orientation of 230°, slightly off from the orientation of the estuary inlet and the real-life dominant direction. Steps of +30° relative to scenario 1 were chosen so there could be a total of 3 scenario's before the orientation is perpendicular to the real-life situation. In addition, the geometry of the shore won't allow for a realistic wave direction when the direction is changed counter-clockwise, or steps of -30°.

Scenario 3: Waves with an orientation of 260°

This scenario has a wave orientation of 260° which is of significantly from the dominant wave direction, while still generally in the direction of the estuary inlet. The reasoning in section 3.1.2.2 also applies here.

3.1.3 Clay Mineral Simulations

Lastly, the model was ran with three cohesive sediment fractions. These approach chlorite, illite and kaolinite. The parameters that are used to do this are density, fresh settling velocity and saline settling velocity. Three simulation were ran.
The first with parameters from literature, which will be explained in section 4.3.1. The second and third clay minerals simulations will have different density and settling velocities compared to the first clay mineral simulation, respectively. This allows for the distillation of the effect of these parameters. All parameters will be listed in section 4.3

3.2 Numerical Modeling in Delft3D

This section will give a short general introduction of 3D models in Delft3D and will go into more detail about sediment transport, post-processing and cohesive sediment parameters as they are relevant to the study and needed to interpret the results.

3.2.1 3D models

Delft3D is hydrodynamic, morphodynamic and sediment transport simulator of coastal systems. The modeling method can be described as forward, process-based modeling. In other words: after specifying

an initial situation, boundary conditions and a period to be simulated , Delft3D will simulate the effect of the specified processes for the corresponding period, one short time step at a time. It allows for the simulation on multiple spatial- and time scales. It consist of multiple modules, but the bulk of the work in this study will be done by the FLOW- and Wave modules.
The FLOW module incorporates a large number of features, including but not limited to (Delft3D Flow manual):

- Tidal forcing
- Density driven flows
- Sediment transport and deposition
- Four options for advanced turbulence models
- Temperature
- Salinity
- Space and time varying wind and atmospheric pressure
- Time varying boundary conditions

FLOW simulation are ran simultaneously with other modules, where the hydrodynamic conditions are used as input for the other modules (Delft3D Flow manual). This study only makes use of the Wave module. As the name implies, the Wave module simulates random, short-crested, wind-generated waves nearshore (Delft3D Wave manual).

The domain on which a Delft3D simulation is ran, consist generally of a 2D grid and it's bathymetry. The user has a choice to create a 3D simulation by manually choosing an amount of layers. Because grid cells can be curvilinear and have any chosen orientation, cells are indexed in terms of M and N.
Boundary conditions are set at manually set boundaries on the grid. These boundary conditions can simulate the behaviour of rivers and the sea and are the driving force in the model. The types of available boundary conditions are (Delft3D Flow manual):

- Water level
- Current
- Neumann
- Discharge (total or per cell)
- Riemann

Which can be forced in the following four types:

- Astronomic
- Harmonic
- Time-series
- QH-relation (only for water level boundary conditions)

Lastly, at the boundaries, the transport conditions can be set. At every boundary the quantity of constituents in the incoming water can be set. These constituents can be temperature, pollutants, salinity, sediment and more.

3.2.2 Governing Equations

Delft3D defines two types of of sediment classes. First, cohesive sediment, also indicated as mud. The clay minerals this study focuses on are simulated as a cohesive sediment. The second class is non-cohesive sediment, also indicated as sand. Both classes are governed by a set of mostly different equations and parameters. This section will only go into the relevant governing equations for cohesive sediment transport and deposition.

3.2.2.1 Sediment Deposition from Water Column to Bed

Delft3D computes the present sediment in both the water column (divided vertically in grid blocks) and the bed. When sediment has be transport from water column to bed, it is considered deposited. By default the model assumed perfect mixing of the sediments in the bed by default. A system can be used where Delft3D saves the order of deposition, the bed stratigraphy, which is a not used in this study but a possible addition for future work.

To compute the transport of cohesive sediment from water column to bed, Delft3D uses the Partheniades-Krone formulations. It makes use of a depositional (D) and erosional (E) flux, which are calculated per sediment fraction at the bottommost water layer cell (Delft3D Flow manual).

$$E = M * Max(0, \frac{\tau_{cw}}{\tau_{cw,e}} - 1)^n \tag{3.1}$$

$$D = w_s * c_b * \Gamma \tag{3.2}$$

where:
E erosion flux from the bed $[kg * m^{-2}s^{-1}]$
M user-defined erosion parameter $[kg * m^{-2}s^{-1}]$
n user-defined power for erosion

D deposition flux $[kg * m^{-2}s^{-1}]$

w_s fall velocity (including hindered settling) [m s^{-1}]

c_b average sediment concentration in the bottommost computational layer of thickness [kg m^{-3}]

Γ dimensionless reduction factor for deposition flux [-]

τ_{cw} maximum bed shear stress due to current and waves as calculated by the wave-current interaction model selected by the user

$\tau_{cr,e}$ user-defined critical erosion shear stress [N m^2]

$\tau_{cr,d}$ user-defined critical deposition shear stress [N m^2]

Where

$$\Gamma = \begin{cases} 1 - \frac{\tau_{cw}}{\tau_{cr,d}}, & \text{where } \delta<0 \\ \delta, & \text{where } 0 \leq \delta \leq 1 \end{cases}$$

If the critical bed shear stress for sedimentation If the bed shear stress is larger than this value, no sedimentation takes place. In addition, lowering the critical bed shear stress for sedimentation reduces the depositional flux according to equation 3.2 While used in modeling, this parameter is a point of discussion, as it was suggested that it doesn't or might not exist and is difficult or impossible to obtain (van Maren, 2009), (Shi et al., 2015). One may imagine that differentiating between critical shear stresses for sedimentation for clay minerals from literature would be highly difficult to do, which is part of the reasoning of leaving it out for the scope of this study.

3.2.2.2 Cohesive Sediment Settling (Flocculation)

Flocculation is the main process in the deposition and settling of clay. Delft3D uses the following equation to compute the settling velocity of cohesive sediment, depending on that cohesive sediment fraction's parameters for fresh and saline settling velocity and the salinity of the water. The maximum saline settling is achieved at the value set as SALMAX or S_{max}, in the case of this study, the default 31 ppt. This is computed seperately for every cohesive sediment fraction.

$$\mathrm{w}_{s,0}^{(l)} = \begin{cases} \frac{w_{s,max}^{(l)}}{2}(1 - cos(\frac{\pi S}{S_{max}})) + \frac{w_{s,f}^{(l)}}{2}(1 - cos(\frac{\pi S}{S_{max}}), & \text{when } S \leq S_{max} \\ w_{s,max}^{(l)}, & \text{when } S > S_{max} \end{cases} \quad (3.3)$$

where:

$w_{s,0}^{(l)}$ the (non-hindered) settling velocity of sediment fraction (l)

$w_{s,max}^{(l)}$ WSM, settling velocity of sediment fraction (l) at salinity concentration SALMAX

S_{max} SALMAX, maximal salinity at which WSM is specified (31 ppt)

$w_{s,f}^{(l)}$ WS0, fresh water settling velocity of sediment fraction (l)

S salinity

3.3 Postprocessing of Simulation Data

The following subsections explain how the results were computed from the simulation data using postprecessing.

3.3.1 Preserved mass of sediment of the base case

The mass that is present in the sediment column at the last time step was extracted from the data for each sediment fraction per grid cell. The mass per grid cell was then divided by the area of each grid cell to account for the different sizes of grid cells.
It was then plotted as interpolated map using the coordinates of the grid cells using 'linear' interpolation.

3.3.2 Relative difference in preserved sediment

The method of extracting the preserved mass was repeated for each of the scenario's, excluding the interpolation. For each grid cell, the difference in mass per m^2 between the base case and the scenario's was computed. This difference in each grid cell was then divided by mass in the base case to get the relative difference for each grid cell. It was plotted as interpolated map using 'linear' interpolation.

3.3.3 Dependency of changes in preserved sediment on erosion and deposition

To interpret the physical meaning of relative changes in preserved sediment, it is important to know the cause of these changes. Changes in preserved mass at the end of the simulated time are assumed to be a results of: i) an increase or decrease in sediment that is deposited into the sediment column during the simulation, ii) an increase or decrease in erosion during the simulation or iii) a combination of both. To differentiate between this, the dependency of changes in preserved sediment on erosion and deposition is computed as described below.

First, the total erosion over the whole simulated time is calculated for the base case and the scenario's per grid cell. The total erosion of a grid cell is defined as the sum of all negative changes between two time steps. In other words, when the amount of mass of sediment 1 at time step x+1 is lower as the mass of sediment 1 at time step x, this is assumed to be due to erosion. These eroded masses are subsequently summed for all time steps of the simulation. The time step of the simulations were all taken to be 1 day.

Secondly, the difference in total erosion between the base case and the scenario's was calculated for every grid cell.

Lastly, the changes in total erosion where compared to the changes in preserved mass. This was done by dividing the differences in erosion by the differences in preserved mass.
This results in a value that represent the dependency of changes in preserved mass on erosion.
A value of roughly 1 means that the difference in erosion is very similar to the difference in preserved sediment. For instance, when running a scenario results in 0.5 kg more erosion in a grid cell over the whole simulated time, it will result in a value of 1 when running the scenario also results in 0.5 kg less preserved sediment in that grid cell. Hence, the change in preserved sediment is caused by more erosion and not by less deposition
Using the same reasoning, values closer to 0 represent little dependency on erosion. In such a case a decease in preserved sediment is dominantly caused by a decrease in deposition of that sediment.
Values of >0.5 are assumed to be grid cells where changes in erosion are dominant. Values of ≤ 0.5 are assumed to be grid cells where changes in deposition are dominant.

3.3.4 Relative Masses of Clay Minerals

The results of section 5.3 are the ratio's of the masses of chlorite, illite and kaolinite relative to the sum of all three clay minerals. This was done to better compare them to the clay mineral indexes from literature (section 2.5). These are computed per grid cell at the last time step at 180 days. The total cumulative mass is the sum of the three clay minerals. The relative masses were interpolated and plotted on their own scale to improve the visibility of the relative small differences.

Data and model setup

This section will explain the creation of the grid, the input parameters and if relevant, the data the input parameters are based on.

4.1 Base Case

4.1.1 Grid and Bathymetry

The grid and bathymetry of the model are shown in figures 4.1 and 4.2, respectively. The grid was made manually, following the outline also present in the figures. This outline was at 6m elevation, extracted from LiDAR measurements. It has 62 grid blocks in N direction, 144 in M direction. The grid was optimized in numerous iterations to improve its quality as much as possible following the criteria by Deltares, 2011:

- Orthogonality: A value of 0.04 in the inner model area. Larger values (0.05 - 0.10) may be tolerated in the outer parts.
- Smoothness: ratio of neighbouring grid cells in M and N direction. Should be less than 1.1 in area of interest, further out up to 1.4.
- Aspect ratio, the ratio if a grid cell's dimensions in M and N direction. In the range of 0.5 - 2.

The bathymetry is corrected for mean sea level (further explained in chapter 4.1.3) and extracted from LiDAR measurements.

The four boundaries in the model are shown in figure 4.3. They represent the open sea and the rivers Irt, Mite and Esk.

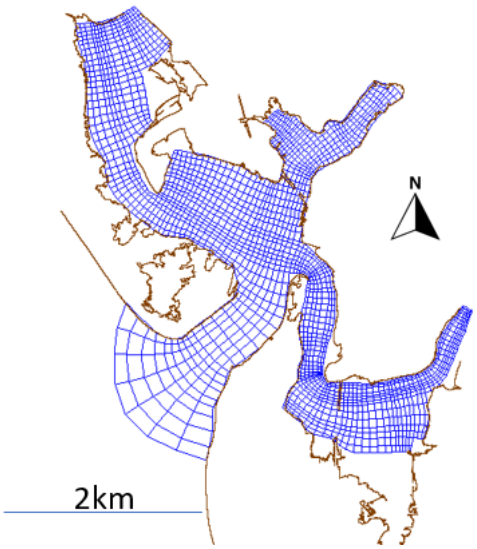

FIGURE 4.1: Model grid and outline

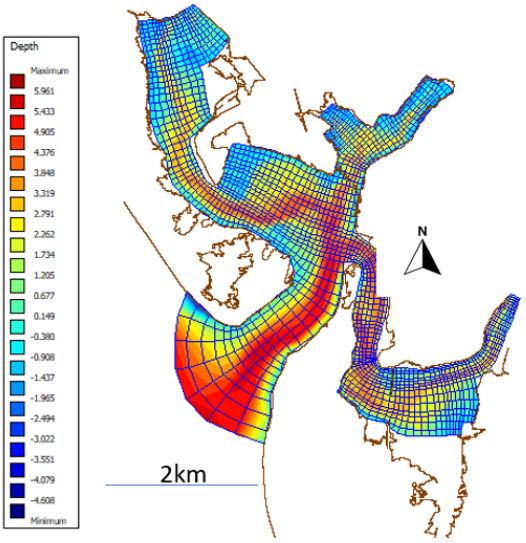

FIGURE 4.2: Bathymetry of model, corrected for mean sea level. Note that everything below mean sea level is positive.

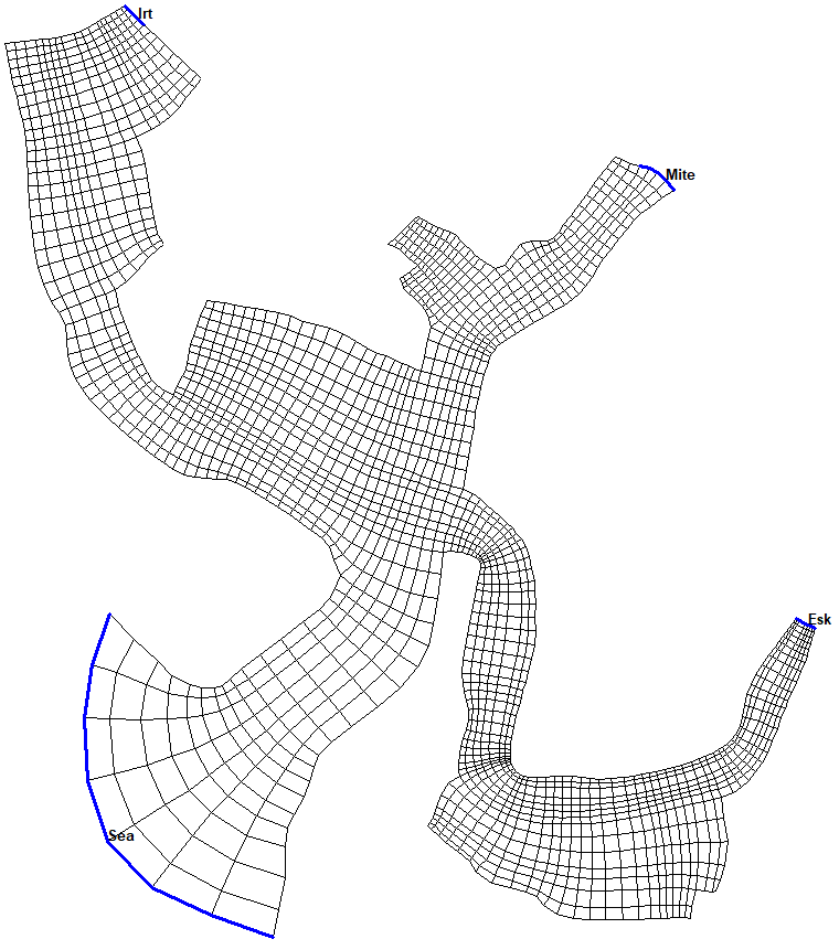

FIGURE 4.3: Location of the boundaries

4.1.2 River Discharges

The river Irt, Mite and Esk have mean flow rates of 3.4 m^3s^{-1} , 0.3 m^3s^{-1} and 4.2 m^3s^{-1} , respectively (Boucher, 1999). The max flow rates are 24.02 m^3s^{-1} for the Irt and 75.06 m^3s^{-1} for the Esk while the

max flow rate for the Mite is unknown (Boucher, 1999).
Because the rates are so small, they have been set higher in the model (but in a realistic range) to improve sediment input for the sensitivity analysis for the sake of computational time.
These discharges are:

- Irt: 20 $m^3 s^{-1}$
- Mite: 10 $m^3 s^{-1}$
- Esk: 20 $m^3 s^{-1}$

4.1.3 Tides

Parsons et al., 2013 reported a spring tidal range of over 7 meters. This is supported by measurements of the tide gauge in Workington, 20 km to the north of the Ravenglass Estuary (National Oceanography Centre, 2021). To illustrate, the spring-neap cycle from the station is shown in figure 4.4. The mean sea level is roughly 4.5 meters and the neap tidal range can be as low as 2.5 m.

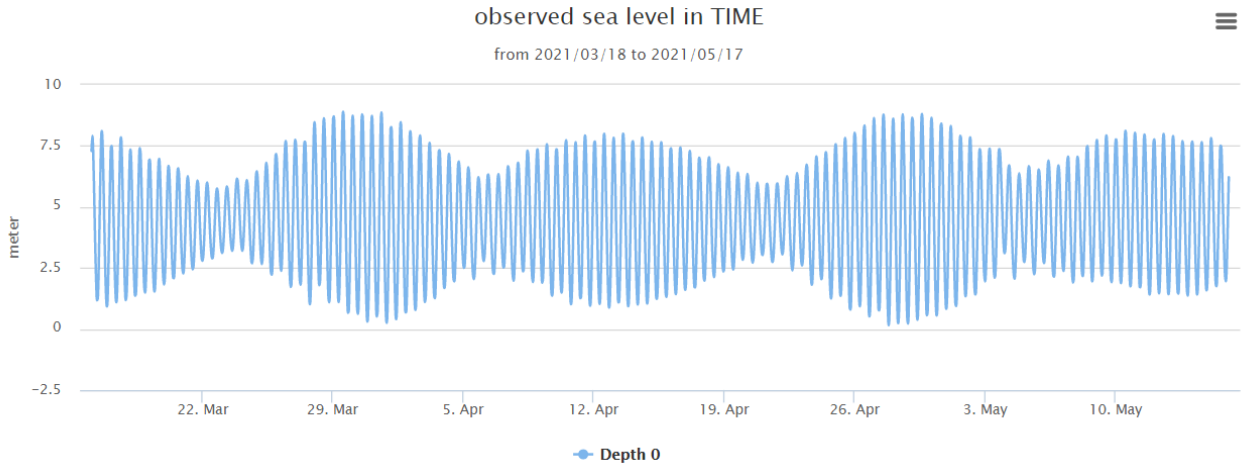

FIGURE 4.4: Tide measurements at the Workington tide gauge (National Oceanography Centre, 2021)

The boundary condition at the 'Sea' boundary was set as a harmonic sea level. It has a semidiurnal frequency (28,8 deg/h) and an amplitude of 1.5 m. This approximates the mean tidal range.
The salinity of sea water was set to 31 ppt. This corresponds to the default maximum salinity value as computed by Delft3D, or in other words, the salinity level at which the saline settling velocity is applied to cohesive sediment.

Simulated Tide Parameters	**Value**	**Unit**
Mean sea level	4.5	m
Spring tide sea level	6	m
Neap tide sea level	3	m
Frequency	28.6 (semidiurnal)	deg/h
Sea water salinity	31	ppt

TABLE 4.1: Parameter values of tides

4.1.4 Bottom Roughness

The bottom roughness of the model was set to be spatially varying. The roughness is computed following the White-Colebrook equation:

$$C = 18^{10} log(\frac{12H}{k_s}) \tag{4.1}$$

Where C is the Chevy friction coefficient, H the water depth and k_S the equivalent geometrical roughness of Nikuradse. k_s is user-specified.
k_s was set be equal to $3d_{50}$ as suggested by (Van Rijn, 1984). Where d_{50} is the mean grain diameter. The grain size distribution in the Ravenglass estuary was taken from Griffiths et al., 2019a.

4.1.5 Modeling Parameters

With the exception of the parameters discussed before, all modeling parameters are listed in table 4.2.

Parameter /setting	**Unit**	**Values**
Simulated time	6	months
Time step	0.3	minutes
Initial water level	0	m
Initial salinity	0	ppt
Initial sediment concentration	0	kg/mˆ3
Gravity	9.81	m/sˆ2
Water density	1000	kg/mˆ3
Horizontal eddy viscosity	1	mˆ2/s
Horizontal eddy diffusity	10	mˆ2/s
3D turbulence model	k-epsilon	-
Morphological Scale factor	1	-
Spin-up interval	720	minutes
Minimum depth for sediment calculation	0.1	m
van Rijn's reference height factor	1	-
Threshold sediment thickness	0.05	m
Estimated ripple height factor	2	-

TABLE 4.2: Model parameters of the base case

4.2 Sensitivity Analysis of the Base Case

The sediment input for the sensitivity analysis consist of the following three sediment fractions and are constant for all base case runs:

Sediment Parameter	**Fine Sand**	**Very Fine Sand**	**Mud**
Reference density kg/mˆ3][	1600	1600	1600
Specific density [kg/mˆ3]	2650	2650	2650
Dry bed density [kg/mˆ3]	1600	1600	500
Saline settling velocity [mm/s]			0.25
Fresh settling velocity [mm/s]			0.25
Median sediment diameter [μm]	200	100	
Critical shear stress for sedimentation [N/mˆ2]			1000
Critical shear stress for erosion [N/mˆ2]			0.5
Sediment erosion rate [kg/(mˆ2 s)]			0.0001
Initial sediment layer at bed [m]	0.05	0.05	0.05

Table 4.3: Sediment parameters for the base case

The sediment discharges are set to 3 kg m^{-3} for all three rivers. No sediment is coming in from the sea.

4.2.1 Sensitivity analysis of the base case without Waves

Three scenario's are here described, all parameters not mentioned are the same as in the base case.

4.2.1.1 Scenario 1: Higher Mean Sea Level

This scenario has an increased mean sea level of +1 m relative to the base case.

4.2.1.2 Scenario 2: Initial conditions for sediment

This scenario has 3 kg m^{-3} of each sediment fraction present in the water column at the start of the simulation.

4.2.1.3 Scenario 3: Increased Horizontal Eddy viscosity

This scenario has an increased Horizontal Eddy viscosity value of 1.3 m^2/s (from 1 m^2/s) relative to the base case. This was based on the stability limitation (Delft3D Flow manual):

$$\Delta t * v_H(\frac{1}{\Delta x^2} + \frac{1}{\Delta y^2}) < 1 \tag{4.2}$$

Where the timestep Δ t was set to 15 seconds, and the horizontal grid cell dimensions Δx^2 and Δy^2 to the lowest values found: 8 m and 8 m respectively. V_h is the horizontal eddy viscosity.

4.2.2 Sensitivity Analysis of the Base Case with Waves

To study the effect of waves on the sediment distribution in the Ravenglass estuary, three scenario's were ran. The wave parameters are shown in table 4.4. The wave height and peak period are taken as the values that were measured most often by Fugro GEOS, 2001. Because the shores of west England are sheltered by Ireland, the wave climate is relatively mild. Therefore it was chosen to study the effect of three different wave orientations and leave the peak period and wave height constant.

Delft3D wave parameter	**Value**	**Unit**
Significant wave height	1	m
Peak Period	4.5	s
Orientation	200, 230 & 260	nautical degrees
Directional spreading	4 (default)	-
Implemented at boundary	'Sea' Boundary as depicted in figure 4.3	

TABLE 4.4: Wave parameter input

4.3 Clay Mineral Simulations

This section lists all parameters of the cohesive sediment fractions that approach the behaviour of chlorite, illite and kaolinite. The parameters that are used to do this are density, fresh settling velocity and saline settling velocity.
Three simulation were ran. The first with parameters from literature, which will be explained in section 4.3.1.
The second and third clay minerals simulations will have different density and settling velocities compared to the first clay mineral simulation, respectively. This allows for the distillation of the effect of these parameters.

4.3.1 Clay Mineral Simulation 1: Clay mineral Parameterization according to values from Literature

These parameters were used in the first clay mineral simulation, and will be referred to as 'Parameters from literature'.

The effect of salinity on the settling of kaolinite is a point of discussion. This study follows an inverse relation between settling rate and salt concentration as reported by Palomino and Santamarina, 2005, Liu et al., 2018 and Jeldres et al., 2017 .

The dry bed density was taken to be 1/5th of the specific density. The Critical bed shear stress for sedimentation was set at 1000 N/m^2, which is the default and limit in Delft3D. Because the scope of this study doesn't include erosion and reworking, it was decided to leave it at the default 1000 N/m^2. For the same reasoning, the critical bed shear stress for erosion was set at the upper limit of 100 N/m^2.

* The fresh settling velocity of chlorite was based on the work of Whitehouse et al., 1958 . It concluded that in quiet saline water, chlorite settles faster than kaolinite and slower than illite. Because chlorite's settling behavior is most similar to illite, the fresh water settling velocity was chosen to have the same ratio to illite's fresh settling velocity as both saline settling velocities have to each other as found by Whitehouse et al., 1958.

	Chlorite	
Delft3D parameters for cohesive sediment	Value	Source
Specific density (kg/mˆ3)	3000	(Worden et al., 2020)
Dry bed density (kg/mˆ3)	600	
Fresh settling velocity (mm/s)	0.010	*
Saline settling velocity (mm/s)	0.026	(Whitehouse et al., 1958)
Critical bed shear stress for sedimentation (N/mˆ2)	1000	Default
Critical bed shear stress for erosion (N/mˆ2)	100	Delft3D upper limit
Erosion paremeter (kg/m2/s)	0	No erosion
Initial sediment layer thickness in at bed (m)	0.05	Default

TABLE 4.5: Sediment parameters for the Chlorite sediment class

	Illite	
Delft3D parameters for cohesive sediment	Value	Source
Specific density (kg/mˆ3)	2810	(Worden et al., 2020)
Dry bed density (kg/mˆ3)	562	
Fresh settling velocity (mm/s)	0.013	(Liu et al., 2018)
Saline settling velocity (mm/s)	0.032	(Whitehouse et al., 1958)
Critical bed shear stress for sedimentation (N/mˆ2)	1000	Default
Critical bed shear stress for erosion (N/mˆ2)	100	Delft3D upper limit
Erosion paremeter (kg/m2/s)	0	No erosion
Initial sediment layer thickness in at bed (m)	0.05	Default

TABLE 4.6: Sediment parameters for the Illite sediment class

	Kaolinite	
Delft3D parameters for cohesive sediment	Value	Source
Specific density (kg/mˆ3)	2630	(Mindat, 2021)
Dry bed density (kg/mˆ3)	526	
Fresh settling velocity (mm/s)	0.027	(Jeldres et al., 2017)
Saline settling velocity (mm/s)	0.013	(Jeldres et al., 2017)
Critical bed shear stress for sedimentation (N/mˆ2)	1000	Default
Critical bed shear stress for erosion (N/mˆ2)	100	Delft3D upper limit
Erosion paremeter (kg/m2/s)	0	No erosion
Initial sediment layer thickness in at bed (m)	0.05	Default

TABLE 4.7: Sediment parameters for the Kaolinite sediment class

4.3.2 Clay Mineral Simulation 2: Changes in Clay Mineral Density

This simulation used a larger density value of 3300 kg/m^3 for Chlorite and smaller density value of 2600 kg/m^3 for Illite. The dry bed density was also set to 1/5th of this. These values where within the range of density for their respective mineral groups (Mindat, 2021) and chosen in order to increase the potential difference in their distribution. Exact values listed in table 4.8. Parameters not listed remain the same

as depicted in chapter 4.3.1.

Parameter	Simulation 1 - from literature	Simulation 2 - changes in density
	Chlorite	
Specific density (kg/mˆ3)	3000	3300
Dry bed density (kg/mˆ3)	600	660
	Illite	
Specific density (kg/mˆ3)	2810	2600
Dry bed density (kg/mˆ3)	562	520
	Kaolinite	
Specific density (kg/mˆ3)	2630	2630
Dry bed density (kg/mˆ3)	526	526

TABLE 4.8: Changed density values in simulation 2

4.3.3 Clay Mineral Simulation 3: Changes in Fresh and Saline Settling Velocity

For this simulation, the difference between the fresh and saline settling velocity relative to simulation 1 was doubled. This was done for each clay mineral in order to distill the effect of the settling velocity. Exact values are listed in table 4.9. Parameters not listed remain the same as depicted in chapter 4.3.1.

Parameter	Simulation 1 - from literature	Simulation 3 - changes in settling velocity
	Chlorite	
Fresh settling velocity (mm/s)	0.010	0.002
Saline settling velocity (mm/s)	0.026	0.034
	Illite	
Fresh settling velocity (mm/s)	0.013	0.006
Saline settling velocity (mm/s)	0.032	0.042
	Kaolinite	
Fresh settling velocity (mm/s)	0.027	0.034
Saline settling velocity (mm/s)	0.013	0.003

TABLE 4.9: Changed settling velocity values in simulation 3

Results

5.1 Base Case

This section shows the sediment distribution for the Base Case at the last time step of the simulated period for each of the three sediment fractions. Masses are expressed in mass per m^2 to compensate for grid cell size differences.

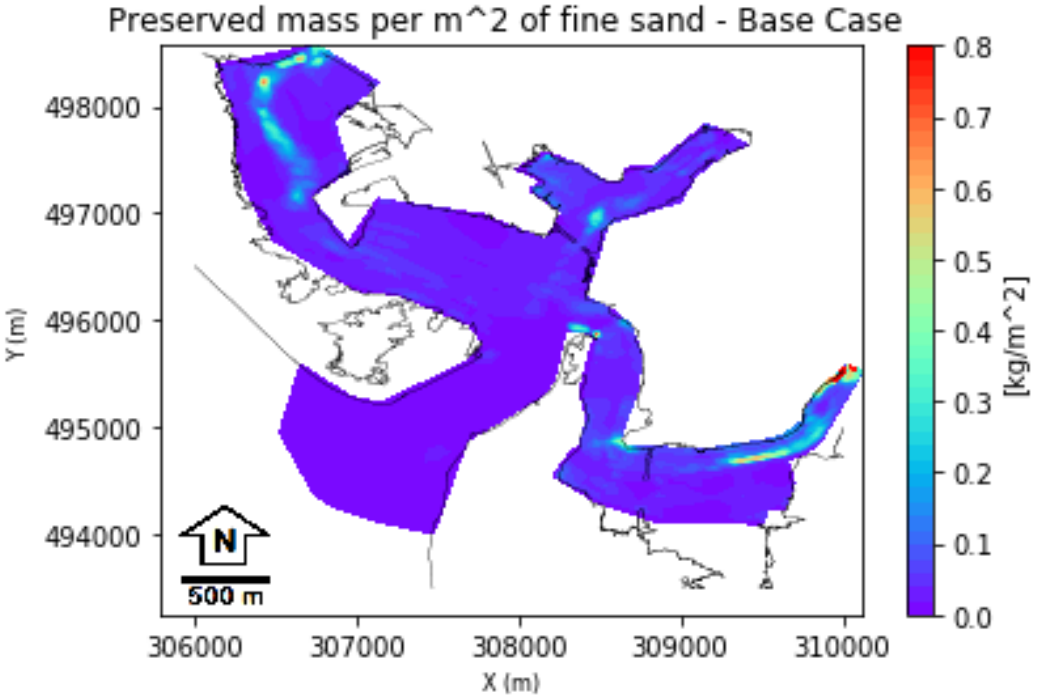

FIGURE 5.1: Deposited mass per m^2 of the fine sand sediment fraction

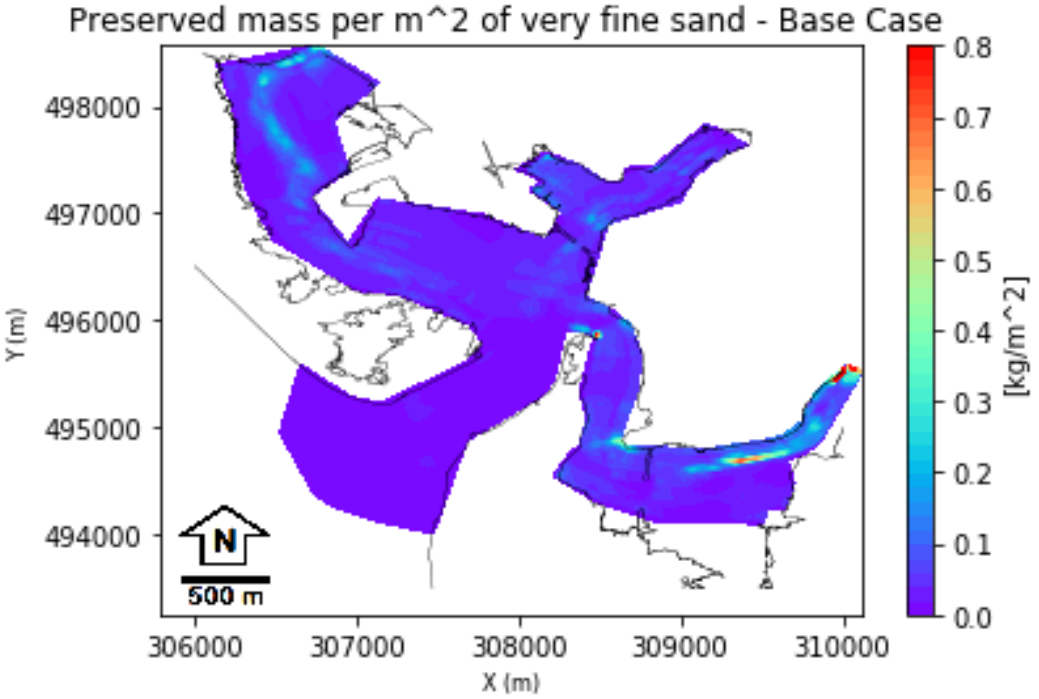

FIGURE 5.2: Deposited mass per m^2 of the very fine sand sediment fraction

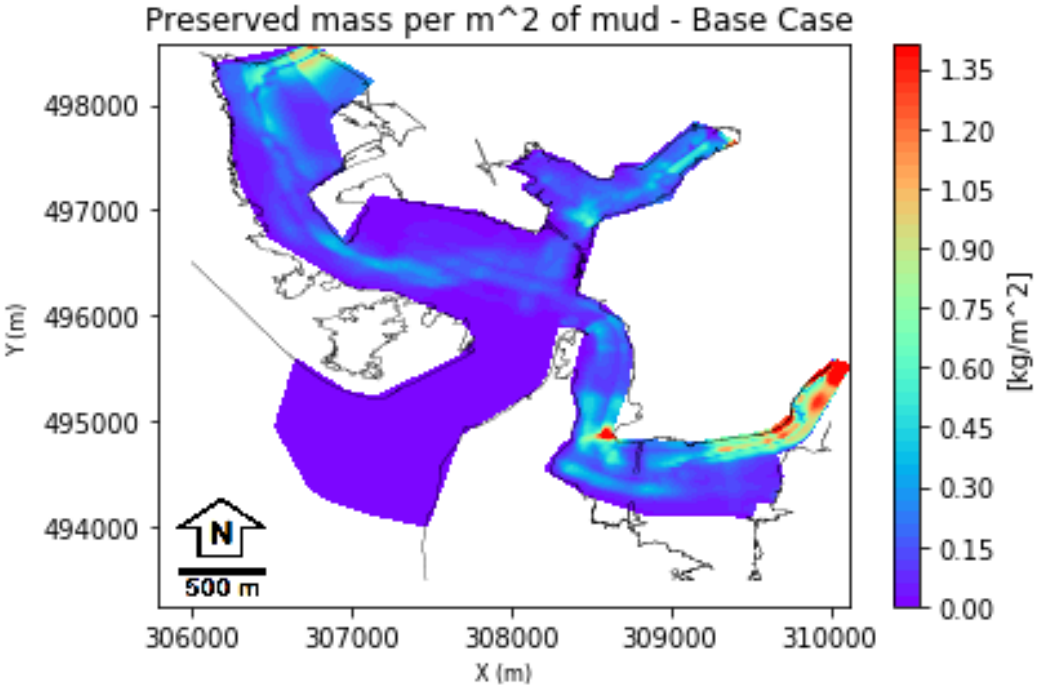

FIGURE 5.3: Deposited mass per m^2 of the mud sediment fraction

5.2 Sensitivity Analysis of the Base Case

5.2.1 Sensitivity Analysis of the Base Case without Waves

The following subsections show the results of the scenario's that were ran. Each subsection includes the relative difference in preserved mass compared to the base case, and the dependency of these changes on

erosion and deposition.

When other figures were needed to interpret the results, these are also shown here.

5.2.1.1 Scenario 1: Higher Mean Sea Level

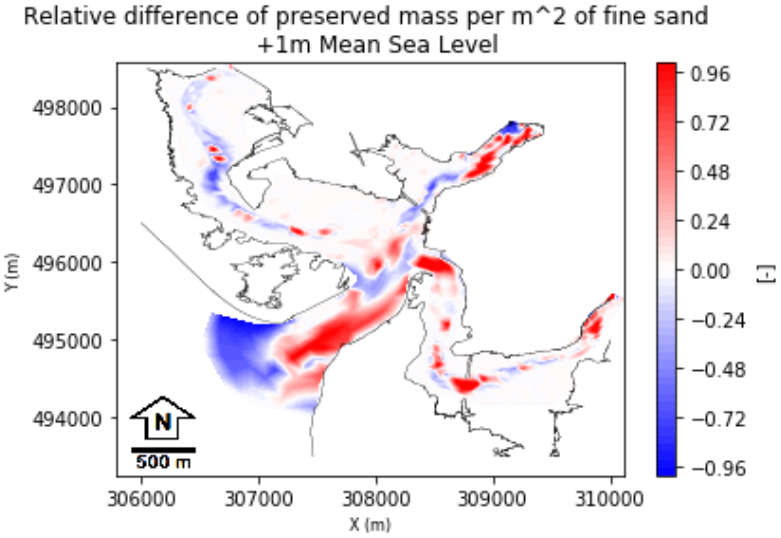

FIGURE 5.4: Relative difference of deposited mass per m^2 of fine sand between the base case and the scenario 'Higher Mean Sea Level' (+1m)

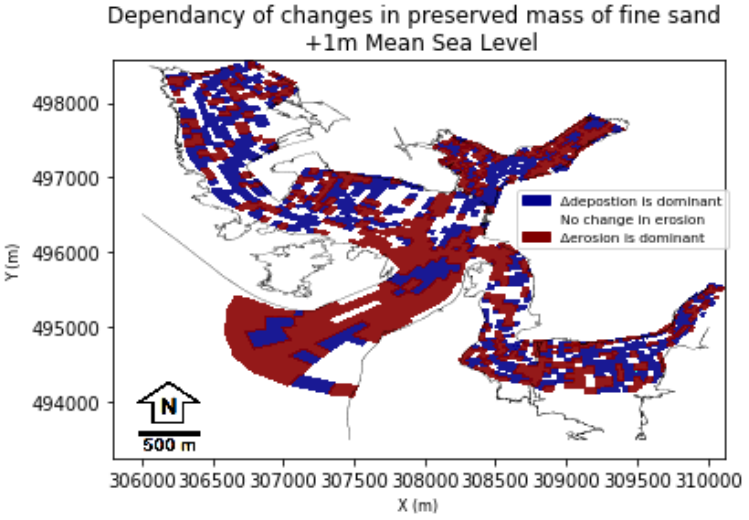

FIGURE 5.5: The dominant factor that results in differences in preserved sediment of fine sand for the scenario 'Higher Mean Sea Level'

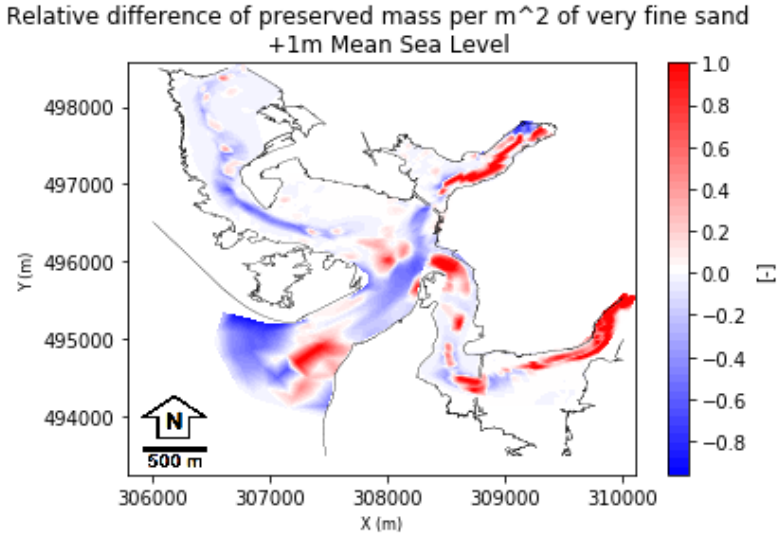

FIGURE 5.6: Relative difference of deposited mass per m^2 of very fine sand between the base case and the scenario 'Higher Mean Sea Level' (+1m)

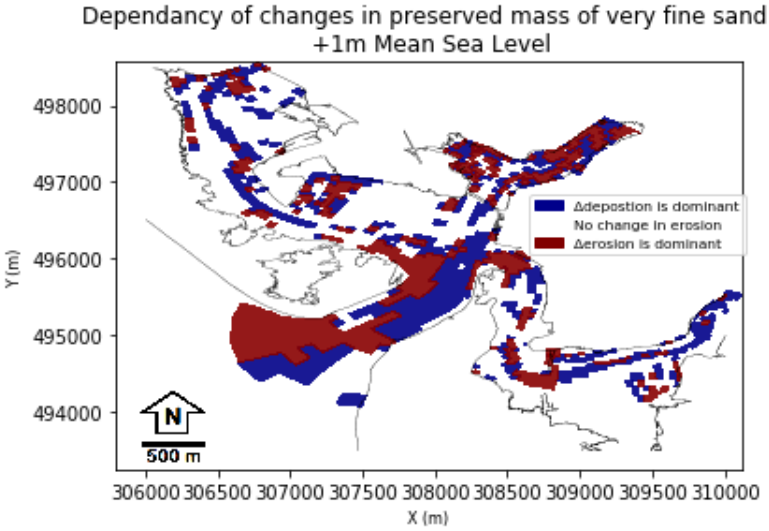

FIGURE 5.7: The dominant factor that results in differences in preserved sediment of very fine sand for the scenario 'Higher Mean Sea Level'

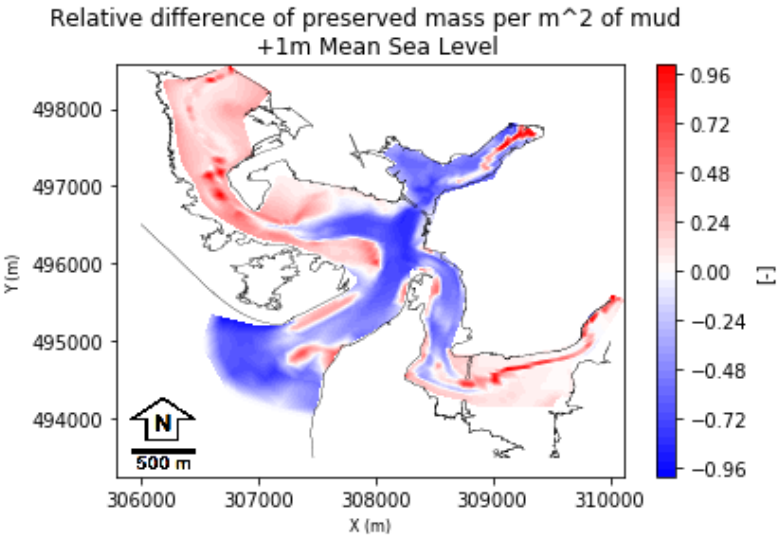

FIGURE 5.8: Relative difference of deposited mass per m^2 of mud between the base case and the scenario 'Higher Mean Sea Level' (+1m)

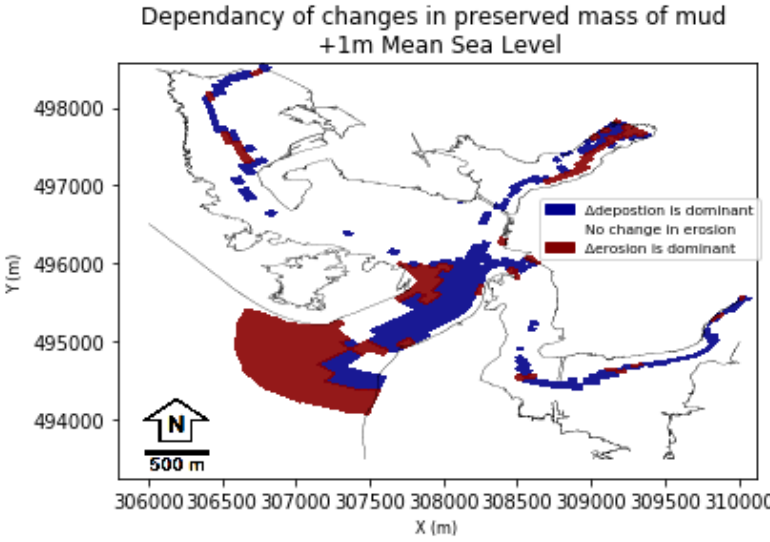

FIGURE 5.9: The dominant factor that results in differences in preserved sediment of mud for the scenario 'Higher Mean Sea Level'

Additional figures

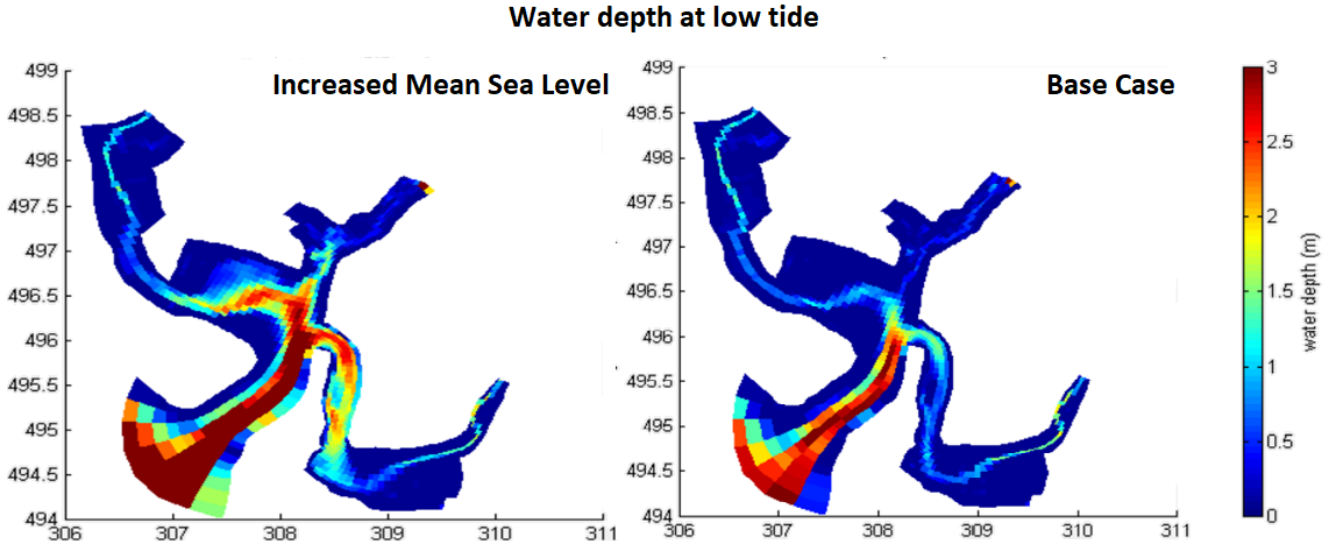

FIGURE 5.10: Water depth at low tide for the scenario 'Higher Mean Sea Level (l) and the Base Case (r)'

5.2.1.2 Scenario 2: Initial Conditions for Sediment

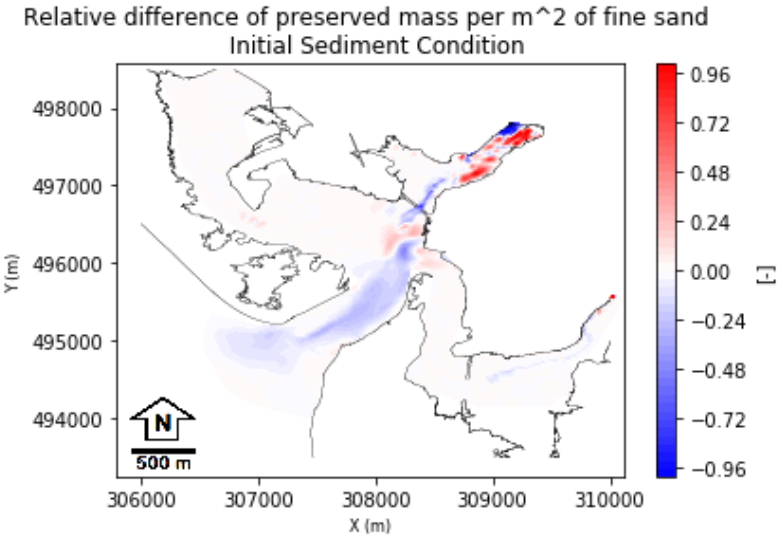

FIGURE 5.11: Relative difference of deposited mass per m^2 of fine sand between the base case and the scenario 'Initial Sediment Condition'

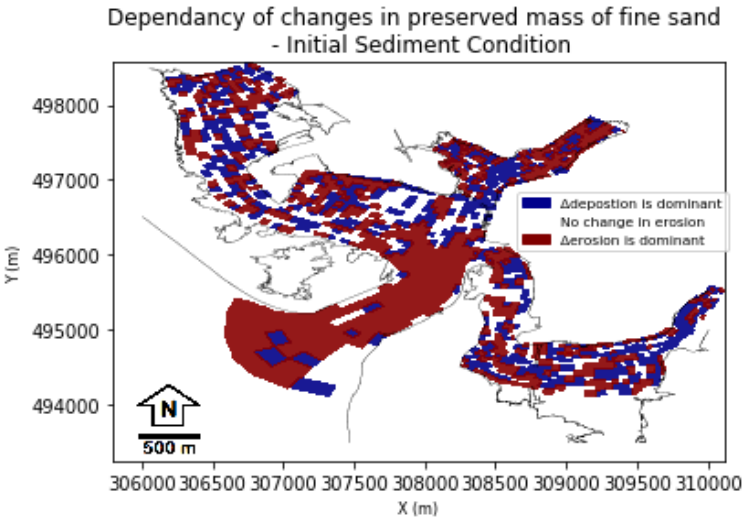

FIGURE 5.12: The dominant factor that results in differences in preserved sediment of fine sand for the scenario 'Initial Sediment Condition'

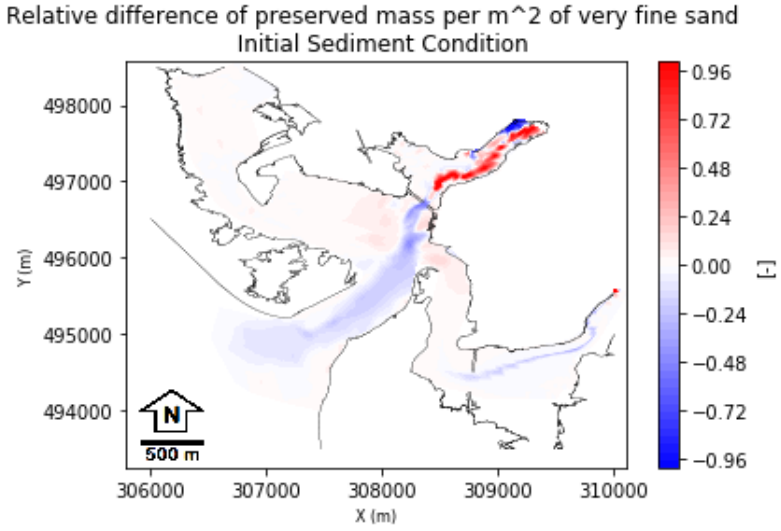

FIGURE 5.13: Relative difference of deposited mass per m^2 of very fine sand between the base case and the scenario 'Initial Sediment Condition'

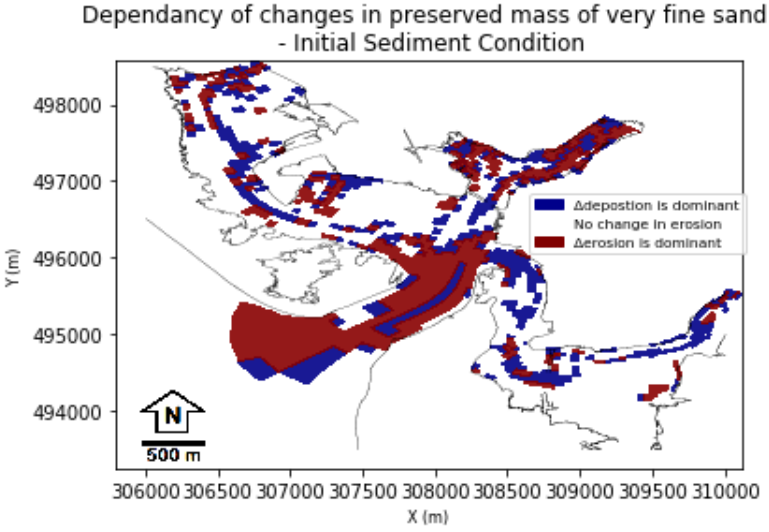

FIGURE 5.14: The dominant factor that results in differences in preserved sediment of very fine sand for the scenario 'Initial Sediment Condition'

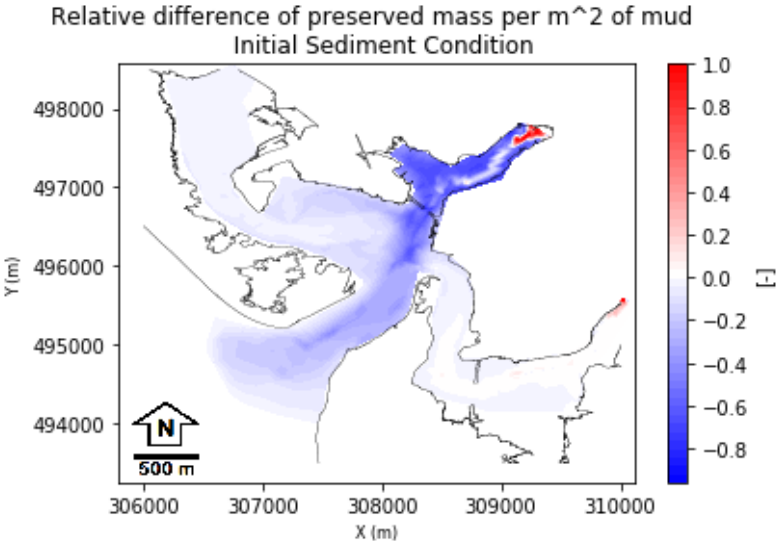

FIGURE 5.15: Relative difference of deposited mass per m^2 of mud between the base case and the scenario 'Initial Sediment Condition'

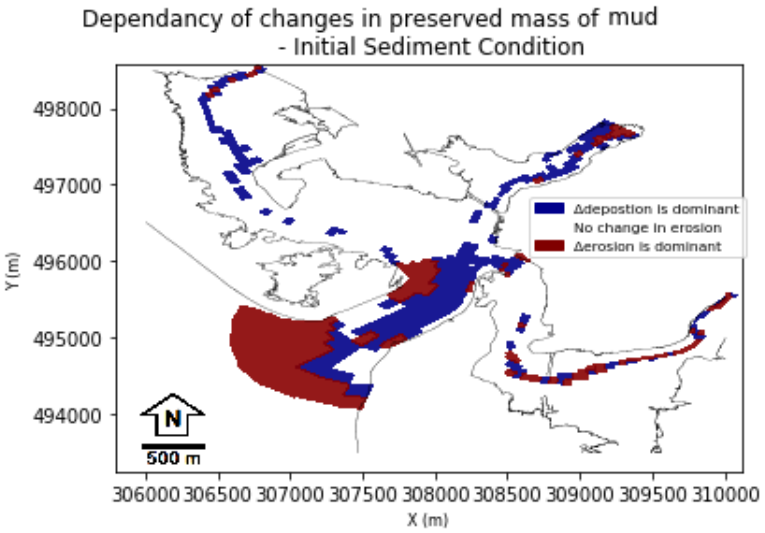

FIGURE 5.16: The dominant factor that results in differences in preserved sediment of mud for the scenario 'Initial Sediment Condition'

Additional figures

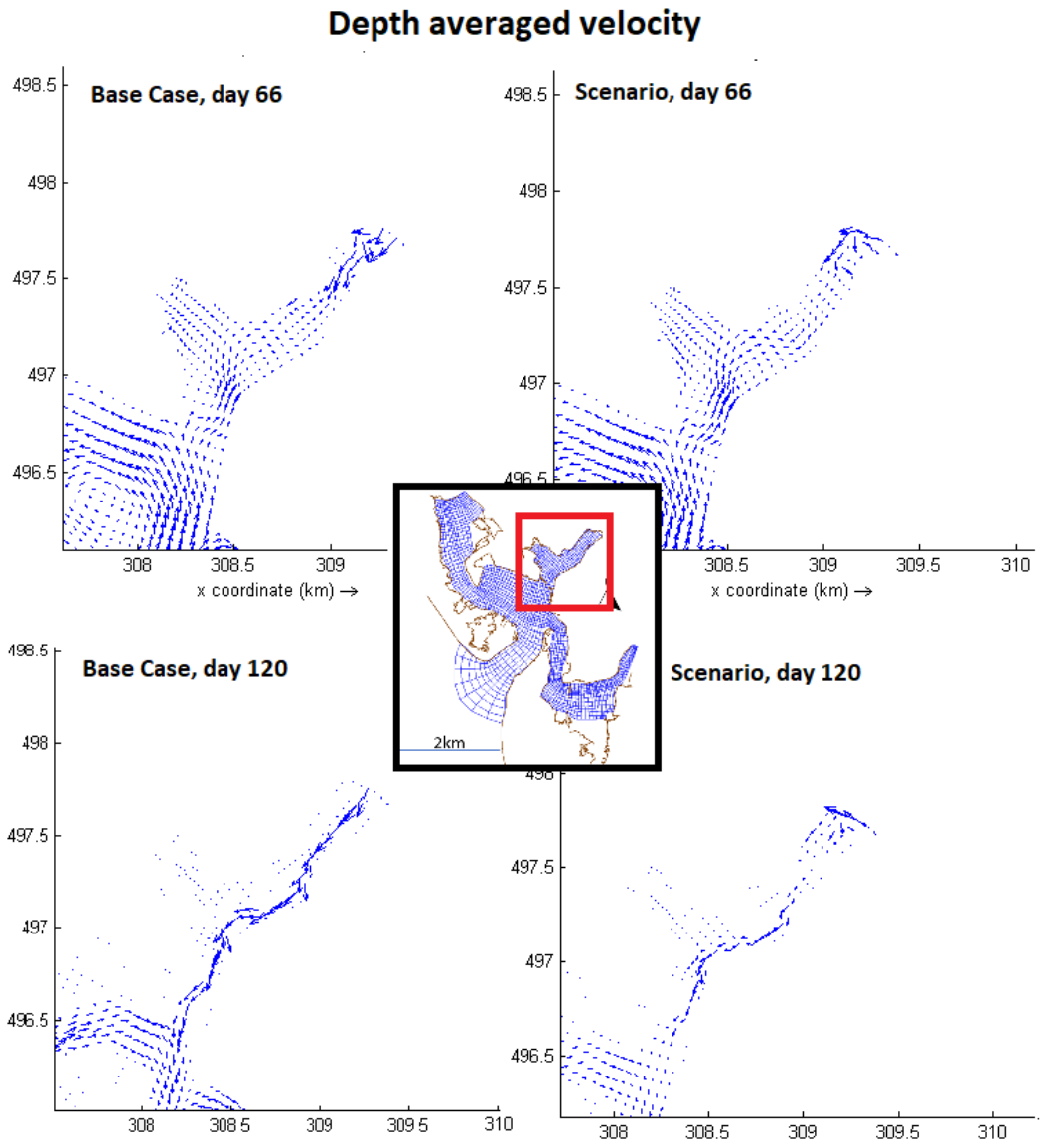

FIGURE 5.17: Comparison of depth-averaged velocities in the Mite-arm of the estuary at two time steps

5.2.1.3 Scenario 3: Increased Horizontal Eddy Viscosity

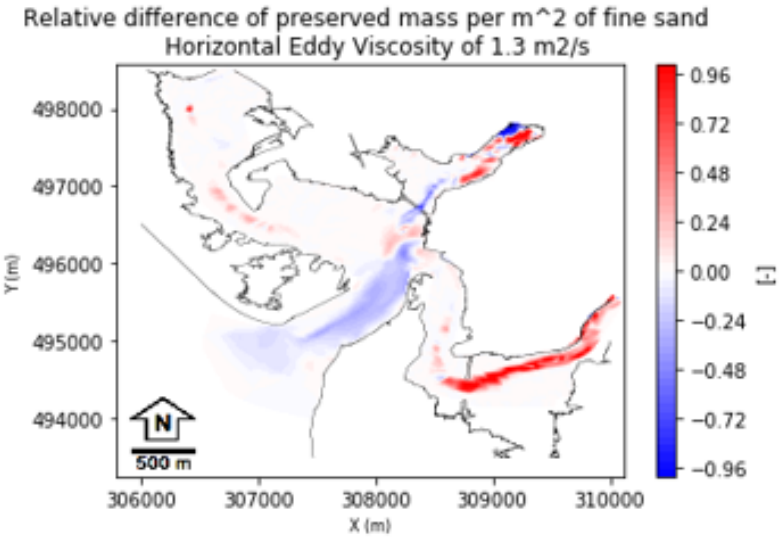

FIGURE 5.18: Relative difference of deposited mass per m^2 of fine sand between the base case and the scenario 'Increased Horizontal Eddy Viscosity'

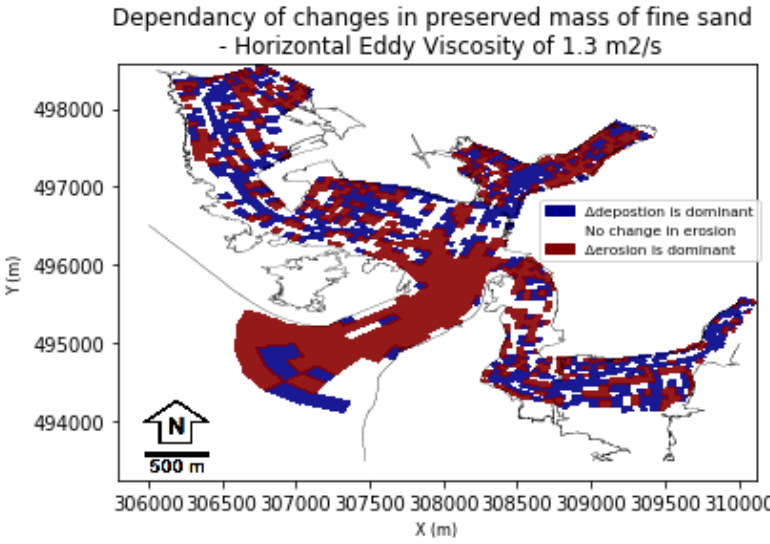

FIGURE 5.19: The dominant factor that results in differences in preserved sediment of fine sand for the scenario 'Increased Horizontal Eddy Viscosity'

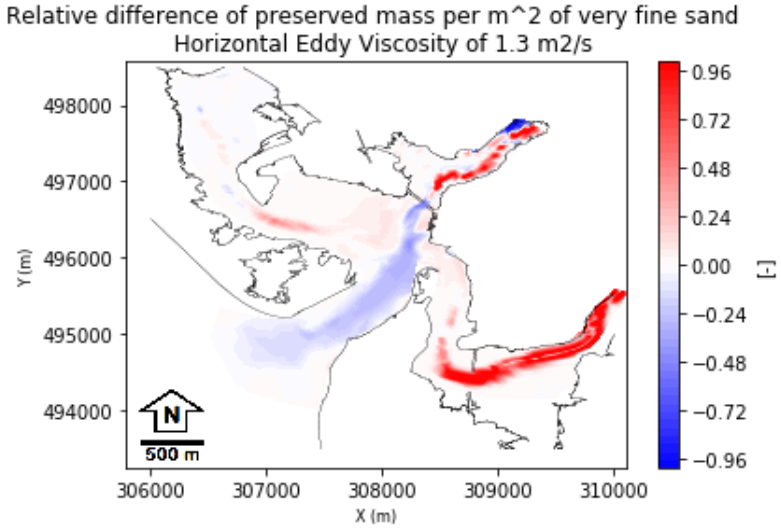

FIGURE 5.20: Relative difference of deposited mass per m^2 of very fine sand between the base case and the scenario "Increased Horizontal Eddy Viscosity'

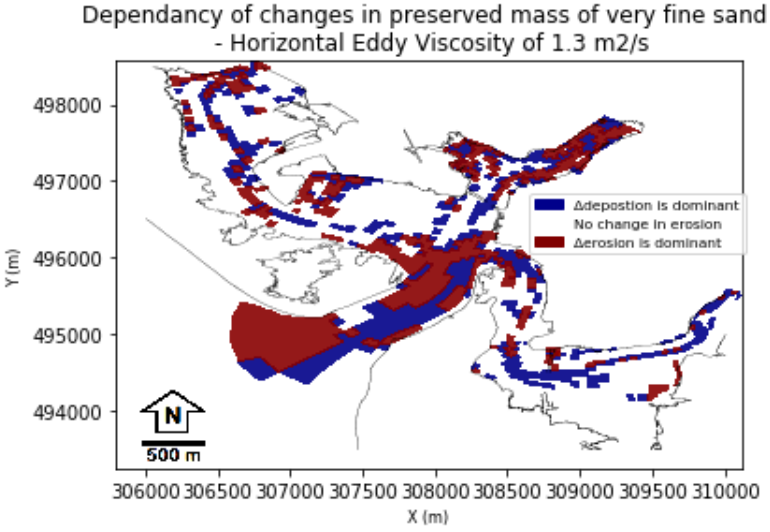

FIGURE 5.21: The dominant factor that results in differences in preserved sediment of very fine sand for the scenario 'Increased Horizontal Eddy Viscosity'

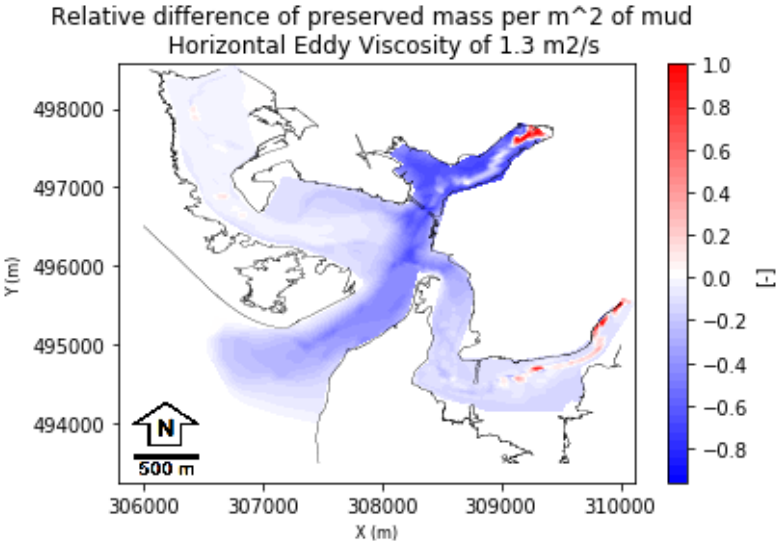

FIGURE 5.22: Relative difference of deposited mass per m^2 of mud between the base case and the scenario 'Increased Horizontal Eddy Viscosity'

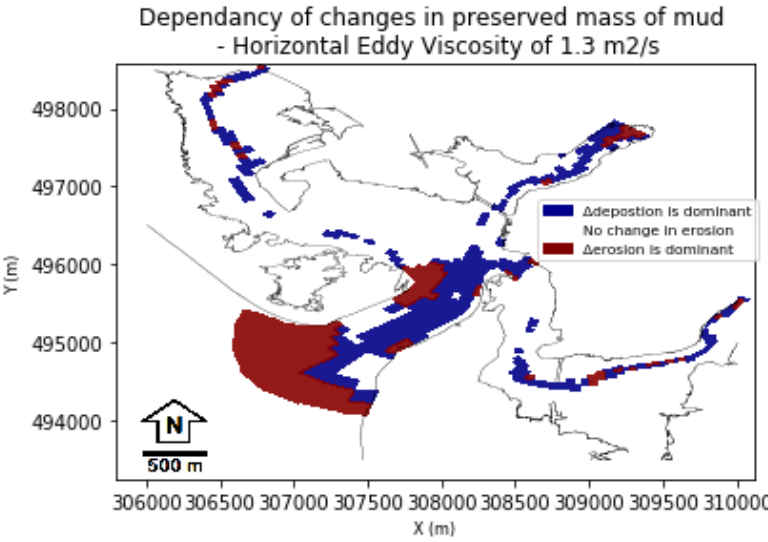

FIGURE 5.23: The dominant factor that results in differences in preserved sediment of mud for the scenario 'Increased Horizontal Eddy Viscosity'

Additional Figures

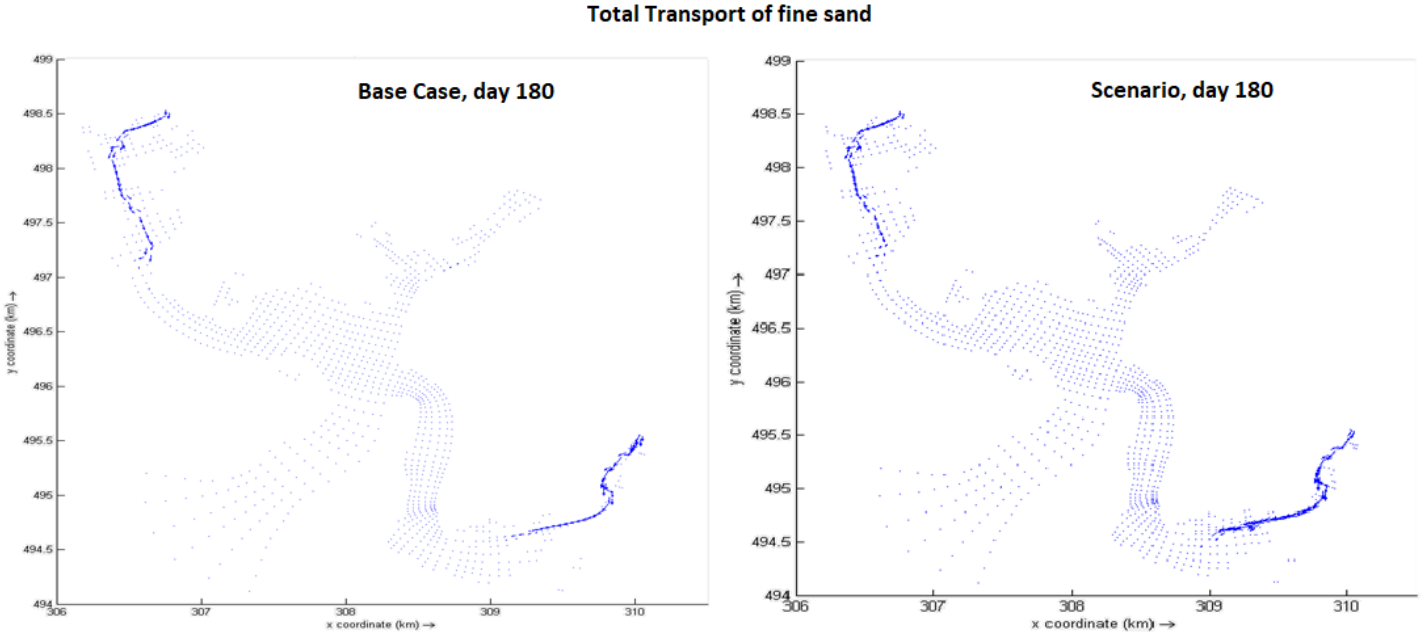

FIGURE 5.24: Comparison of transport of fine sand

5.2.2 Sensitivity analysis of the Base Case with waves

5.2.2.1 Scenario 1: Waves with an orientation of 200°

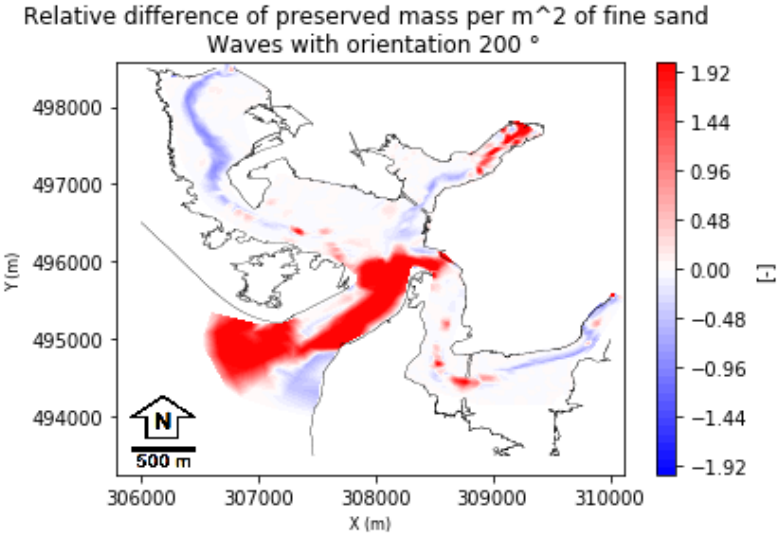

FIGURE 5.25: Relative difference of deposited mass per m^2 of fine sand between the base case and the scenario 'Waves with an orientation of 200°'

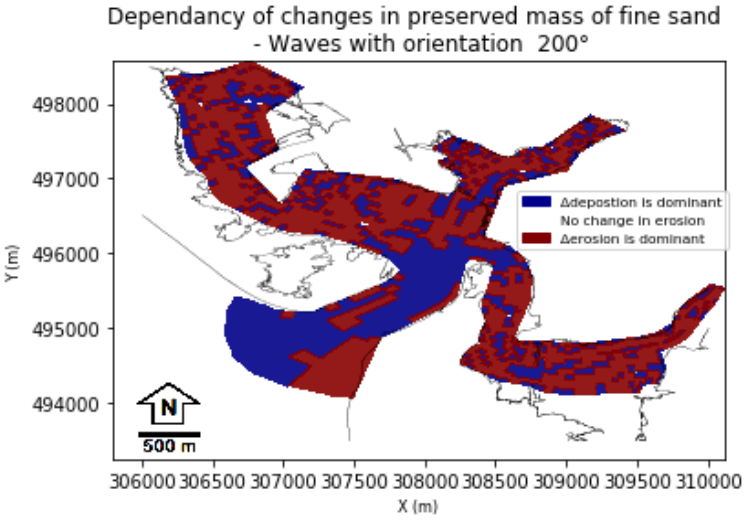

FIGURE 5.26: The dominant factor that results in differences in preserved sediment of fine sand for the scenario 'Waves with an orientation of 200°'

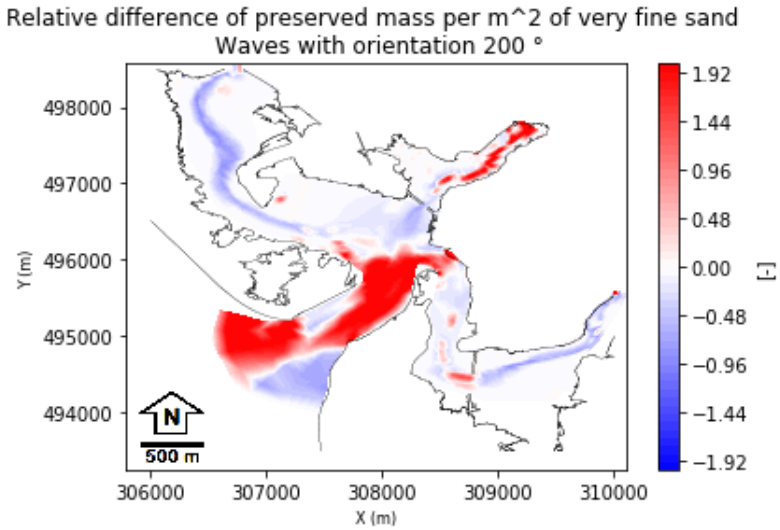

FIGURE 5.27: Relative difference of deposited mass per m^2 of very fine sand between the base case and the scenario 'Waves with an orientation of 200°'

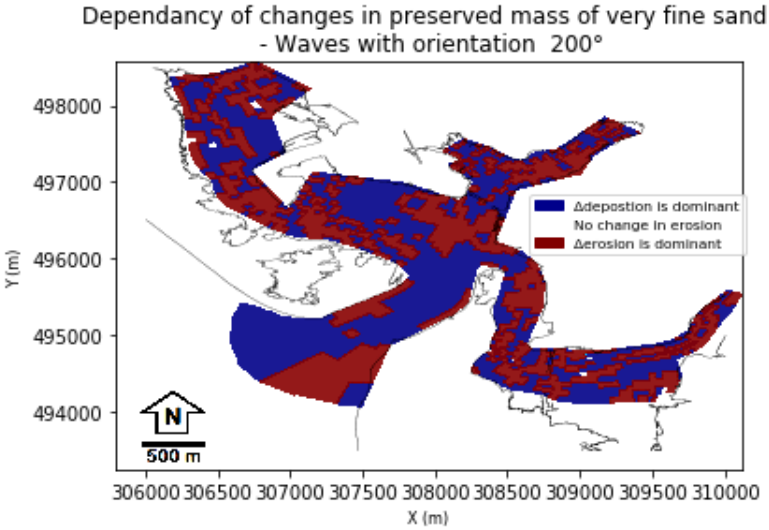

FIGURE 5.28: The dominant factor that results in differences in preserved sediment of very fine sand for the scenario 'Waves with an orientation of 200°'

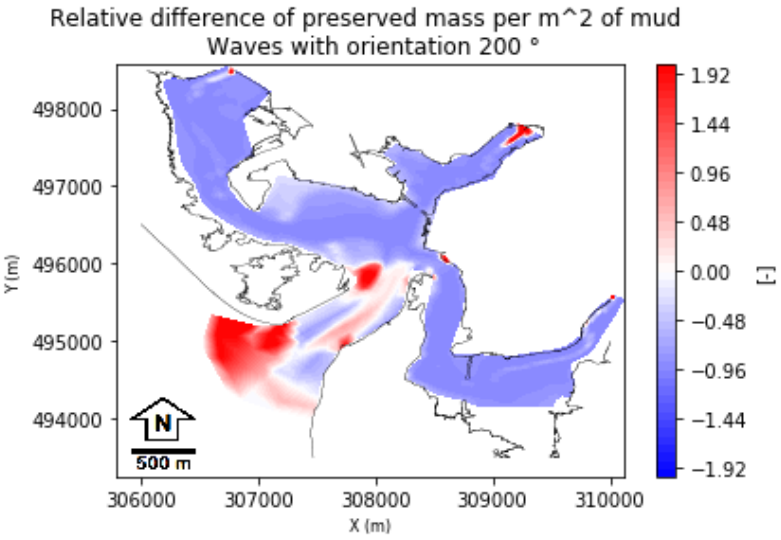

FIGURE 5.29: Relative difference of deposited mass per m^2 of mud between the base case and the scenario 'Waves with an orientation of 200°'

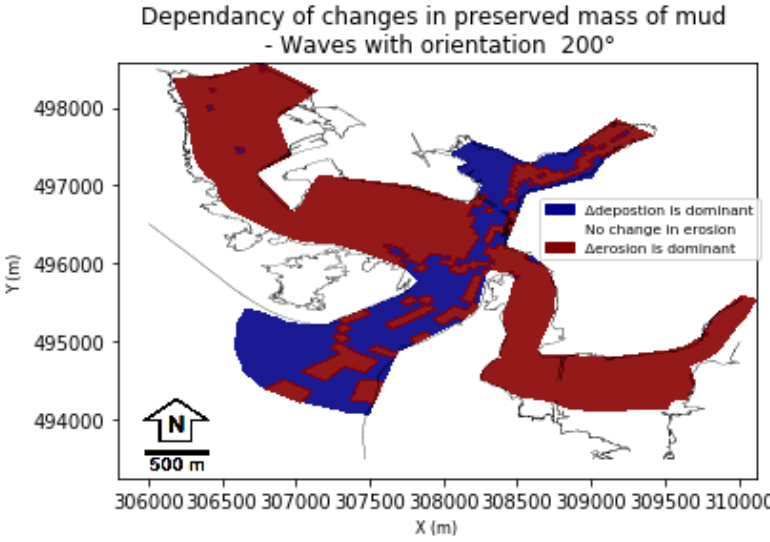

FIGURE 5.30: The dominant factor that results in differences in preserved sediment of mud for the scenario 'Waves with an orientation of 200°'

5.2.2.2 Scenario 2: Waves with an orientation of 230°

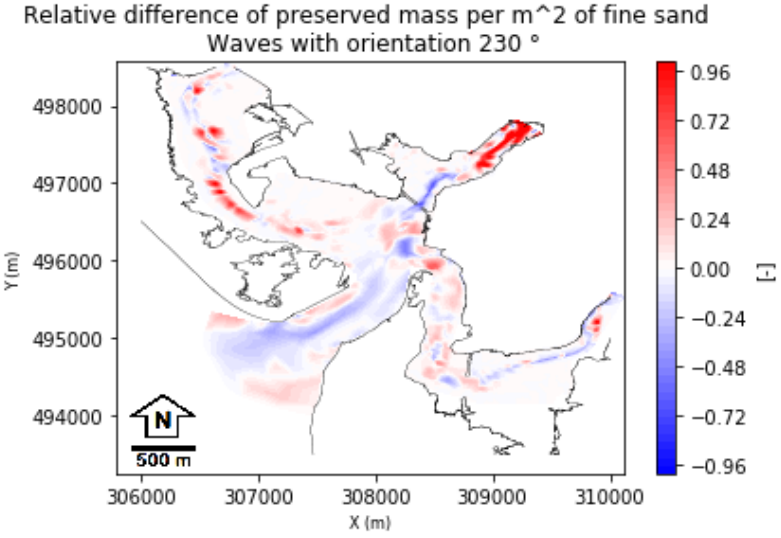

FIGURE 5.31: Relative difference of deposited mass per m^2 of fine sand between the base case and the scenario 'Waves with an orientation of 230°'

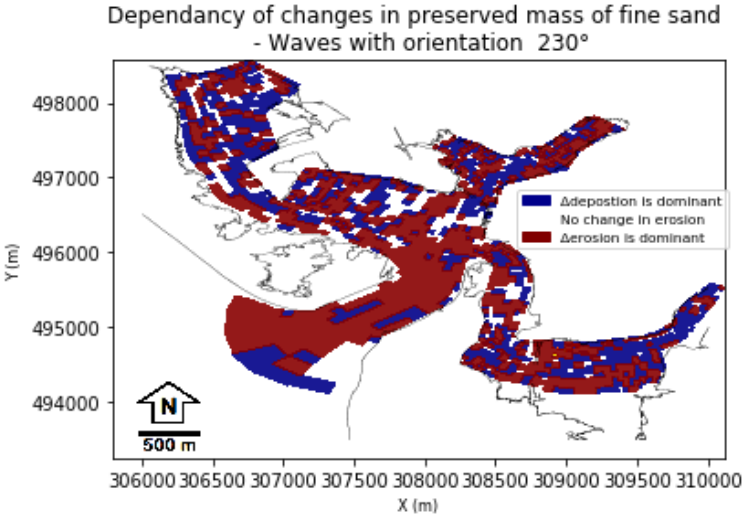

FIGURE 5.32: The dominant factor that results in differences in preserved sediment of fine sand for the scenario 'Waves with an orientation of 230°'

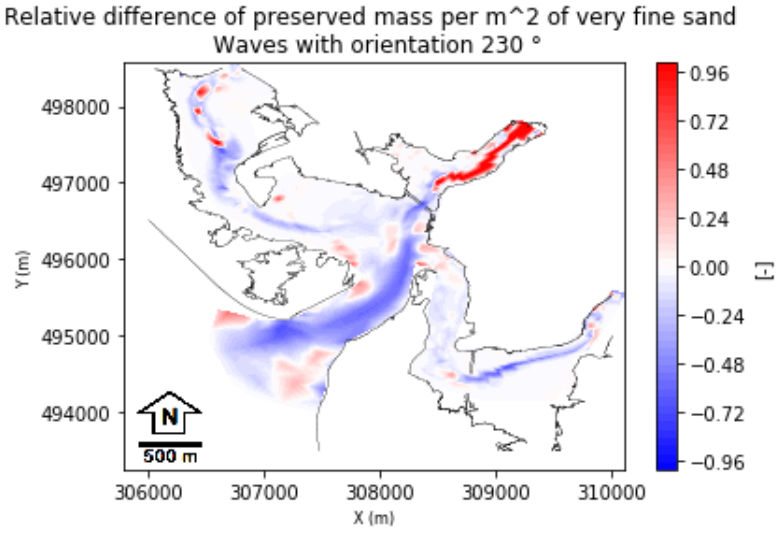

FIGURE 5.33: Relative difference of deposited mass per m^2 of very fine sand between the base case and the scenario 'Waves with an orientation of 230°'

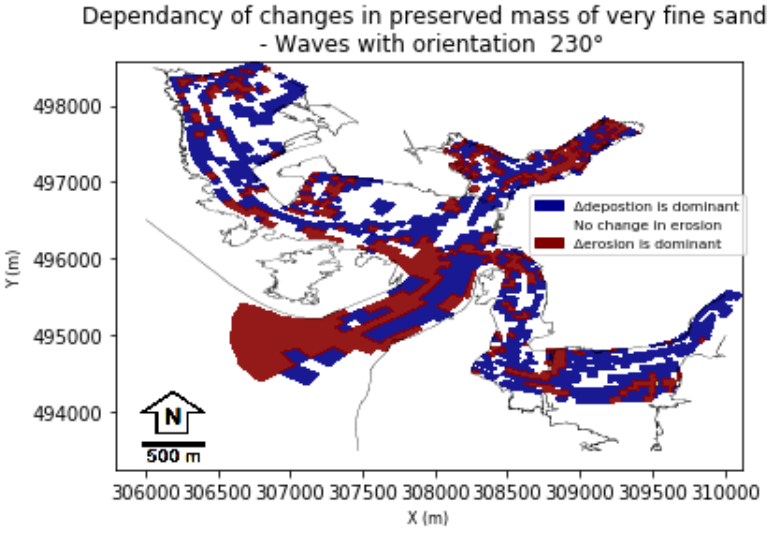

FIGURE 5.34: The dominant factor that results in differences in preserved sediment of very fine sand for the scenario 'Waves with an orientation of 230°'

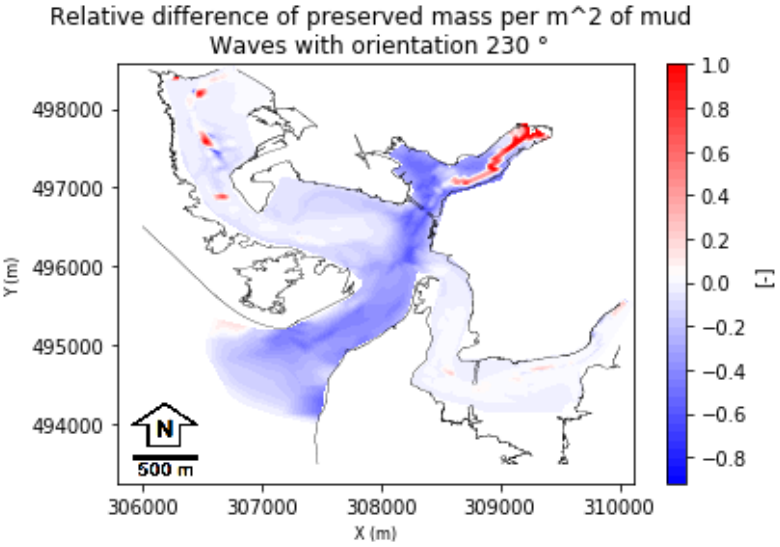

FIGURE 5.35: Relative difference of deposited mass per m^2 of mud between the base case and the scenario 'Waves with an orientation of 230°'

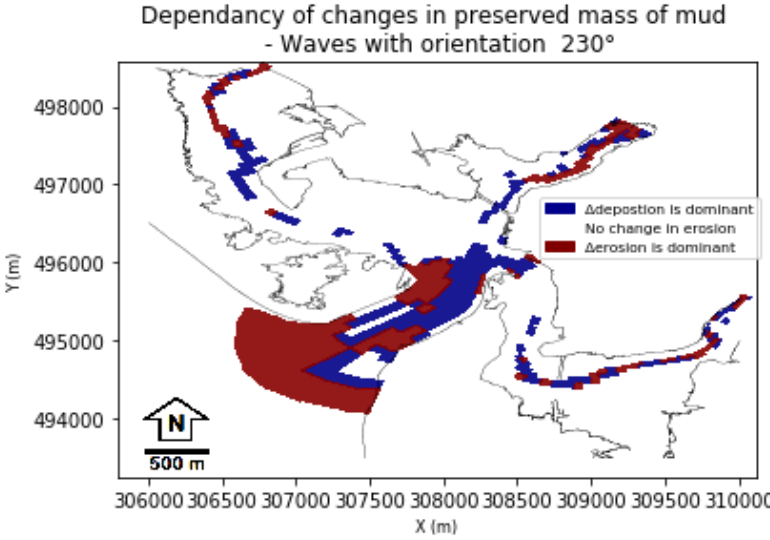

FIGURE 5.36: The dominant factor that results in differences in preserved sediment of mud for the scenario 'Waves with an orientation of 230°'

5.2.2.3 Scenario 3: Waves with an orientation of 260°

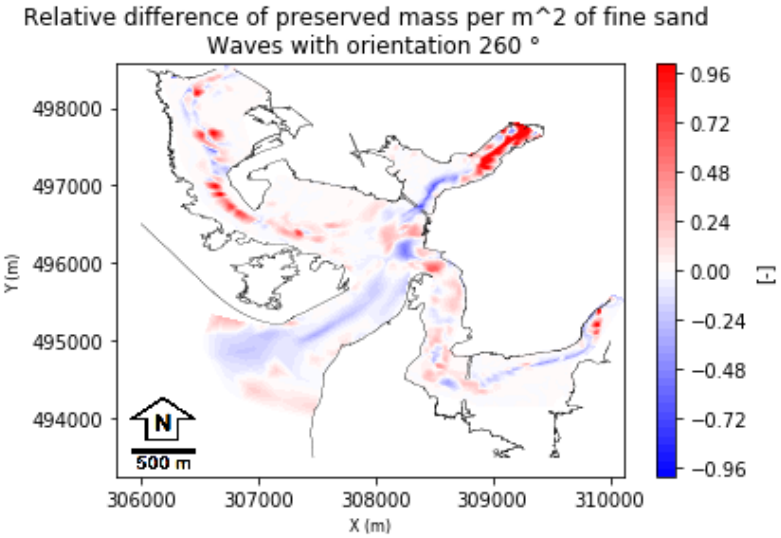

FIGURE 5.37: Relative difference of deposited mass per m^2 of fine sand between the base case and the scenario 'Waves with an orientation of 260°'

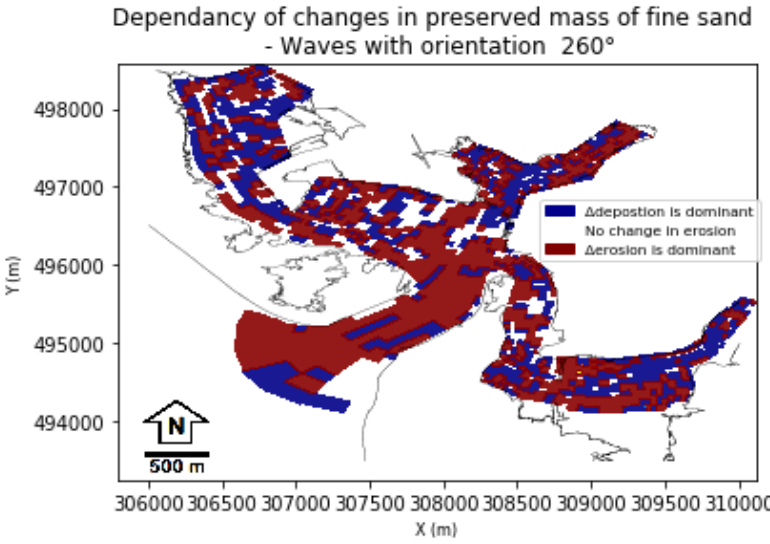

FIGURE 5.38: The dominant factor that results in differences in preserved sediment of fine sand for the scenario 'Waves with an orientation of 260°'

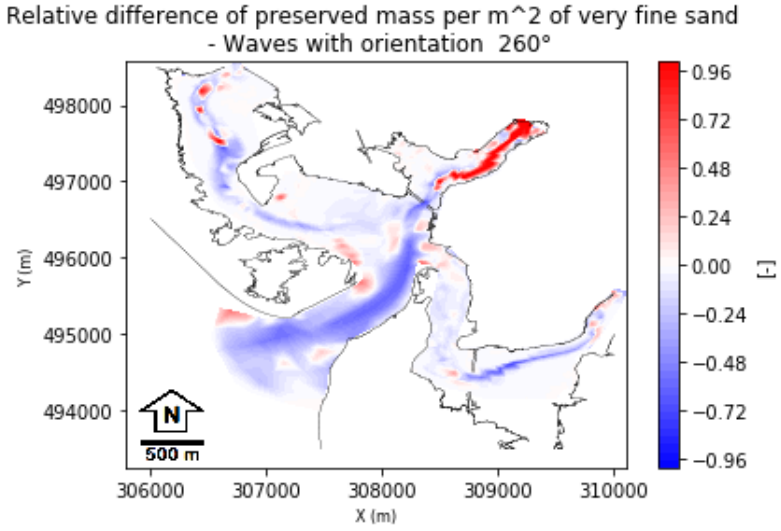

FIGURE 5.39: Relative difference of deposited mass per m^2 of very fine sand between the base case and the scenario 'Waves with an orientation of 260°'

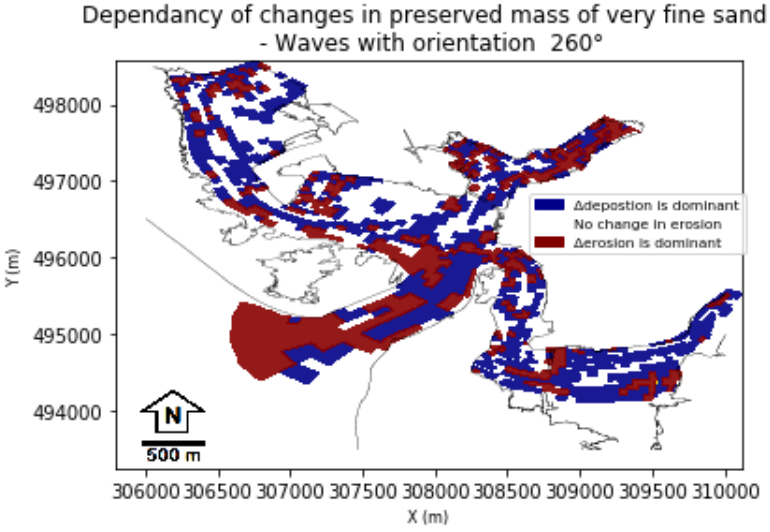

FIGURE 5.40: The dominant factor that results in differences in preserved sediment of very fine sand for the scenario 'Waves with an orientation of 260°

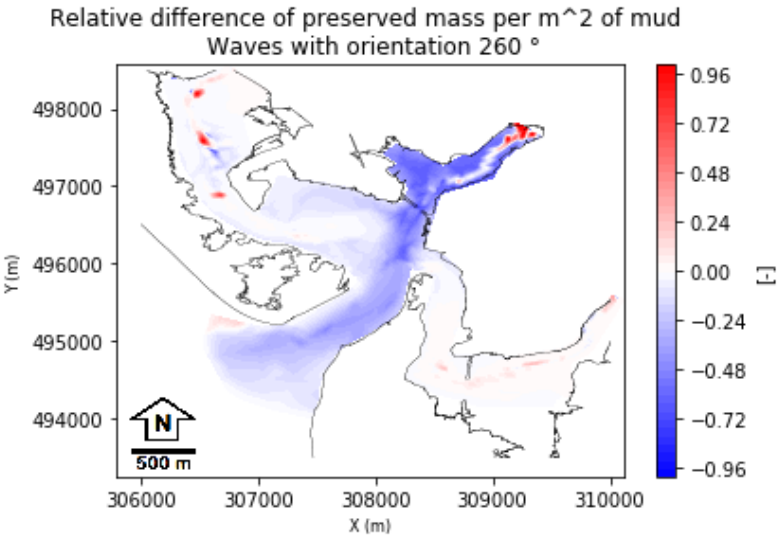

FIGURE 5.41: Relative difference of deposited mass per m^2 of mud between the base case and the scenario 'Waves with an orientation of 260°'

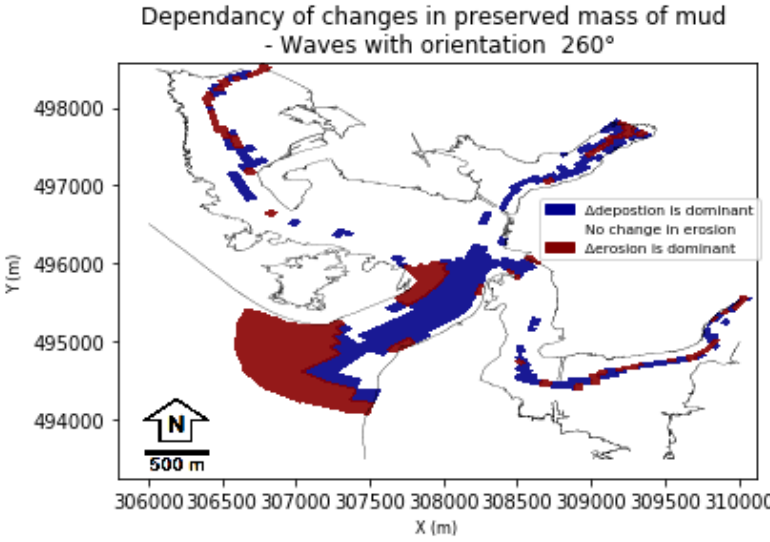

FIGURE 5.42: The dominant factor that results in differences in preserved sediment of mud for the scenario 'Waves with an orientation of 260°

5.3 Clay Mineral Simulations

This chapter depicts the relative mass distribution of the three separate clay minerals which behaviour are approached, as well as total cumulative mass of these three minerals. For the sake of clarity, the relative masses are not plotted on a scale of one to zero to improve the visibility of these small differences.

5.3.1 Clay mineral Simulation 1: Parameters from Literature

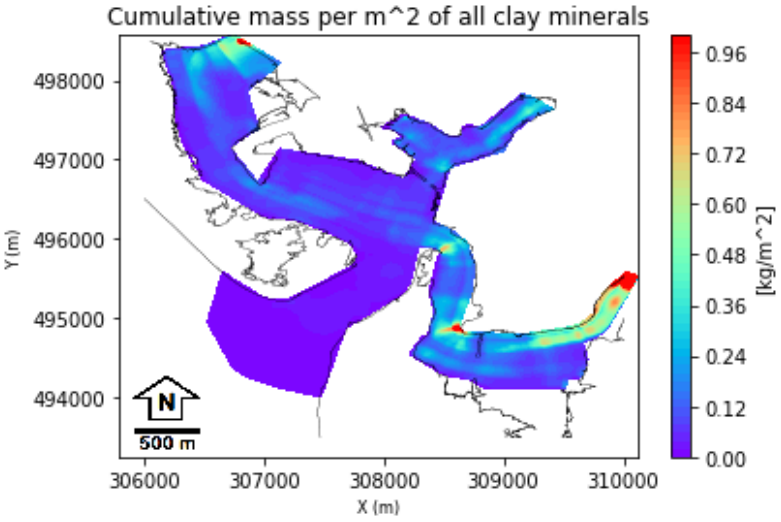

FIGURE 5.43: Total cumulative mass of Chlorite, Illite and Kaolinite

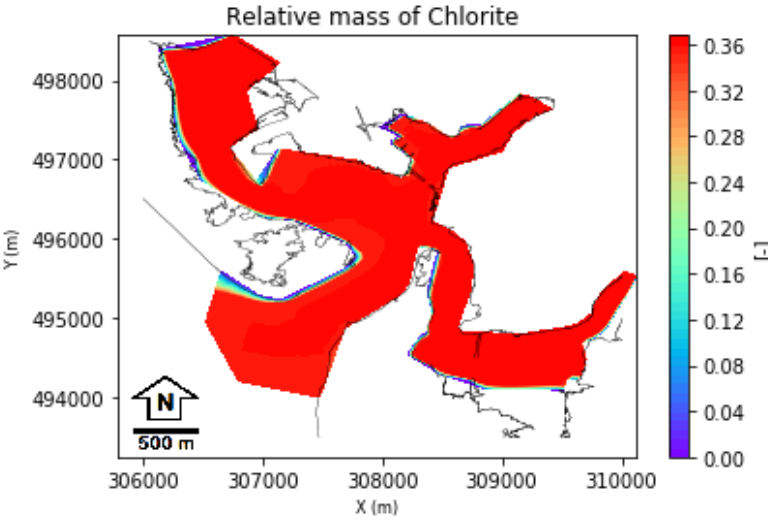

FIGURE 5.44: Relative mass of Chlorite with respect to the total mass of Chlorite, Illite and Kaolinite

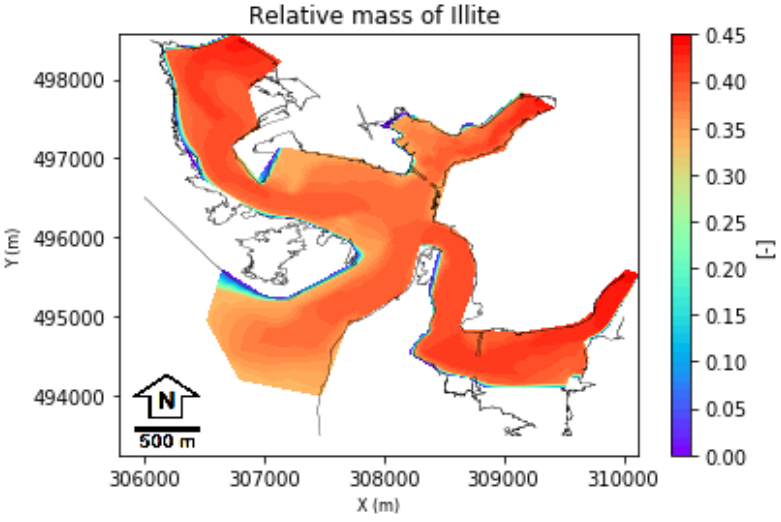

FIGURE 5.45: Relative mass of Illite with respect to the total mass of Chlorite, Illite and Kaolinite

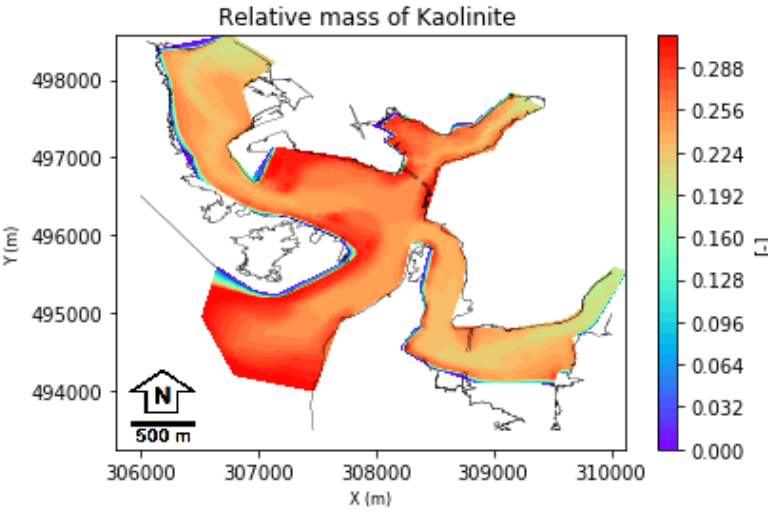

FIGURE 5.46: Relative mass of Kaolinite with respect to the total mass of Chlorite, Illite and Kaolinite

5.3.2 Clay Mineral Simulation 2: Changes in Clay Mineral Density

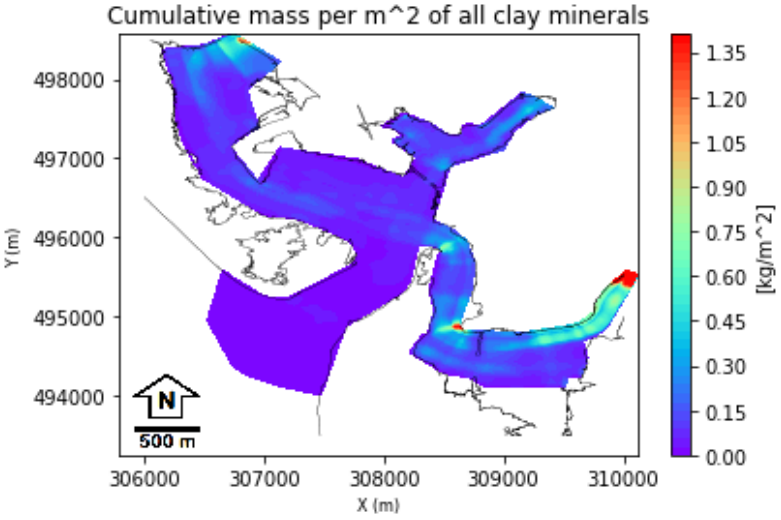

FIGURE 5.47: Total cumulative mass of Chlorite, Illite and Kaolinite

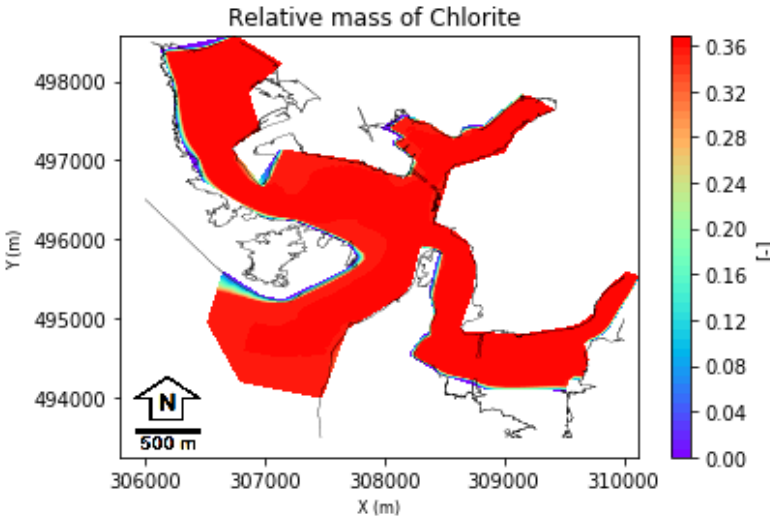

FIGURE 5.48: Relative mass of Chlorite with respect to the total mass of Chlorite, Illite and Kaolinite

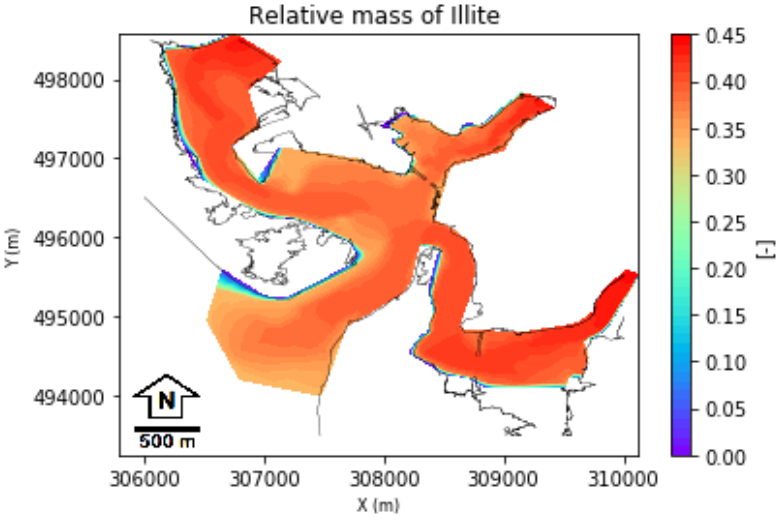

FIGURE 5.49: Relative mass of Illite with respect to the total mass of Chlorite, Illite and Kaolinite

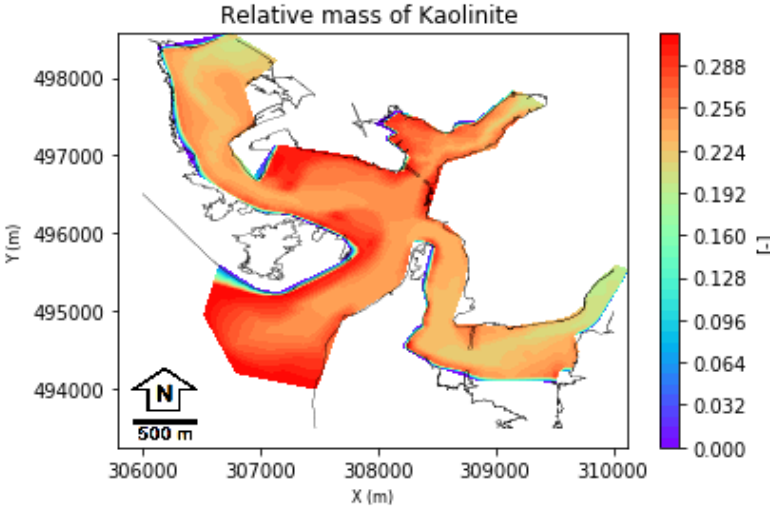

FIGURE 5.50: Relative mass of Kaolinite with respect to the total mass of Chlorite, Illite and Kaolinite

5.3.3 Clay Mineral Simulation 3: Changes in Clay Mineral Fresh and Saline Settling Velocity

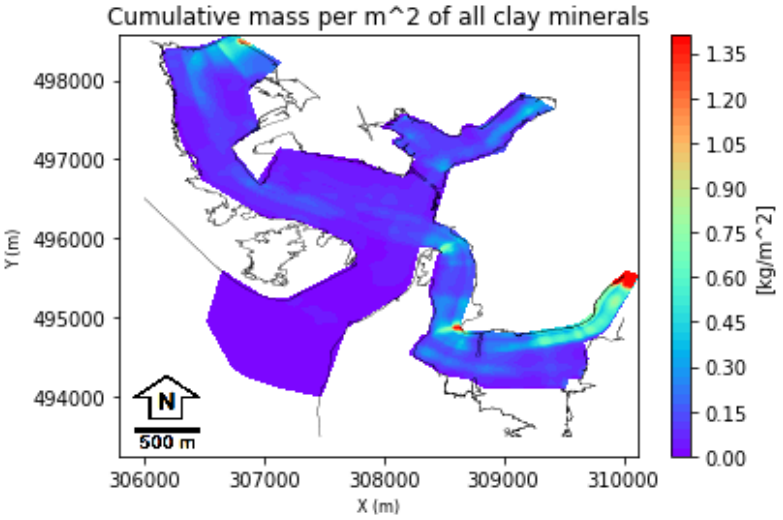

FIGURE 5.51: Total cumulative mass of Chlorite, Illite and Kaolinite

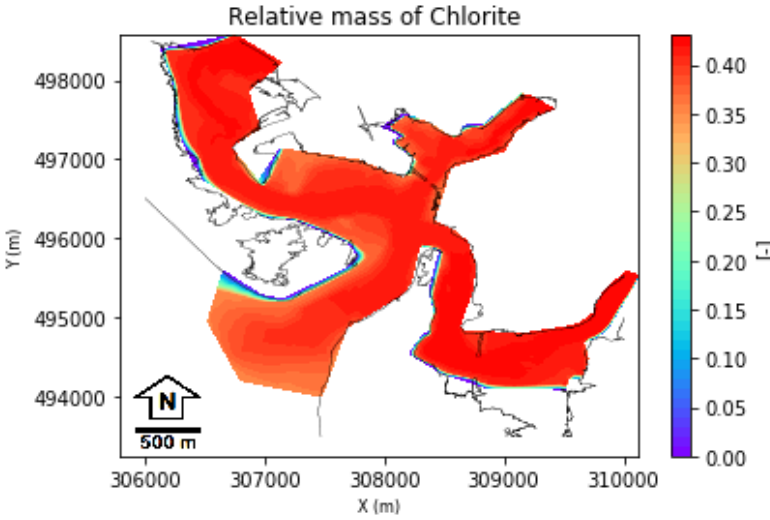

FIGURE 5.52: Relative mass of Chlorite with respect to the total mass of Chlorite, Illite and Kaolinite

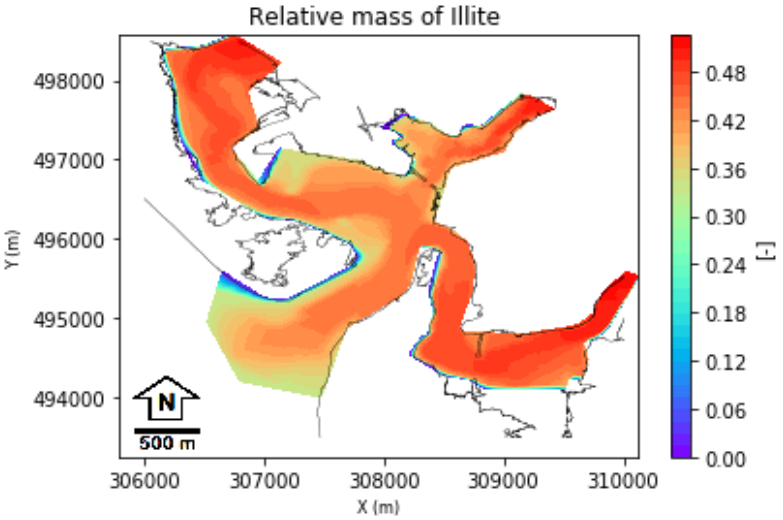

FIGURE 5.53: Relative mass of Illite with respect to the total mass of Chlorite, Illite and Kaolinite

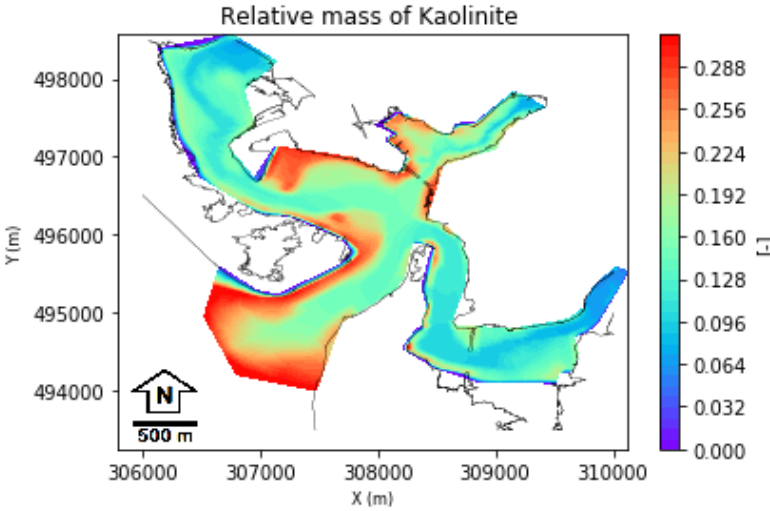

FIGURE 5.54: Relative mass of Kaolinite with respect to the total mass of Chlorite, Illite and Kaolinite

Interpretation

6.1 Base Case

The distribution of the three sediment fractions in the base case follow the trend of heavier sediments being concentrated more in the higher-energy channel. The heaviest sediment - fine sand - is dominantly present in the main channels, this is the clearest in the Irt-arm of the estuary. The very fine sand is slightly less concentrated in the channels, but follows the same general trend. The mud is deposited mostly on the flats next to the main channel, the absence of mud in the main channel is best demonstrated in the Irt-arm of the estuary in figure 5.3. All three sediment fractions are nearly absent in the outer estuary and the inlet, which can be explained by large impact of the tides. In other words, the energy in the area is too high for the material to be deposited.

6.2 Sensitivity Analysis

6.2.1 Sensitivity Analysis of the Base Case without waves

6.2.1.1 Scenario 1: Higher Mean Sea Level

Increasing the mean sea level showed similar changes for both the very fine sand and fine sand fraction. The changes in the Irt-arm of the estuary show a decrease in deposited material, but the quantities are still in the same range. This may be explained by higher flow velocities in the channel, which prevents sand from being deposited in the sediment column. These increases in flow velocities is a logical result of increasing the mean sea level, because the tides are now able to reach further upstream. This is also suggested by the dependency of changes in preserved mass, which show a dominant role for a decrease in deposition in the main channel of the Irt-arm.
The Esk- and Mite arms show area's of increasing mass of the sand fractions, which all coincide with the outside of bends in the channel. When comparing to the initial base case distributions, this might be explained by the fact that little preserved mass is present in these area's in the base case. The area's of increases in preserved sediment for the sand fractions also seem to correlate well with the area's with a

dominant role for deposition, for instance at the lower Esk-arm. This coincides with the influence of the sea at low tide (figure 5.2.1.2), which results in lower flow velocities than that of a un-interrupted river.

The mud distribution shows a decrease in preserved mass in the area's that seem to correlate with area of tidal influence at low tide. This is what one would expect, as the constant moving water won't allow mud to settle. This is also found in previous modeling work by van de Lageweg et al., 2018. Similarly, an increase can be seen in the areas that are only effected by the water at high tide, after which mud has time to be deposited into the sediment column. This is backed up by the fact that a change in deposition is the dominant factor on differences in preserved mud for the bulk of the estuary area.

6.2.1.2 Scenario 2: Initial conditions for sediment

Adding more sediment in the system by applying initial conditions of 3 kg/m^3 for each of the three fractions, results in similar relative differences for fine and very fine sand. The differences in the Esk-arm and inlet are relatively small. The Mite-arm of the estuary shows the largest differences for both sand fractions: an increase in the main channel. This seems to be dominantly caused by a decrease in erosion. Studying the time-series for other flow and transport properties showed no visible differences between the scenario and Base Case for bed shear stresses and available sediment in the water column. One change was noticed in the depth averaged flow velocities in the Mite arm (figure 5.17). Over time, the flow path in the Mite-arm changed due to accumulation of sediment. A change in flow path explains an overall decrease in erosion in the old flow path as found in the results.

The relative difference in deposited mud is negative for almost the entire estuary, where the Mite-arm has a clearly higher decrease than the rest. This is dominantly caused by a decrease in deposition. Referring to the changed flow path and the fact that there is a large sediment accumulation in the upper Mite-arm, the results may suggest that sediment that is fed into the estuary through the Mite-Arm is now deposited in the upper Mite-arm before it can be distributed over the rest of the estuary, resulting in an overall small decrease in preserved sediment.

However, if the addition of initial sediment in the water column results in a large sediment accumulation in the upper Mite-arm, this would also mean that the incoming tide has a tendency to transport more sediment into the Mite-arm. This is supported by the fact that the simulation starts with incoming tide. Unfortunately, it's not possible to study the time-series for transport for this because data is saved in steps of 24 hrs which won't show a single tidal cycle.

6.2.1.3 Scenario 3: Increased Horizontal Eddy viscosity

Increasing the horizontal eddy viscosity, and hence increasing turbulence, results mainly in an increase in the Esk-arm of the estuary for the two sand fractions. The very fine sand to a larger degree than the fine sand. Mud shows a decrease over practically the entire estuary. Physically this makes sense in

comparison to the heavier sand fractions because the deposition of lighter sediment is more dependent on flow properties like bed level turbulence than heavier sediments, which is mainly dependent on gravity and flow velocity. This is also backed up by the fact that an increase in deposition is the dominant factor on changes in preserved mud.

More turbulence makes it easier to transport sand grains, which is illustrated in figure 5.24 in the Esk-arm of the estuary. Other time-series, more specifically, flow velocity and bed shear shear stresses showed no visible changes. More transport through the Esk-arm of the estuary makes more sediment available for deposition, this is backed up by the fact that deposition is the dominant factor on changes in preserved very fine sand in the Esk-arm.

6.2.2 Sensitivity Analysis of the Base Case with waves

6.2.2.1 Scenario 1: Waves with an orientation of 200°

The effect of the waves on sediment distribution extents from the sea all the way upstream to the upper parts of the three rivers. For the two sand fractions, the changes in preserved sediment are mainly located in the main channels and the inlet. A strong correlation can seen between the area's of increased preserved sediment and a dependency on deposition. This is also the area of the estuary that is always covered by water, even at low tide. At 200°, the waves have an optimal orientation to reach into the estuary and interact with the tides. When relating this to the description of the estuary, where the outer estuary, inlet and lower Esk arm show characteristics of wave-dominated estuary's, the area correlates. In other words, the waves seems to have a negative influence on the overall energy level in the area's that are normally wave-dominated (and were tide-dominated in the base case).

Studying of the time-series for flow velocities doesn't show significant changes in the arms of the estuary, where small decreases in preserved sand can be seen. These decreases may result from increased bed shear stresses, as Delft3D superimposed the shear stress induced by waves and by currents. This is backed up by the dominant role of erosion on preserved sediment. Mud shows a strong decreases in most of the estuary, with the exception of the outer estuary and inlet. Similar to the sands, the area's of increased preserved sediment coincides with a dominant role of deposition. Because the deposition of mud is more dependant on bed shear stresses and flow properties relative to sands, the distribution make physical sense when compared.

All three sediment fractions show a strong increase on the western foreshore. This is a similar pattern that is observed in previous studies. To be specific, in chlorite distribution (figure 2.12). This phenomenon was attributed as direct results of the dominant wave direction.

6.2.2.2 Scenario 2: Waves with an orientation of 230°

The changes in preserved sediment for all sediment classes are significantly smaller compared to waves with an orientation of 200°. The results for very fine sand show that decreases in preserved sediment coincide with a dominant role of deposition. Opposite to waves with an orientation of 200°, this distribution supports a situation where waves enhance the effect of tides, creating a area where there is too much energy for sands to be deposited, but restricted to the inlet and the main channels.
The distribution of mud shows an overall decrease in preserved sediment, which is dominantly caused by a decrease in deposition. Similarly to waves with an orientation of 200°, this is largely attributed to the increase of bed shear stresses due to the addition of bed shear stresses resulting from waves, relative to only bed shear stresses resulting from currents.

6.2.2.3 Scenario 3: Waves with an orientation of 260°

The results of this scenario are practically identical to the results of waves with an orientation of 230°. Therefore the same interpretation holds.
The fact that these two scenario's are so extremely similar while the waves with an orientation of 200° show very different characteristics, supports the fact that for the Ravenglass estuary, the specific wave orientation has a strong control on the sediment distribution. In extension, one could argue on a strong role of estuary geometry, as the narrow 200°-oriented inlet is probably the cause of the dependency on wave orientation.

6.3 Clay Mineral Simulations

6.3.1 Clay Mineral Simulation 1: Clay Mineral Properties from Literature

The total cumulative mass of all clay minerals shows an extremely similar distribution to the mud distribution in the base case, while the quantity is lower. This suggests that distribution trends are not strongly governed by settling velocities, which are a factor 10 smaller than the mud in the base case, but may still have a smaller impact. The quantities however, seem to be influenced by the settling velocities. This is backed up by the fact that three times the cohesive sediment being discharged into the system, with overall higher density, results in lower total mass.

When examining the relative masses of chlorite, illite and kaolonite, two particular phenomena stands out. Firstly, the homogeneous distribution of chlorite, while illite and kaolinite show relatively small spatial differences. Secondly, kaolinite shows lower relative masses in the fluvial-dominated area's: upstream where less tidal influence is present and along the main channels. This is opposite to what one would expect, considering the inverse relationship between kaolinite's settling velocity and water salinity. Because chlorite's relative mass is distributed homogeneously, this also implies that illite's relative mass is distributed following the exact opposite trend as kaolinite: larger quantities in area's of a larger fresh

water influence, where settling velocity is expected to be lower.
When comparing the relative masses to present-day clay mineral indexes in the Ravenglass Estuary (Chapter 2.5), chlorite and kaolinite show no similarities between the simulation results and literature data. Illite however, shows a similar trend where there is a small increase from the estuary inlet towards the estuary arms further upstream. The abundance in the outer estuary however, is not found in the simulation results.

6.3.2 Clay Mineral Simulation 2: Changes in Clay Mineral Density

The results of this simulation show identical trends in distribution of relative masses of chlorite, illite and kaolinite, as well as total cumulative mass of all clay minerals when compared to the results of with clay mineral properties from literature. To only difference seems to be the total quantity of mass, which is higher but still of a similar order.
This suggests that cohesive sediment density is not a governing factor in distribution trends, but contributes to the quantity of deposited mass.
Because of the extremely similar results, the interpretation as stated in chapter 6.3.1 also holds here.

6.3.3 Clay Mineral Simulation 3: Changes in Clay Mineral Fresh and Saline Settling Velocity

Changing the ratio between the fresh and saline settling velocities for each of the clay mineral classes results in a distribution in total cumulative mass of the three clay minerals that is once again extremely similar to results of the base case and the other clay mineral mineral simulations.
The relative mass distribution of chlorite shows a small degree of heterogeneity in this simulation, with a very small decrease at the inner estuary mudflat, inlet, and outer estuary.
Illite and kaolinite show distributions in relative mass that have the same trend as previous results, but seem exaggerated. This suggests that settling velocity has large impact on clay mineral distribution trends, but changes won't result into an entirely different distribution pattern. In addition, the trends that are found in the simulation results are more general, larger scale trends than the distribution patterns that are found in the present day Ravenglass Estuary. For instance, trends on the scale of depositional facies or even individual bars or flats.

Discussion

7.1 Sensitivity Analysis

While the results of the sensitivity analysis, for both the base case with and without waves, can be physically explained and show similar characteristics with the real-life situation, the question rises to what extend these can be used to answer the research questions.

First of all, this study has made a lot of assumptions and simplifications in order to create the base case. The main simplifications are: i) using the mean tidal range of 5 m while the present-day situation has a neap tidal range of 2.5 m and a spring tidal range of 8 and ii) using constant river discharges (both water and sediment). Estuarine hydrodynamics are in principle governed by the interaction between tides, waves and river discharge. The latter of which the Ravenglass estuary has three of. Therefore, hard conclusions on the specific controls on sediment distribution should be drawn with caution. However, it does allow for the studying of more general trends.

The fact that on the relatively short timescale of 6 months enough sediment accumulated in certain spots to (slightly) alter the flow path suggest that in hindsight, the sediment discharges were too high. For this study, the effect seems minimal. More generally speaking, this has two effects. Firstly, this can create a situation where it is very hard for a sedimentary system to reach a state of equilibrium. A result of large sediment accumulation that changes the flow paths in the system, which quickly results in large accumulations in other locations that in turn again changes the flow path and vice versa. Note that the Ravenglass Estuary is especially sensitive to this as it is a very shallow estuary that dominantly transports sediment through narrow channels. Secondly, it is more difficult to distill the effect of a single parameter when not only the hydrodynamic changes are applied, but also secondary morphological changes occur.

Tidal cycles happen on a timescale of 6-7 hours while the data in this study is saved in steps of 24 hours. In other words, effects of individual tidal cycles on sediment deposition and erosion is not captured in the data. This also means there is a small error in the computation of the total erosion, which is used when determining the dependency of changes in preserved sediment. Decreasing the time step the data is saved will give more information on tidal cycles and the interaction of tides with river discharges and waves.

The sensitivity analysis of the base case without waves shows that the model is very sensitive to small changes, supported by the fact that all three scenario's show area's with double the amount of preserved sediment on a simulated period of only 6 months. Again underlining the remark that conclusion should be drawn on trends in deposition instead of exact locations. The analysis also shows that distribution patterns can be explained by the energy levels in the estuary as caused by the tidal-fluvial interaction.

The sensitivity analysis of the base case with waves show that the orientation of the waves has a strong influence on sediment distribution. The waves with an orientation of 200°, the dominant direction in the present-day estuary, show characteristics that approach the present day situation best. This in turn is a direct result of the estuary geometry. However, erosion plays a strong role on the distribution for mud in this scenario, which is highly probable to behave the most similar to the clay minerals. This should be kept in mind when interpreting the results for the clay minerals simulations, as these do not include erosion and reworking.

7.2 Clay Mineral Simulations

On first glance, the simulation results suggest that density has an effect on the quantity of deposited material, and no clear effect on the relative masses. However, one might assume that if the relative mass of a sediment fraction doesn't change while the density has increased, relatively more sediment has been deposited. While this might seem intuitive, it is not correct due to the way Delft3D computes deposition from the water column to the sediment column. From equation 3.2 it follows that the deposition flux is already calculated in terms of mass, not volume. This flux in turn is dependant on (total) sediment concentration in the water column and settling velocities. Because settling velocity doesn't change in simulation 2, this increased deposition is a result of sediment concentration. This in turn, is again influenced by sediment density.

Compared to the results of the base case, it makes sense to expect higher quantities of cohesive sediment because the concentrations of cohesive sediment input through the rivers is three times as high. This might be explained by the fact that the sand sediment classes from the base case are transport dominantly through bedload transport. In other words, compared to cohesive sediment the higher concentration will occur in the bottommost computation layer, the same layer where deposition is calculated.
The simulation results show clear differences in distribution pattern of the relative masses of illite and chlorite after the change in settling velocities. The distribution pattern has not been changed characteristically; one might describe the trend over the entire estuary in the same manner for both simulation. The change might be better described as an exaggeration of this same trend.

At the same time, the change in settling velocities also resulted in an increase in the quantity of deposited mass. This is attributed to chlorite and illite, as both show an overall relative increase in mass. This coincides with the two clay minerals that increased their saline settling velocity, whereas kaolinite had it lower compared to the first simulation. This makes logical sense as the marine influx of salt water into the estuary is significantly larger than the fresh fluvial water. It does, however, not fully explain the

trend of increased deposited clay in area's of more fluvial influence for illite. And the opposite for kaolinite.

Instead of only the saline fresh settling velocity, it might also be possible that the ratio of fresh- to saline settling velocity is the most important control on distribution. This connects several suggested controls on literature: i) the ratio of fluvial-marine currents (Dowey, 2012), and ii) the physical characteristics of different clay minerals (Dowey, 2012), which is the origin of their flocculation-behaviour. This also may explain why the observed trends from the simulation-results are counter-intuitive.

The fact that the distribution pattern of the clay minerals hardly change relative to the mud distribution in the base case, also suggests that erosion and reworking is not a strong control on distribution, which was not a part of these simulation. This is backed up by the fact that the total quantity decreased, while a lack of erosion, which was was observed to be present but not a dominant factor in the sensitivity analysis, per definition cant lead to a decrease in deposited sediment.

7.3 Approximation of Clay Mineral Behaviour by Cohesive Sediment in Delft3D

The distribution of both the mud in the sensitivity analysis and the clay minerals in the clay mineral simulation follow the same distribution pattern. This pattern shows similarities to the distribution of the percentage of clay fraction in the present-day Ravenglass estuary (figure 2.10).
The very heterogeneous distribution of a subgroup of this clay fraction, the clay minerals chlorite, illite and kaolinite, seems to be not even close to being recreated using modeling in Delft3D. The clay mineral behaviour in this study is approached with only three physical parameters: density, saline settling velocity and fresh settling velocity. Studying the differences when changing these parameters does not suggest that more complex distribution patterns can be created in Delft3D, or that the distribution pattern may change significantly from a 'default' cohesive sediment fraction.

In addition, there are three other parameters that influence the distribution of a cohesive sediment in Delft3D: critical shear stress for erosion, critical shear stress for sedimentation and the sediment erosion rate. While the critical shear stress for erosion was increased from 0.5 N/m^2 for mud in the sensitivity analysis to 100 N/m^2 in the clay mineral simulation, the results do not suggest a large effect of this parameter on the distribution. Critical shear stress for sedimentation has been constant for all cohesive sediment in this study. It is possible that this parameter has a profound impact on the distribution pattern, although no results suggest that. In the hypothetical scenario that this is the case, this would come with additional complications as it was suggested that this parameter doesn't or might not exist and is difficult or impossible to obtain (van Maren, 2009), (Shi et al., 2015). Therefore it is not likely that this parameter is the best option going forward in trying to approach the clay mineral behaviour as a cohesive sediment in Delft3D.

7.4 Possible Controls on Clay Mineral Distribution and the further use of Modeling in Delft3D

This study does not take into account several potential controls on clay mineral distribution. Studying these further, with or without (hydrodynamic) modeling, would be a good next step in understanding and predicting clay mineral distribution.

Physical characteristics of the different clay minerals are suggested to be a potential strong control on clay mineral distribution. More specifically: lattice type, structure, shape and size. And in extension of these: the breakup of flocs and small-scale surface processes. These are currently not implemented in Delft3D in any way. Studying the effects of the physical characteristics of clay minerals would probably involve lab work or other basic modeling work outside of Delft3D.

It is also possible that simplifications of the hydrodynamic input of this research, especially the mean tides and river discharges, excluded possible strong controls on clay mineral distribution. Three possible processes that can be modeled in Delft3D would be: flood events, neap-spring tidal cycles and sediment supply.

Flood events can have a large impact on a shallow estuary with small river discharges like the Ravenglass estuary. These event may occur in short periods of high precipitation in the catchment area, where three rivers can transport it into the estuary. Flood events in theory could deposited much more sediment in a matter of hours than a 'normal' tidal cycle could deposited in weeks or even longer. Relative to the simplified mean values used in this study, it could largely alter the hydrodynamics within the estuary.
The tidal range in the present-day Ravenglass estuary varies from 8 m at spring tide to 2,5 m at neap tide. A mean tidal cycle with a constant tidal range of 4,5 is therefore a major oversimplification. As the inner estuary is tide-dominated, this would have a large effect on the hydrodynamics, and in turn, the sediment distribution. In addition, this would largely influences the high-energy area's, where the unusual abundance of chlorite occurs in the bars. It would also exaggerate one of the more characteristic hydrodynamic features of the estuary: the highly asymmetrical tidal cycle.

Clay mineral distribution is strongly influenced by sediment supply (Griffiths et al., 2019a) and the deposition of cohesive sediment as computed by Delft3D is influenced by the concentration of sediment. In this study, supply was kept constant. In addition, the results show most sediment was deposited close to the river boundaries and the sensitivity analysis found hints of a tendency to transport sediment into the Mite-arm. Therefore, distilling the effect of sediment supply would be useful in improving our understanding of sediment distribution.

While further modeling work in Delft3D could prove useful in terms of understanding the hydrodynamics and it's effect on cohesive sediment distribution, the results of this study no not suggest that simulated cohesive sediment fractions can be parameterized in such a way, that it will approach or predict the very heterogeneous distribution patterns as observed in the present-day Ravenglass estuary. However, this should be studied further in order to conclude on this with certainty.

7.5 Implications for the Prediction of Clay Mineral Distribution and Clay-coated Sand Grains in other Paralic Depositional Environments

The results of this study do not suggest that clay mineral distribution, and in extension, the distribution of clay-coated sand grains can be predicted using hydrodynamic modeling in Delft3D. However, it has also no been disproven, and so the work done can be used as a first step in order to gain more insight in the possible benefits of hydrodynamic modeling.
Next possible steps in this process would be to delve deeper into the parameterization of different cohesive sediment fractions and to what extent these fractions can differ from each other and create vastly different, heterogeneous distribution patterns like observed in the Ravenglass estuary. If Delft3D does not allow for this, later modeling work may be scoped down to studies on controls on cohesive sediment distribution or more realistic modeling work of hydrodynamics of the Ravenglass estuary, including a focus on validation of the model.

7.6 Implications for the Prediction of Clay Mineral Distribution and Clay-coated Sand Grains in Reservoirs

Prediction of clay minerals and clay-coated sand grains in reservoirs should be studied after the distribution is well understood in present-day paralic depositional environments. Therefore, it is too soon for this study to provide direct implications for reservoirs or reservoirs analogues.
It is beneficial to keep this goal in mind in further studies nonetheless. To illustrate, the results if this study hint at an important role for the geometry of the estuary, where the two spits shelter a large part of the inner estuary and indirectly create a vital role of wave direction on the hydrodynamics and sediment distribution in the estuary. If the geometry or paleocurrents of a depositional environment corresponding to a certain reservoir cannot be determined accurately, this can greatly reduce ones ability to predict the distribution of clay minerals and clay-coated sand grains using hydrodynamic modeling. This problem could be counteracted by using a combination of different prediction methods, such a prediction based on knowledge of grain size, clay fraction and depositional facies (Wooldridge et al., 2017b).

Conclusions

8.1 What are the most important Hydro- and Morphodynamic processes in the Ravenglass Estuary that can lead to the observed Clay Mineral Distributions?

The most important processes that were identified was the interaction between the incoming marine currents versus the outgoing fluvial currents and the orientation of waves. Both are strongly influenced by estuary geometry and both have also been found or suggested in other studies. The data also suggests a possible important role for the ratio between a sediments saline- and fresh settling velocity and sediment supply, which should be studied further. Outside of hydrodynamic modeling, suggested processes are effects of characteristic physical properties of clay minerals and small scale bed-level processes.

8.2 What are the key Hydrodynamic and Morphodynamic processes in the Ravenglass Estuary as identified by hydrodynamic modeling in Delft3D?

The results from the sensitivity analysis for the Base Case with and without waves suggest that the area of fluvial-tidal interaction has a large role in the distribution of sediment. Cohesive sediment distribution seem to be controlled by the area of tidal influence, where more sedimentation is seen in area's effected by high tides, but not by low tides. In addition, deposition of non-cohesive sediment can be explained by the effect of tides on the flow velocity in the main channels of the estuary. Here the flow velocity of the river can be either increased by the outgoing tide, resulting in less deposition. Closer to shoreline at low tide, where there is generally a low-energy zone, the flow velocity of the river discharge is decreased as it is comes into contact with the seawater, resulting in an area that is more favourable for sedimentation of sand. The effect of waves on sediment distribution can be physically explained by the effect incoming mild waves have on the tides, which is generally a decreases in energy in area's influenced by waves. Because the Ravenglass estuary has a narrow inlet, this effect is more prominent when the wave orientation coincides with the orientation of the inlet. This supports the fact that wave orientation is a strong

control in the Ravenglass Estuary, but this is local-specific due to the unsual estuary geology and may very well not translate to other paralic depositional environments.

8.3 How can the behaviour of Chlorite, Illite and Kaolinite Clay Minerals be Approximated in Delft3D?

This study approximated the behaviour of chlorite, illite and kaolinite as cohesive sediment fractions in Delft3D, mainly by using the density, fresh settling velocity and saline settling velocity parameters as listed in tables 4.5, 4.6 and 4.7. The observed distributions in the present-day Ravenglass Estuary were not approached and it is not certain if that is even a possibility. To conclude on this for certain, the extent to how different cohesive sediment fractions can be distributed in different patterns should be studied further. Possible important sediment parameters for this are the critical shear stress for sedimentation and the ratio of fresh settling velocity to saline settling velocity.

8.4 Can hydro- and morphodynamic modelling explain and predict clay mineral distribution in the Ravenglass Estuary and what does this imply for the use of modeling and prediction of clay mineral distributions in other paralic depositional environments?

The observed clay mineral distribution in the Ravenglass Estuary cannot be explained and predicted by modeling in Delft3D according to the findings of this study, but more work should be done in order to completely disprove this.
Aside from the suggested step in section 8.3, more work should be done on the effects of marine-fluvial interaction on the distribution of cohesive sediment that was outside of the scope of this study, including but not limited to: spring-neap tides, flood events and the effect sediment supply. Another suggestion for future work is improving on the realism of the model of the Ravenglass Estuary by hydrodynamic validation.

8.5 What do the Results and Analysis of the Ravenglass Estuary potentially mean for the Distribution of Clay Minerals and Clay-coated Sand Grains in various Paralic Depositional Environments and can this be used as a Reservoir Analogue?

The findings of this study do not suggest that the distribution of clay minerals, and in extension, clay coated sands grains can be predicted in other paralic depositional environments or reservoirs. However, the work done provides a good first step for further work on this topic and suggests that it can improve our understanding on estuarine hydrodynamics and controls on sediment distribution.

8.6 Main Research Question: Why do Clay Minerals Accumulate at specific locations in the present-day Ravenglass Estuary and what implication does that have as an analogue for Clay Mineral Distribution in Paralic Depositional Environments?

The cause of the, sometimes counter-intuitive, observed distribution of clay minerals in the present-day Ravenglass Estuary is still not well understood after the completion of this study. However, important hydro- and morphodynamic processes have been identified and should be studied further. From this, it can be concluded that hydrodynamic modeling can help, at the very least, in the overall understanding of estuarine hydrodynamics and it's effects on sediment distribution. So, before clay mineral distribution other paralic depositional environment can be predicted, more work has to be done on this topic. Expanding on the work done in this study, and continuing on using the Ravenglass Estuary as an analogue, seems to be a promising next step.

Recommendations

- Study the effect of more complex possible controls on sediment distribution, including but not limited to: sediment supply, spring-neap tides and flood events
- Expand on the parameterization of cohesive sediment fractions, and the potential ability to create distribution patterns that differ significantly from each other
- Improve on a model of the Ravenglass Estuary, preferably with more hydrodynamic validation
- Use smaller timesteps (e.g. hourly) in order to accurately study the effect of an individual tide cycle
- Use smaller amounts of sediment input in order to prevent morphodynamic changes and be able to distill certain effects better
- Expand on the effects of the physical properties of the clay minerals on distribution
- Expand on or incorperate knowledge of small-scale surface based processes that are not approached or incorporated in Delft3D

Bibliography

Assinder, D., Kelly, M., and Aston, S. (1985). Tidal variations in dissolved and particulate phase radionuclide activities in the esk estuary, england, and their distribution coefficients and particulate activity fractions. *Journal of Environmental Radioactivity*, 2(1):1–22.

Bennet, R. and Hulbert, M. (1986). *Clay microstructures*. Springer.

Boucher, A. (1999). Ravenglass estuary: Basic characteristics and evaluation of restoration options. Technical report, Westlakes Scientific Consulting Ltd,.

Dalrymple, R., Zaitlin, B. A., and Boyd, R. (1992). Estuarine facies models; conceptual basis and stratigraphic implications. *Journal of Sedimentary Research*, 62(6):1130–1146.

Daneshvar, E. (2015). *Role of provenance on clay minerals and their distribution in modern estuaries*. PhD thesis, University of Liverpool.

Deer, W., Howie, R., and Zussman, J. (1975). *An introduction to rock-forming minerals*. Longman group ltd, London.

Dowey, P. (2012). *Prediction of Clay Minerals and Grain-coatings in Sandstone Reservoirs Utilising Ancient Examples and Modern Analogue Studies*. University of Liverpool.

Ehrenberg, S. N. (1993). Preservation of anomalously high porosity in deeply buried sandstones by grain-coating chlorite: Examples from the norwegian continental shelf. *AAPG Bulletin (American Association of Petroleum Geologists); (United States)*, 77:7.

Fairbridge, R. (1980). *THE ESTUARY: ITS DEFINITION AND GEODYNAMIC CYCLE*. CHEMISTRY AND BIOGEOCHEMISTRY OF ESTUARIES.

Flemming, B. (2011). Geology, morphology, and sedimentology of estuaries and coasts. *Treatise on Estuarine and Coastal Science*, 3(6):7–38.

Fugro GEOS (2001). Wind and wave frequency distributions for sites around the british isles. Technical report, Prepared by Fugro GEOS for the Health and Safety Executive. Note: Data taken of grid point 15920.

Griffiths, J., Worden, R., Wooldridge, L., Utley, J., Duller, R., and Edge, R. (2018). Estuarine clay mineral distribution: Modern analogue for ancient sandstone reservoir quality prediction. *Sedimentology*, 66.

Griffiths, J., Worden, R. H., Wooldridge, L. J., Utley, J. E. P., and Duller, R. A. (2019a). Compositional variation in modern estuarine sands: Predicting major controls on sandstone reservoir quality. *AAPG Bulletin*, 103(4):797–833.

Griffiths, J., Worden, R. H., Wooldridge, L. J., Utley, J. E. P., Duller, R. A., and Edge, R. L. (2019b). Estuarine clay mineral distribution: Modern analogue for ancient sandstone reservoir quality prediction. *Sedimentology*, 66(6):2011–2047.

Heald, M. T. and Baker, G. F. (1977). Diagenesis of the Mt. Simon and Rose Run sandstones in western West Virginia and southern Ohio. *Journal of Sedimentary Research*, 47(1):66–77.

Jeldres, R., Leiva, W., Toledo, P., Piceros, E., and Herrera, N. (2017). Viscoelasticity and yielding properties of flocculated kaolinite sediments in saline water. *Colloids and Surfaces A: Physicochemical and Engineering Aspects*, 529.

Kelly, M. and Emptage, M. (1991). The relationship between sediment and plutonium budgets in a small macrotidal estuary: Esk estuary, cumbria, uk. *Journal of Environmental Radioactivity*, 13(1):55–74.

Liu, D., Edraki, M., and Berry, L. (2018). Investigating the settling behaviour of saline tailing suspensions using kaolinite, bentonite, and illite clay minerals. *Powder Technology*, 326:228–236.

Mindat (last visited january 2021). Mineral data. *URL: mindat.org, by the Hudson Institute of Mineralogy.*

Parsons, A., Pye, K., Pontee, N., and Allan, E. (2013). North west estuaries processes reports – ravenglass estuary. Technical report, Halcrow Grup ltd a CH2M Hill Company.

Partheniades, E. (2009). Chapter 3 - forces between clay particles and the process of flocculation. In Partheniades, E., editor, *Cohesive Sediments in Open Channels*, pages 47–88. Butterworth-Heinemann, Boston.

Perillo, E. (1995). *GEOMORPHOLOGY AND SEDIMENTOLOGY OF ESTUARIES: AN INTRODUCTION*, volume 53 of *Geomorphology and Sedimentology ofEstuaries. Developments in Sedimentology.* Elsevier Science.

Pittman, E. D., Larese, R. E., and Heald, M. T. (1992). Clay Coats: Occurrence and Relevance to Preservation of Porosity in Sandstones. In *Origin, Diagenesis, and Petrophysics of Clay Minerals in Sandstones.* SEPM Society for Sedimentary Geology.

Pritchard, D. W. (1967). Observations of circulation in coastal plain estuaries. *Estuaries.*

Reading, H. G. (1996). *Sedimentary Environments: Processes, Facies and Stratigraphy, 3rd Edition.* Wiley-Blackwell.

Schubel, J. R. (1984). *Estuarine sedimentation*, pages 400–402. Springer US, New York, NY.

Shi, B., Wang, Y. P., Yang, Y., Li, M., Li, P., Ni, W., and Gao, J. (2015). Determination of critical shear stresses for erosion and deposition based on in situ measurements of currents and waves over an intertidal mudflat. *Journal of Coastal Research*, 31:1344–1356.

Storvoll, V., Bjørlykke, K., Karlsen, D., and Saigal, G. (2002). Porosity preservation in reservoir sandstones due to grain-coating illite: a study of the jurassic garn formation from the kristin and lavrans fields, offshore mid-norway. *Marine and Petroleum Geology*, 19(6):767–781.

van de Lageweg, W. I., Braat, L., Parsons, D. R., and Kleinhans, M. G. (2018). Controls on mud distribution and architecture along the fluvial-to-marine transition. *Geology*, 46(11):971–974.

van Maren, B. (2009). An introduction to cohesive sediment transport modelling. *https://slidetodoc.com/an-introduction-to-cohesive-sediment-transport-modelling-bas/ Accessed: {2021\OT1\textendash05-06}*,, 31:1344–1356.

Van Rijn, L. (1984). Sediment transport, part i: Bed load transport. *Journal of hydraulic engineering*, 110.

Villars, M. and Delvigne, G. (2001). *Estuarine Processes*. Delft Hydraulics.

Whitehouse, U., Jeffrey, L., and Debbrecht, J. D. (1958). Differential settling velocities of clay minerals in saline waters. *Clays and clay minerals*, 7(6):1–79.

Wolanski, P. E. and Elliott, M. (2014). *Estuarine Ecohydrology : An Introduction*. ProQuest Ebook Central,. Elsevier Science Technology.

Wooldridge, L., Worden, R., Griffiths, J., Thompson, A., and Chung, P. (2017a). Biofilm origin of clay-coated sand grains. *Geology*, 45.

Wooldridge, L., Worden, R., Griffiths, J., and Utley, J. (2017b). Clay-coated sand grains in petroleum reservoirs: Understanding their distribution via a modern analogue. *Journal of Sedimentary Research*, 87:338–352.

Wooldridge, L., Worden, R., Griffiths, J., and Utley, J. (2018a). Clay coat diversity in marginal marine sediments. *Sedimentology*.

Wooldridge, L., Worden, R., Griffiths, J., Utley, J., and Thompson, A. (2018b). The origin of clay-coated sand grains and sediment heterogeneity in tidal flats. *Sedimentary Geology*, 373:191–209.

Worden, R., Griffiths, J., Wooldridge, L., Utley, J., Lawan, A., Muhammed, D., Simon, N., and Armitage, P. (2020). Chlorite in sandstones. *Earth-Science Reviews*, 204:103105.

Worden, R. and Morad, S. (2000). Quartz cementation in oil field sandstones: A review of the key controversies. *Spec. Publ. Int. Assoc. Sed.*, 29:1 – 20.

Cover image by: Thomas Nugent, *url: https://www.geograph.org.uk/photo/4652500*